THE 40AR/39AR GEOCHRONOLOGY AND THERMOCHRONOLOGY OF THE LATIR VOLCANIC FIELD AND ASSOCIATED INTRUSIONS: IMPLICATIONS FOR CALDERA-RELATED MAGMATISM

By

Matthew Joseph Zimmerer

Submitted in Partial Fulfillment
of the Requirements for the

Masters of Science in Geochemistry

New Mexico Institute of Mining and Technology
Department of Earth and Environmental Science

Socorro, New Mexico

August, 2008

ABSTRACT

Volcanic and plutonic rocks exposed in the Latir volcanic field, Sangre de Cristo Mountains of northern New Mexico, provide a unique opportunity to study caldera-related magmatism and understand the spatial and temporal relationship between the volcanic and plutonic record. Fifty-one samples were dated using $^{40}Ar/^{39}Ar$ method. The results indicate a 10 Ma period of Latir volcanic field related magmatism. The volcanic geochronology provides point-in-time information about magmatism whereas the thermochronology of plutonic rocks establishes their emplacement and cooling history.

Volcanic rocks provide information about the earliest magmatism associated with Latir volcanic field. Precaldera volcanism began at 28.3 Ma and ended at 25.3 Ma, based on $^{40}Ar/^{39}Ar$ analysis of hornblende, biotite, and sanidine from exposed volcanic rocks. Combining the published geochemistry with ages of precaldera volcanism from this study indicates that the earliest magmatism was characterized by multiple, small magma chambers, rather than a single, large magma chamber. Peak magmatism occurred during the eruption of the 500 km^3 peralkaline Amalia Tuff from the Questa caldera. Sanidine analyses from eleven samples yielded a mean age of 25.23 Ma for the Amalia Tuff.

Following the eruption of the Amalia Tuff, four resurgent plutons were emplaced in the shallow crust near the center of the caldera. K-feldspar multiple diffusion domain

(MDD) thermal models indicate that the plutons cooled rapidly after emplacement. By 24.7 Ma, within 500 ka of caldera eruption, all the plutons cooled to 150°C. A biotite from the previously undated Canada Pinabete pluton, a resurgent pluton chemically similar to the Amalia Tuff, yields an age 25.28 Ma. Because the Canada Pinabete pluton and Amalia Tuff are geochemically similar and their ages are analytically indistinguishable, the Canada Pinabete pluton is interpreted as non-erupted Amalia Tuff. This supports the idea that ignimbrite magma chambers may not completely drain during eruption and plutons can be directly correlated to large-scale ignimbrite sheets. The remainder of the resurgent plutons are slightly younger than the Amalia Tuff and record a compositional transition to lesser-evolved magmas. Three postcaldera rhyolites yield sanidine ages between 24.9 and 25.0 Ma indicating coeval volcanism with emplacement of the resurgent plutons.

After resurgent plutonism, three plutons, probably cupolas of a larger, single intrusion, were emplaced and are now exposed along the southern caldera margin. Biotite ages from the Red River, Sulfur Gulch, and Bear Canyon plutons are 24.8, 24.5, and 24.3 Ma, respectively, suggesting incremental emplacement of the larger intrusion along the southern caldera margin. K-feldspar monotonic MDD thermal histories from the individual plutons display differences of rates and timing of cooling. MDD models suggest the Red River pluton experienced a period of isothermal cooling at 300°C between 24 and 22 Ma, followed by rapid cooling at 21 Ma. One K-feldspar MDD thermal model from the Bear Canyon indicates rapid cooling at 21 Ma, but another Bear Canyon K-feldspar thermal model indicates rapid cooling at 23 Ma, followed by isothermal conditions at 200°C between 22 and 18 Ma. The unconstrained MDD thermal

models suggest reheating by younger thermal events possibly related to magma emplacement.

The two youngest plutons, Rio Hondo and Lucero Peak, were emplaced 5-15 km south of the caldera. An associated study of U-Pb zircon ages suggest that the Rio Hondo pluton was possibly incrementally emplaced between 23 and 22.5 Ma. Biotite collected from multiple locations in the Rio Hondo pluton yield ages of ~21 Ma, indicating that following incremental emplacement, the different increments comprising the pluton cooled to 350°C at the nearly the same time. K-feldspar MDD monotonic cooling models indicate a period of slow to isothermal cooling between 21 and 16 Ma. Alternatively, the unconstrained modeling results show a thermal perturbation at 16.5 Ma, which corresponds to the age of a Rio Hondo hosted rhyolite dike. A single age of 22.5 Ma from a postcaldera andesite on Brushy Mountain suggests coeval volcanism with the emplacement of the Rio Hondo pluton. Biotite ages are ~19 Ma from both the interior and margin of the Lucero Peak pluton. Similarly, K-feldspar cooling histories from the interior and margin of the pluton both suggest slow cooling between 19 and 16 Ma. The similarity of cooling histories between marginal and interior unites, combined with the lack of robust reheating models, is interpreted to be the result of a complex emplacement history, rather than simple batch emplacement of a pluton. In summary, $^{40}Ar/^{39}Ar$ results from this study describe magmatism at different times associated with caldera-volcanism, and provide insight into the relationship between the volcanic and plutonic record.

TABLE OF CONTENTS

Tables

Appendices

INTRODUCTION

Volcanic and plutonic rocks exposed in the Latir volcanic field provide insight into magmatism during caldera volcanism. Unlike other Oligocene regional volcanic fields in which multiple calderas spatially and temporally overlap (McIntosh, 1992; Lipman, 2007), the Latir field contains only one caldera, the Questa caldera (Lipman et al., 1986), from which the Amalia Tuff erupted at 25.23 Ma (Fig. 1). Having only one caldera within the field insures that the volcanic record has not been complicated by eruptions from other volcanic centers, nor has the thermochronology of the exposed plutons been disturbed by magmatism associated with later generations of caldera growth.

Recent interest has focussed on the nature of plutonism beneath volcanic fields (Coleman et al., 2004; Bartley et al., 2005; Glazner et al., 2006; Lipman, 2007). Studies in the Mesozoic Tuolumne Intrusive Suite have demonstrated that subvolcanic batholiths formed by the incremental emplacement of plutons over durations as long as 10 Ma. During incremental emplacement, individual plutons may not contain any significant melt fraction for a voluminous eruption (Coleman et al., 2004; Glazner et al., 2004). However, the presence of large (>100 km^3), partially to completely molten magma bodies within the upper crust is unquestionably demonstrated by the numerous large-volume

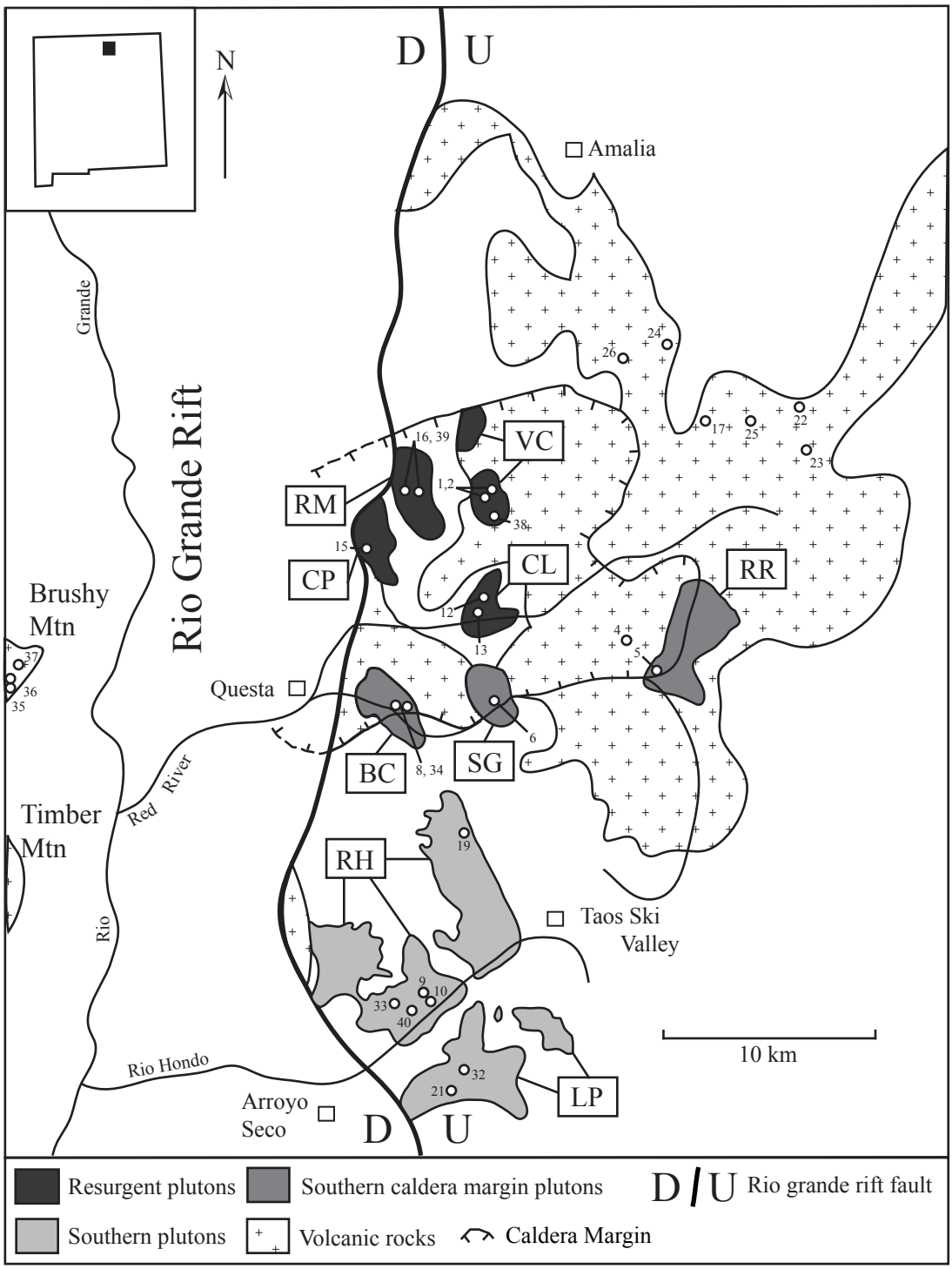

Figure 1 – Generalized geologic map of the Latir volcanic field showing the distribution of the volcanic rocks and plutons, after Czamanske et al (1990). Map also contains the MZQ samples localities (samples along the western margin of the Rio Grande Rift are not shown). Plutons are grouped into three categories (resurgent, southern caldera margin, and south plutons) and the corresponding abbreviations are: VC, Virgin Canyon; RM, Rito del Medio; CP, Canada Pinabete; CL, Cabresto Lake; BC, Bear Canyon; SG, Sulfur Gulch; RR, Red River; RH, Rio Hondo; LP, Lucero Peak.

Tertiary ignimbrites of the San Juan and Mogollon-Datil volcanic fields (McIntosh et al., 1992; McIntosh and Chapin, 2004; Lipman, 2007). Solving this contradiction is difficult because rarely are volcanic rocks and coeval plutons exposed together at the surface. The Latir volcanic field is important in this respect because it is one of the few localities where the plutonic and volcanic records are both preserved and exposed, so the comprehensive complete magmatic history of a volcanic field can be studied.

Though several geochronological studies have examined the timing of volcanism and plutonism in the Latir volcanic field (Pillmore et al., 1973; Lipman et al., 1986; Czamanske et al., 1990; Smith et al., 2002), there is no published comprehensive and precise geochronological study of the volcanic and plutonic record using high-resolution methods. K-Ar dating (Lipman et al., 1986) and detailed mapping (Lipman and Reed, 1989) provided the thorough framework for the geochronology for the Latir field. This study helped to develop a volcanic stratigraphy and recognized an overall younging of plutonism towards the south. Because of the lack of precision and other problems associated with the K/Ar method, subsequent workers have used the $^{40}Ar/^{39}Ar$ dating technique to better understand the timing of volcanism and plutonism. Czamanske et al. (1990) helped determined the timing of the intrusions, but unfortunately the analytical data was not reported, nor the age spectra, and thus the quality and geologic significance of these $^{40}Ar/^{39}Ar$ ages are difficult to assess. Smith et al. (2002) provided the only single-crystal laser-fusion $^{40}Ar/^{39}Ar$ dates on the volcanism and determined the age of the Amalia Tuff to be 25.26 ± 0.1 Ma (corrected for FC-2 = 28.02 Ma)

This paper summarizes the results of 51 new $^{40}Ar/^{39}Ar$ analyses of volcanic and plutonic rocks from the Latir volcanic field. Dating of volcanic rocks associated with

field is important because it determines the timing and duration of the volcanism and constrains the temporal-geochemical trends observed from inception to cessation of the volcanic field. Additionally, timing of volcanism is intrinsically related to the emplacement of magma into the crust that may not be preserved by plutons, either because they are not exposed or were completely erupted. Thermochronology from the plutons contributes to the understanding of how subcaldera plutons are constructed, cool, and change throughout time. Cooling rates are directly related to the level of emplacement, changing geothermal gradients, and thermal perturbations because of melt emplacement. In addition, this paper presents results of multiple diffusion domain (MDD) thermal modeling of plutonic K-feldspars, which has been proven to be useful in deciphering the 300-150°C thermal histories of plutons (Heizler, 1988; Richter et al., 1991).

BACKGROUND

The Latir volcanic field is located in the Sangre de Cristo Mountains of northern New Mexico (see inset Fig. 1). The field is one of numerous Tertiary volcanic fields that form a semi-continuous volcanic belt from Colorado through central Mexico, thought to be the consequence of flat-slab subduction of the Farallon plate beneath the North America plate (Coney et al., 1977; Dickenson et al., 1978). By 45 Ma the rate of convergence had slowed, the subducted slab began to 'roll-back' beneath the western margin of North America, and back-arc crustal stresses began to transition from compression to extension (Chapin et al., 2004; Lawton et al., 1999). Extension across the southwestern North American plate allowed large volumes of silicic magma to intrude into upper levels of the crust, essential for caldera volcanism. Extension has continued until present day, transitioning from ductile to brittle deformation, and eventually forming the present Rio Grande rift (Baldridge and Olsen, 1989; Baldrigde et al., 1995).

The Latir field covers an area of approximately 1200 km^2 and represents the erosional remnants of a much larger field. Like most calderas, compositionally intermediate eruptions characterize volcanism prior to caldera formation (Lipman et al., 1986; Colucci et al, 1991; Lipman, 2007). Basaltic andesite and quartz latite are the most voluminous precaldera volcanic rocks in the field, with minor amounts of precaldera

rhyolitic tuffs and lava flows also erupted. Volcanism climaxed with the formation of the Questa caldera during the eruption of the ~500 km^3 peralkaline Amalia Tuff (Lipman et al., 1986). Most of the postcaldera volcanic rocks are absent from the field because of uplift and subsequent erosion. However, numerous postcaldera volcanic rocks are preserved on the intrarift horst blocks of Brushy and Timber mountains. Similar to precaldera volcanism, postcaldera volcanism is characterized by intermediate and silicic eruptions (Thompson et al., 1986).

Structural and topographic uplift, erosion, and Rio Grande rift faulting has exposed nine plutons throughout the field. Bouguer gravity maps indicate a gravity low centered on the caldera, implying that the plutons connect at depth to form a subvolcanic batholith (Cordell et al., 1986). The plutons are grouped into three categories: resurgent, southern caldera margin, and southern plutons, based on similarities in geographic location, age, and structural position with respect to the subvolcanic batholith (Fig. 1).

The Virgin Canyon, Canada Pinabete, Rito del Medio, and Cabresto Lake plutons comprise the northern resurgent plutons. The Virgin Canyon and Canada Pinabete plutons contain peralkaline and metaluminous granite phases. The geochemical similarity between the Amalia Tuff and the peralkaline phases of the Virgin Canyon and Canada Pinabete suggests they are unerupted Amalia Tuff (Lipman et al., 1986; Johnson and Lipman, 1988). Miarolitic cavities within the granitic Rito del Medio suggest a high level of emplacement within the crust (Czamanske et al., 1991). The Cabresto Lake pluton is more mafic than the other resurgent plutons and may represent a transition between the evolved magmas in the north and the lesser-evolved magmas located in the south (Lipman et al., 1986).

The southern caldera margin plutons, from west to east, are: Bear Canyon, Sulfur Gulch, and Red River. The plutons are characterized by varying degrees of hydrothermal and quartz-sericite-pyrite alteration, as well as, molybdenum mineralization (Leonardson, 1983; Lipman et al., 1986; Czamanske et al., 1990). The Bear Canyon and Sulfur Gulch plutons are relatively homogenous granites that contain minor aplite dikes. In contrast, the Red River pluton consists of granite, quartz monzonite, and numerous dikes of various compositions.

The remaining two southern plutons, Rio Hondo and Lucero Peak, are located 5-15 km south of the southern caldera margin. The Rio Hondo pluton has a main porphyritic granodiorite phase, which is capped by a thin granitic zone directly beneath Precambrian roof rocks (Czamanske et al., 1990). Mafic enclaves and plastically deformed mafic dikes are present in deepest exposed sections of the pluton. Hundreds of northwest-southeast and east-west trending dikes of felsic and mafic composition are located within the main granodiorite phase (Lipman et al., 1986). Unlike the Rio Hondo pluton, the Lucero Peak pluton is a relatively homogenous megacrystic granite with the exception of few dikes in its most eastern section. The Lucero Peak pluton is the youngest known magmatic event in the Latir field (Czamanske et al., 1990).

METHODS

A total of forty-one samples were collected from the Latir volcanic field and surrounding areas during this study. These particular samples are reference to as the MZQ samples. In addition to the collected samples, Peter Lipman provided seven samples from the Lipman et al. (1986) study and Ren Thompson of the USGS provided one. Of the total 49 samples available, 51 mineral separates were analyzed using the $^{40}Ar/^{39}Ar$ dating technique.

Volcanic rocks were collected from the northeastern region of the field to avoid hydrothermal alteration in the southern caldera margin region (Fig. 1). Volcanic rocks were also collected from the horst blocks and distal outflow sheets in the Tusas Mountains, along the west side of the rift. Intrusive rocks were collect from within the caldera, along the southern margin, and south of the caldera. An attempt was made to collect at least two samples from each pluton to better characterize the thermal histories. Outcrops that displayed intense weathering were avoided, as well as locations in close proximity to dikes or other intrusions that might have thermally reset the targeted minerals. Table 1 lists the sampled dated in this study, a short description, UTM coordinates, and the minerals dated.

Sample preparation techniques included crushing, grinding, sieving, ultrasonic cleaning in deionized water and 15% hydrofluoric solution, magnetic separation, and heavy liquids. Minerals were then optically inspected on a binocular microscope and handpicked to obtain monomineralic separates. Samples to be dated were analyzed using a Cameca SX-100 electron microprobe at the New Mexico Bureau of Geology and Mineral Resources to accomplish two goals. First, BSE images obtained from the electron microprobe insure the highest quality of mineral separation. Second, geochemical characterization of samples prior to $^{40}Ar/^{39}Ar$ analysis allows for recognition of any geochemical variation within the samples, which may be the result of alteration or geochemical contamination that would degrade the quality of geochronology results.

Samples were placed in 20-hole aluminum disks and irradiated with the interlabratory standard FC-2 (28.02 Ma) (Renne et al., 1998) in a known geometry. In addition to unknowns and monitors, CaF_2 and K-glass were irradiated to determine calcium and potassium correction factors. Samples were analyzed at the New Mexico Geochronology Research Laboratory between 2006-2008. Sanidine separates were heated using the single-crystal laser-fusion method. Bioite, hornblende, K-feldspar, and groundmass concentrate were step-heated in a double-vacuum Mo resistance furnace. Gas was then cleaned in an all-metal extraction line and analyzed using a MAP 215-50 mass spectrometer. For a complete description of the analytical techniques, refer to Appendix A.

Sample	Description	UTM (NAD 27)	Minerals Dated
79L-64	Rheomorphic flow of Amalia Tuff	13S 0463952 4077218	san
83L-8	Precaldera rhyolite of Cordova Creek	13S 0410405 4037635	san
82L-42H	Outflow vitrophyre of Amalia Tuff	13S 0464613 4068932	san
82L-31	Outflow sheet of Amalia Tuff	13S 0463799 4077053	san
82L-38	Outflow sheet of Amlia tuff	13S 0480246 4087999	san
82L-37	Amalia Tuff, outflow vitrophyre	13S 0460181 4079246	san
78L-183	Postcaldera rhyolite at Commanche point	13S 0471941 4076615	san
TPS04	Unwelded, outflow sheet of Amalia Tuff	13S 0412420 4050596	san
MZQ-1	Peraluminous Virgin Canyon	13S 0455880 4071198	Kspar
MZQ-2	Metaluminous Virgin Canyon	13S 0455754 4701203	Kspar
MZQ-4	intracaldera Amalia Tuff	13S 0455880 4071198	san
MZQ-5	Granite of Red River	13S 0455754 4701203	bt, Kspar
MZQ-6	Granite of Sulfur Gulch	13S 0455880 4071198	bt, Kspar
MZQ-7	Unwelded, silified outflow sheet of Amalia Tuff	13S 0413742 4049489	san
MZQ-8	Granite of Bear Canyon	13S 0455880 4071198	bt, Kspar
MZQ-9	Porphyritic Granodiorite of Rio Hondo	13S 0455754 4701203	bt, Kspar
MZQ-10	Rhyolite dike within Rio Hondo	13S 0455880 4071198	Kspar
MZQ-12	Granite of Cabresto Lake	13S 4054802 4066000	bt, Kspar
MZQ-13	Granite of Cabresto Lake	13S 0454977 0465797	bt, Kspar
MZQ-15	Metaluminous Canada Pinabete	13S 0450662 4068102	bt, Kspar
MZQ-16	Granite Rito del Medio	13S 0452113 4027057	bt, Kspar
MZQ-19	Porphyritic Granodiorite of Rio Hondo	13S 0453613 4055209	bt, Kspar
MZQ-21	Granite Lucero Peak	13S 0454281 4042533	bt, Kspar
MZQ-22	Postcaldera rhyolite at Commanche Point	13S 0472070 4076376	san
MZQ-23	Precaldera hornblende andesite	13S 0472685 4074551	hbl
MZQ-24	Precaldera quartz latite	13S 0464023 4079614	bt
MZQ-25	Rheomorphic flow of Amalia Tuff	13S 0468959 4076642	san
MZQ-26	Precaldera rhyolite of Cordova Creek	13S 0460457 4078175	san
MZQ-32	Granite Lucero Peak	13S 0454405 4042827	bt, Kspar
MZQ-33	Upper Granite of Rio Hondo	13S 0453636 4039302	Kspar
MZQ-34	Granite of Bear Canyon	13S 0450583 4061541	bt, Kspar
MZQ-35	Postcaldera rhyolite at Brushy Mountain	13S 0432601 4062776	san
MZQ-36	Postcaldera andesite at Brushy Mountain	13S 0432550 4062816	gmc
MZQ-38	Metaluminous Virgin Canyon	13S 0455033 4070953	Kspar
MZQ-39	Rito del Medio	13S 0452477 4072046	bt, Kspar
AR-171	Drill Core of Sulfur Gulch	----------	bt

Table 1- Samples used for this study. Minerals abbreviations are: biotite, bt; sanidine, san; K-feldspar, Kspar; hornblende, hbl.

RESULTS

Sanidine single-crystal laser-fusion analyses

Fifteen sanidine separates were dated using the single-crystal laser-fusion method. Eight samples were collected as part of this study and seven Lipman et al. samples were reanalyzed. Results are plotted as apparent ages versus relative probability (Deino and Potts, 1992). Also included with age probability diagrams are auxiliary plots of K/Ca, $\%^{40}Ar^*$, and ^{39}Ar moles auxiliary plots. Results are plotted in figure 2 and summarized in table 2. Full analytical results are in table 1 of Appendix B. Seven to 35 crystals from each sample were analyzed to determine the age. At least 15 grains were analyzed for all the MZQ samples. Samples from the Lipman et al. (1986) (Fig 2A-G) study were originally run as single crystals, but the small size of the crystals (~100-200 μm) resulted in small, imprecise ^{39}Ar signals. To increase precision, the samples were ran again as laser fusion analyses of sets of multiple crystals, typically 5-20 crystals per set. Several criteria were used to determine if an analysis should be included in the age calculation. Analyses with small or imprecise ^{39}Ar mol measurements, radiogenic yield < 95%, and high or low K/Ca values compared to the bulk values were not used for the age calculation. Analyses of xenocrysts were also excluded. Analyses yielding ages that

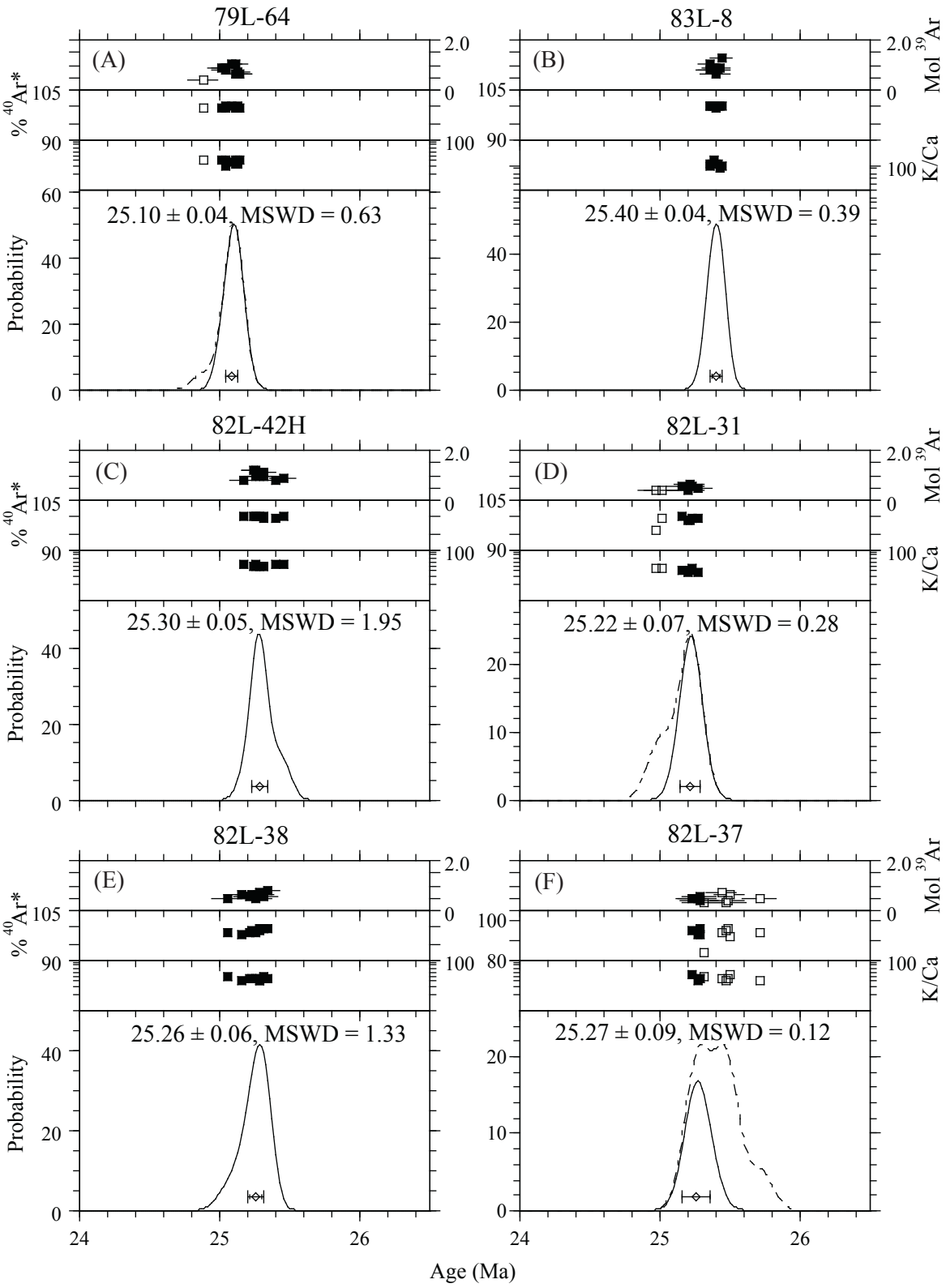

Figure 2 - Ideograms and auxillary plots of precaldera, postcaldera, and Amalia tuff sanidine separates. Moles of 39Ar are in 10^{-14}. All errors are reports at 2 sigma.

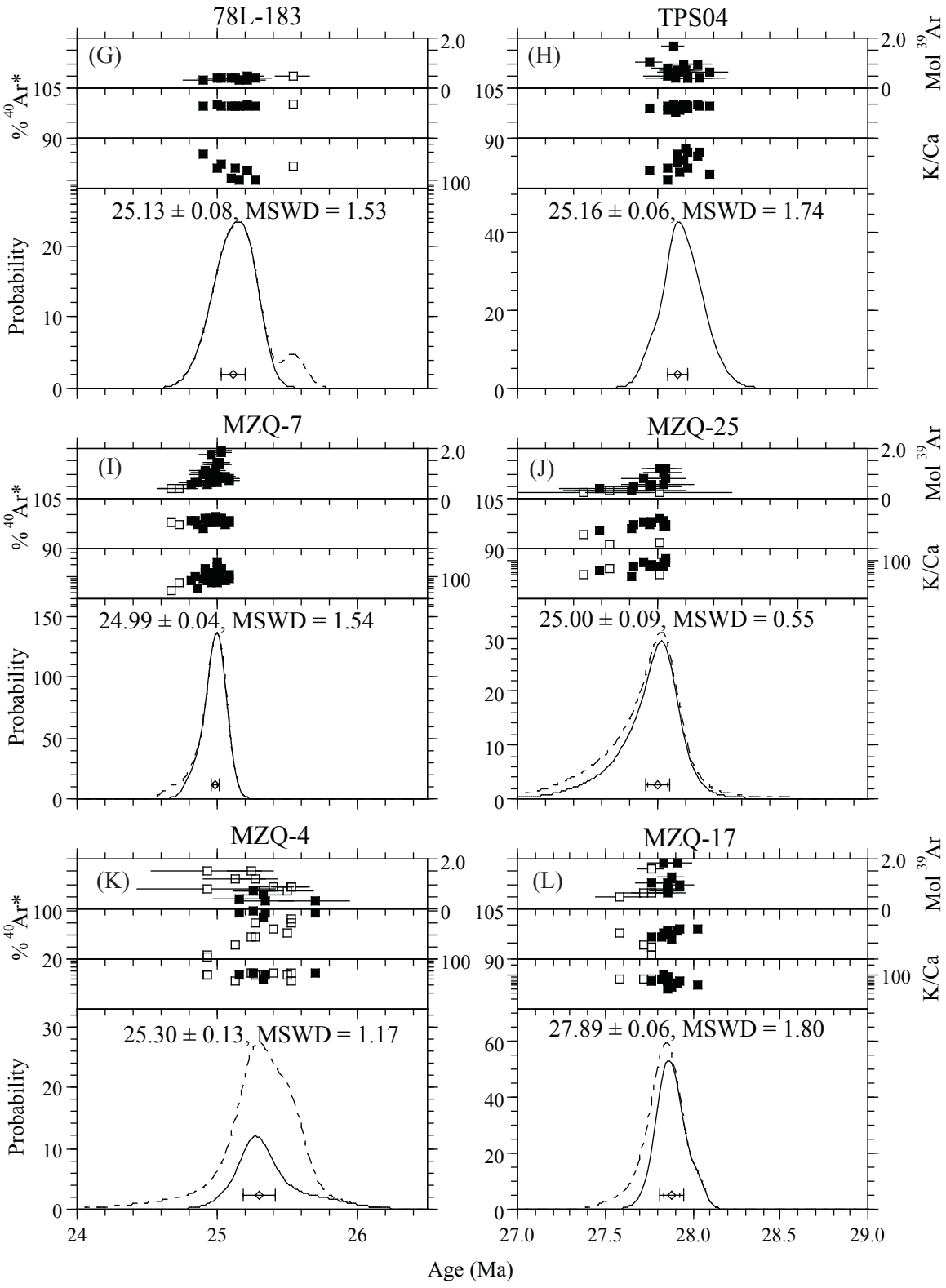

Figure 2 continued

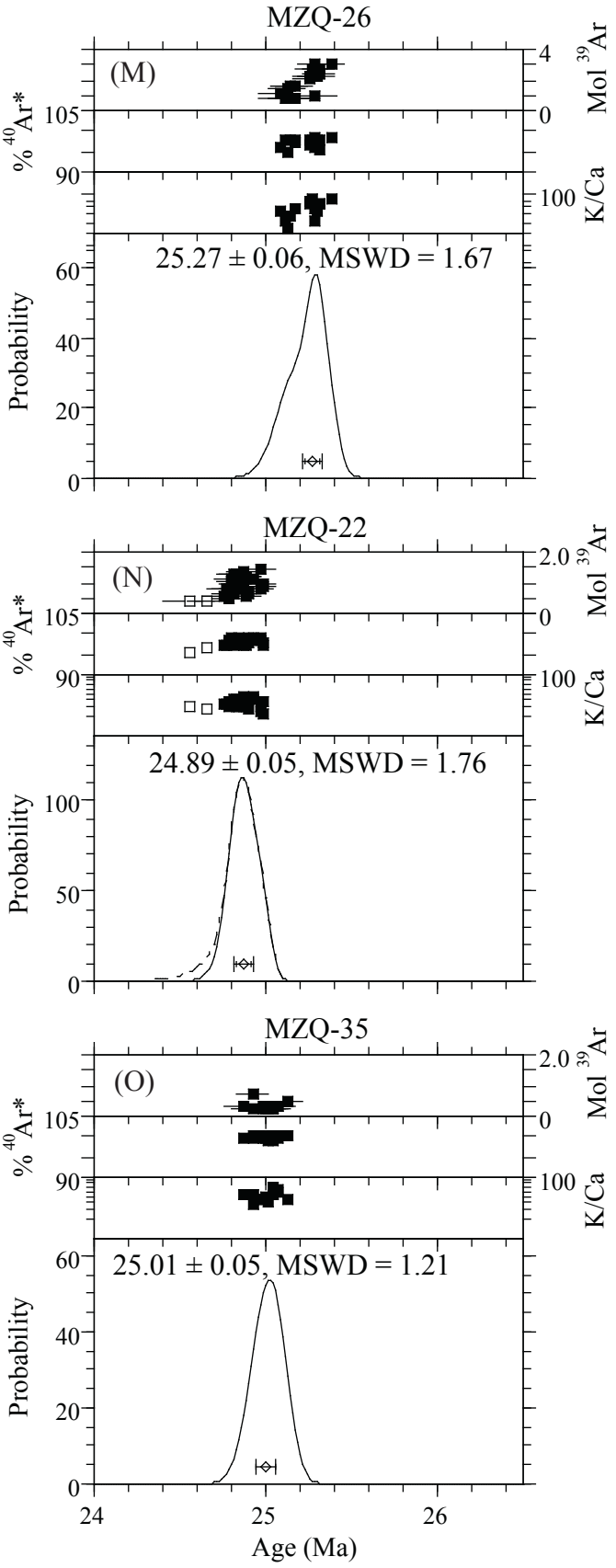

Figure 2 continued

were statistical outliers were omitted from the age calculation only after further investigation to determine the anomalous behavior.

The mean standard weighted deviant (MSWD) is a commonly used criterion for evaluating the statistical robustness of a data set. An MSWD near unity approximates a Gaussian distribution. MSWD values that differ significantly from unity indicate scatter in the data set not solely attributed to analytical error. Whether an anomalously high or low MSWD values is significant is partly a function of the number of analyses. Anomalously high MSWD values may be because of underestimating the errors associated with the ages or may be real geologic scatter. Anomalously low MSWD values may be attributed to an overcorrection during the calculation of the blanks and backgrounds, resulting in an over estimation of error associated with the age (Mahon, 1996).

Signal sizes for the single-crystal laser-fusion analyses ranged from 0.17 to 2.96 e-16 moles ^{39}Ar. The range in moles ^{39}Ar is proportional to the crystal size. Nearly all the analyses had radiogenic yields greater than 95%. K/Ca values for the sanidine analyses ranged from 22 to 260. The variation of K/Ca values commonly reflects the composition of the crystals analyzed. Additionally, because K/Ca values are derived from ^{39}Ar and ^{37}Ar measurements, blank correction induced errors can skew K/Ca values.

For MZQ-4 (Fig. 2K), ten of the fifteen analyses had radiogenic yields <95%. This sample was collected from the hydrothermally altered southern caldera margin. The low radiogenic yield measured for this sample probably reflects mild hydrothermal alteration of the sanidine. BSE microprobe images of MZQ-4 (Fig. 3) indicate minor amounts of clay within fractures. Clay commonly has high atmospheric argon and low

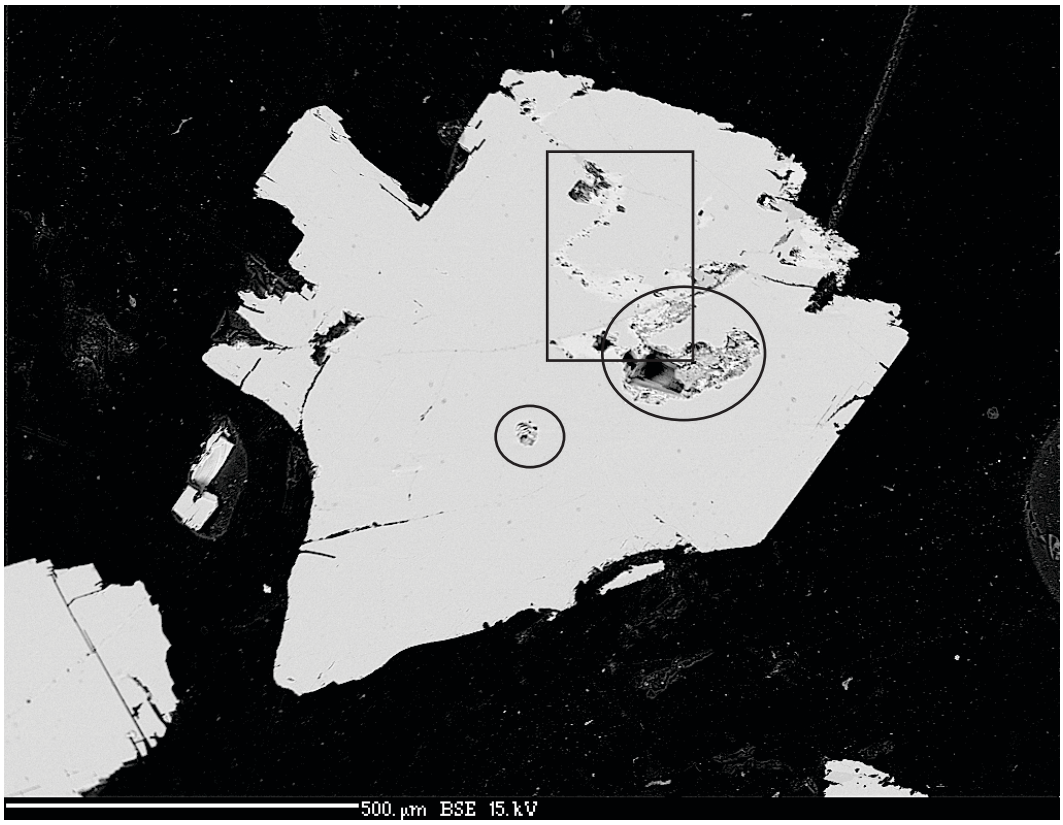

Figure 3 - Backscatter electron microprobe image of MZQ-4 sanidine crystals. The circled region encloses a clay of unknown composition. The square encloses a mineralized fracture. In an attempt to remove the clay, the crystals were cleaned in HF acid for 5-10 minutes, which resulted in removing some, but not all the clay. The HF acid also produced the highly irregular grain surface. In the lower left corner is an example of a grain without any clay or mineralization. Large crystals tended to have more clay resulting in large signals with low radiogenic yields and smaller crystals had no clay, resulting in small signals with higher radiogenic yields (Fig. 2K). The scale is located at the bottom of the image.

radiogenic argon and thus is preferred reason for the overall low radiogenic yields observed in the sample.

Sample	Unit	n	MSWD	K/Ca	Age(Ma)	2s
79L-64	Rhyolite Commache Point	9	0.6	35.1	25.10	0.04
83L-8	Rhyolite of Cordova Creek	8	0.4	99.1	25.40	0.04
82L-42H	Amalia Tuff	9	2.0	48.9	25.30	0.05
82L-31	Amalia Tuff	5	0.3	37.5	25.22	0.07
82L-38	Amalia Tuff	10	1.3	41.3	25.26	0.06
82L-37	Amalia Tuff	4	0.1	43.5	25.27	0.09
78L-183	Amalia Tuff	9	1.5	148.5	25.13	0.08
TPS04	Amalia Tuff	15	1.7	164.3	25.16	0.06
MZQ-7	Amalia Tuff	27	1.5	105.0	24.99	0.04
MZQ-25	Rheomorphic Amalia	12	0.6	68.9	25.00	0.09
MZQ-4	Amalia	5	1.2	45.6	25.30	0.13
MZQ-17	Tuff of Tetilla Peak	11	1.8	64.3	27.89	0.06
MZQ-26	Rhyolite of Cordova Creek	15	1.7	75.4	25.27	0.06
MZQ-22	Rhyolite Commache Point	25	1.8	32.5	24.89	0.05
MZQ-35	Rhyolite at Brushy Mountain	13	1.2	48.7	25.01	0.04

Table 2 – Summary of sanidine single-crystal laser-fusion analyses.

Overall, the age probability plots display single age populations without large age variations between individual ages. Weighted mean ages ranged from 24.89 ± 0.05 Ma to 27.89 ± 0.06 Ma with MSWDs ranging between 0.12 and 1.95. Of the fourteen samples analyzed, seven ages used all the analyses for the mean age calculation. The remainder of the ages omitted between 1 and 10 analyses because of: low radiogenic yields (MZQ-4, MZQ-17, MZQ-25, 82L-37; Fig. 2K, L, J, and F), young apparent ages due to alteration (MZQ-4), small ^{39}Ar signals (79L-64, MZQ-7, MZQ-17, MZQ-22; Fig. 2 A, I, L, and N), or xenocrystic contamination (82L-37, 78L-183; Fig. 2F and G). Xenocrysts are commonly incorporated from vent walls or during erosion of the ground

surface during ignimbrite outflow sheet emplacement (McIntosh et al., 1990). Analysis of sample 78L-183 indicates one xenocryst with an age of 25.55 ± 0.08. Analysis of sample 82L-37 indicates two xenocrystic populations, one population (n=1) with an age of 25.73 ± 0.08 and second, younger population (n=4) with an age of 25.48 ± 0.12.

A total of 11 single-crystal laser-fusion analyses of the Amalia Tuff yield a mean of age 25.23 ± 0.05 Ma (MSWD = 0.73). This age calculation includes two samples from collect as part of this study (MZQ-4 and TPS04), five reanalyzed samples from Lipman et al., and four analyses from Smith et al. (2002). Ages from Smith et al. (2002) used a FC-2 age of 27.84 Ma and the ages were recalculated for FC-2 equal to 28.02 Ma (Renne et al., 1998). Each of the analyses is plotted as a single point on an age probability diagram (Fig. 4). Amalia Tuff sanidine ages range from 25.13 ± 0.08 to 25.30 ± 0.13 Ma. The new weighted mean age for the Amalia Tuff is in close agreement with the previously published age of 25.26 ± 0.1 Ma (Smith et al., 2002; corrected for FC-2 = 28.02 Ma).

Two analyses of Amalia Tuff sanidine, MZQ-7 and MZQ-25 (Fig. I and J), were excluded from the weighted mean Amalia Tuff age calculation because they are slightly younger than the main population. MZQ-7 is from a non-welded distal facies of the Amalia Tuff outflow sheet, in an isolated outcrop on the western margin of the Rio Grande rift. The unit is variably silicified which may have caused mild hydrothermal alteration of the sanidine, although the crystals appeared pristine in BSE images. Hydrothermal fluids can cause argon loss, which may skew results to younger ages. Sample TPS04 yielded an acceptable Amalia Tuff age of 25.16 ± 0.06. Both samples have similar K/Ca values, suggesting that they are from the same eruption.

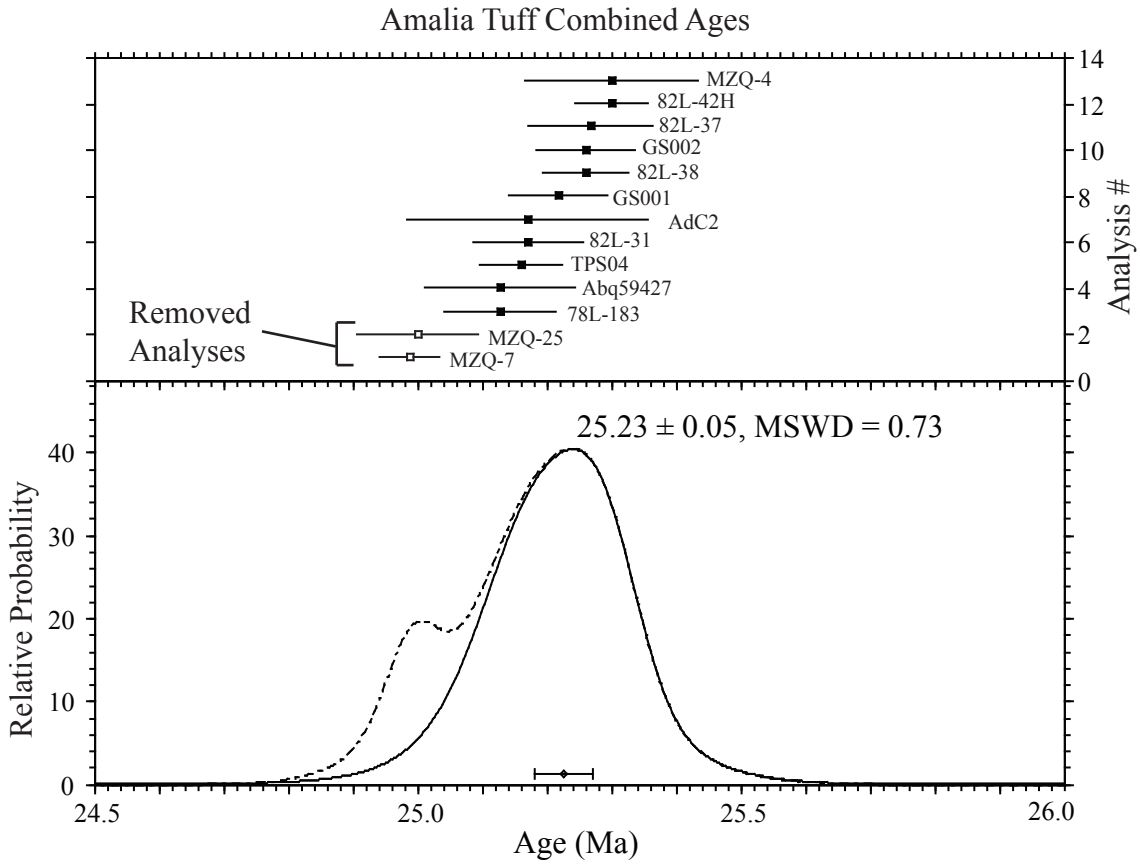

Figure 4 - Ideogram displaying the thirteen ages for the Amalia tuff. Two points were removed from the mean age calculation, see the text for an explanation. Samples Abq59427, AdC2, GS001, and GS002 are sanidine single-crytal laser-fusion analyses from Smith et al., 2002.

Analysis of MZQ-25 sanidine yielded an age 25.00 ± 0.09 (MSWD = 0.55). The sample is what has been mapped as a cogenetic lava or rheomorphic flow of the Amalia Tuff. The results of MZQ-25 appear robust and there is no evidence of alteration, which might have caused argon loss. The interpretation of this rhyolite as rheomorphic flow of the Amalia Tuff may be incorrect. On the geologic map of Lipman and Reed (1989), the outcrop pattern near the sample location could suggest a crude outline of a rhyolitic dome. At the hand-sample scale, the sample displays viscous deformation and flow banding and contained a lower percentage of crystals than typical Amalia Tuff samples (~1 versus >5%, respectively). K/Ca values of MZQ-25 vary from 35 to 104 and are markedly different than the typical values of 50-60 for most of the other Amalia Tuff analyses. The likelihood that the sampled unit is not actually the Amalia Tuff is one that should be investigated more closely. Sample 78L-183, rheomorphic flow of the Amalia Tuff from another part of the field, yields an age of 25.13 ± 0.08 Ma (MSWD = 1.53), indicating that the interpretation that this rhyolite is a rheomorphic phase of the Amalia Tuff is indeed correct.

Two discrepancies exist between the ages of MZQ samples and ages of reanalyzed samples from Lipman et al. For replicate analyses of the rhyolite of Cordova Creek (MZQ-26 and 83L-8, 25.27 ± 0.06 and 25.40 ± 0.04 Ma respectively) (Fig. 2M and B) and the rhyolite at Comanche Point (MZQ-22 and 79L-64, 24.89 ± 0.05 and 25.10 ± 0.04 Ma respectively) (Fig 2M and A), the MZQ samples are younger than their equivalent Lipman et al. samples. Radiogenic yields are > 95% for the all samples indicating that younger ages observed for the MZQ analyses are not the result of radiogenic argon loss. Because 5-20 grains were analyzed for the Lipman et al. samples,

incorporation of xenocrystic grains is a possibility that could skew results to older ages. The small size of the Lipman et al. crystals may have prevented identification of xenocrystic grain during handpicking. If xenocrysts are the reason the Lipman et al. samples are older, the similar K/Ca values of all analyses suggest the xenocyrsts are compositionally indistinguishable or xenocrysts represent a small percentage of crystals analyzed. Because multiple crystals were analyzed together for the Lipman et al. sample, the preferred age for the rhyolites of Costilla Creek and Comanche Point is calculated from the MZQ analyses.

Biotite, Hornblende, and Groundmass analyses

Biotite, hornblende, and groundmass age spectra are shown in figure 5 (A-Q) and the ages are compiled in table 3. Complete analytical results are in table 2 of Appendix B. A total of fifteen biotite samples, one volcanic and fourteen plutonic, were step-heated. Biotites from volcanic rocks were analyzed to determine and eruption age. Alternatively, biotite ages from plutonic rocks indicate timing at which the pluton was 350-300°C. Ages were determined using the integrated or plateau age. A plateau is here defined as three contiguous steps that comprise 50% or more of the $^{39}Ar_K$ released and have ages overlapping within two-sigma error (Fleck et al., 1977).

In addition to age spectra plots, K/Ca and radiogenic yield auxiliary plots are included. K/Ca values during the analyses are similar for all the samples. Initial values are ~100 and values decrease throughout the analysis. This trend is common in biotites and records the progressive degassing of high Ca apatite inclusions at higher temperatures (Lo and Onstott, 1989). BSE microprobe images of biotite confirm the

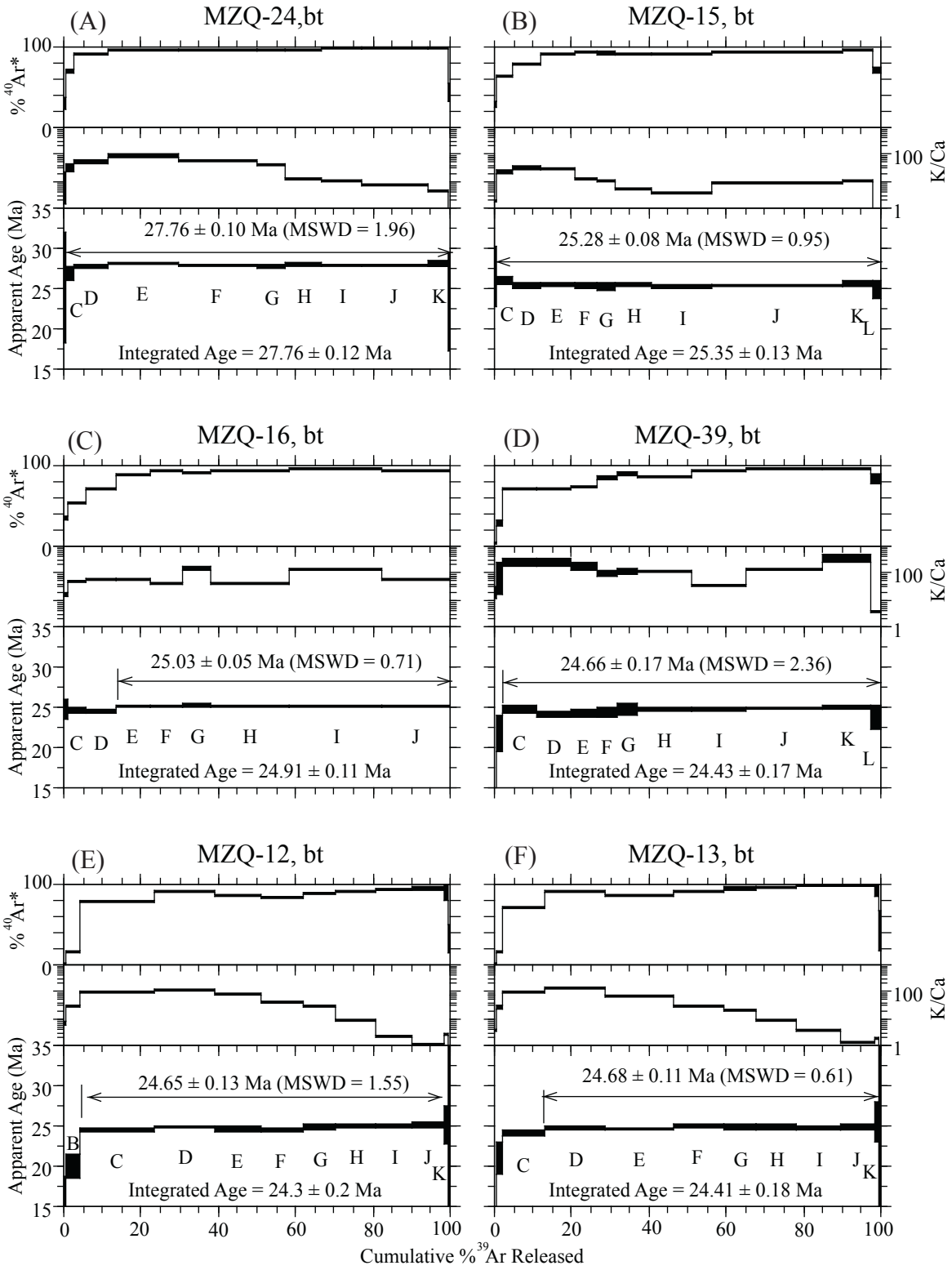

Figure 5- Age spectra and auxiliary plots for biotite (bt), hornblende (hbl), and ground-mass concentrate (gmc). All errors are reported at 2 sigma.

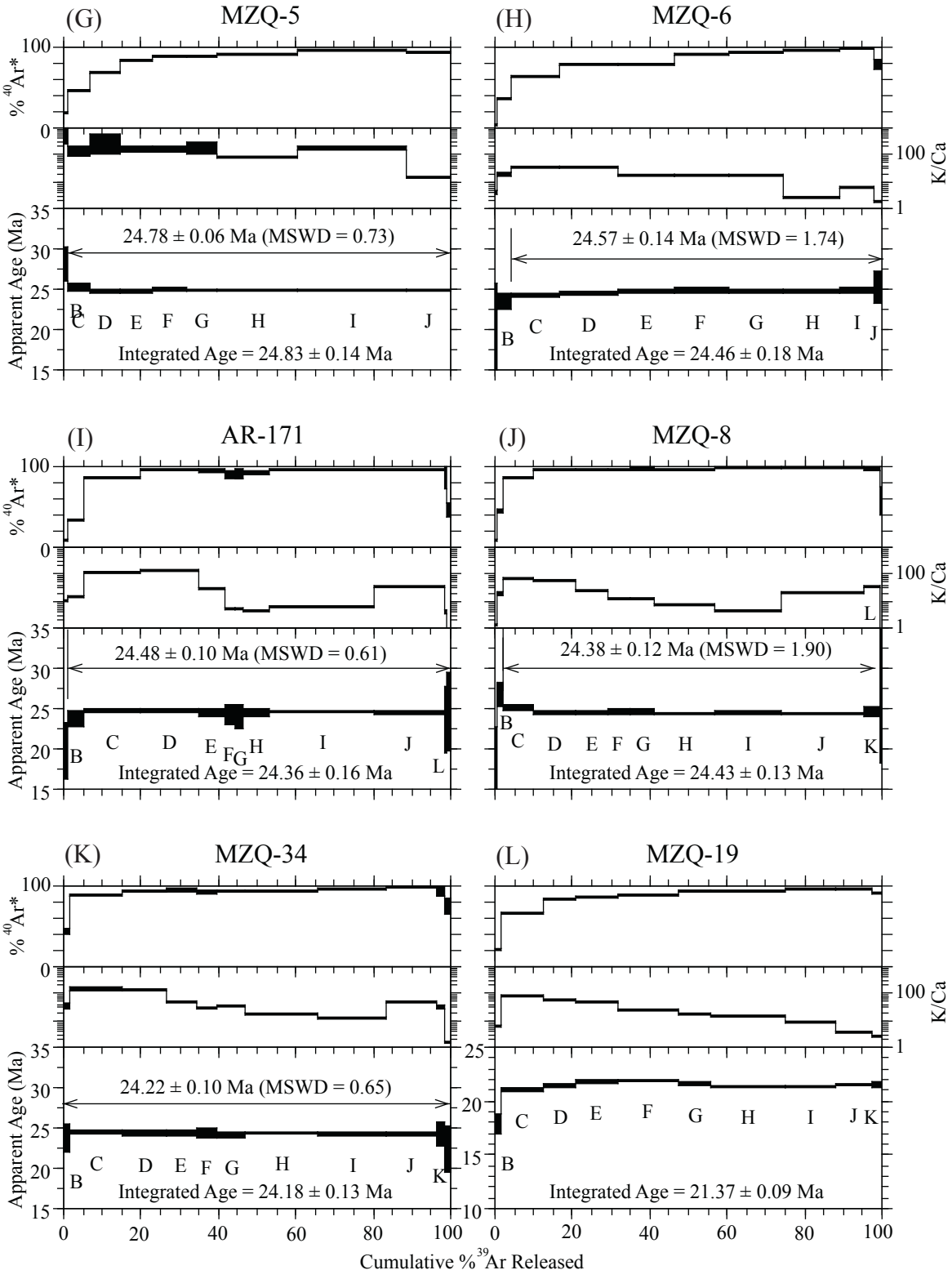

Figure 5 continued

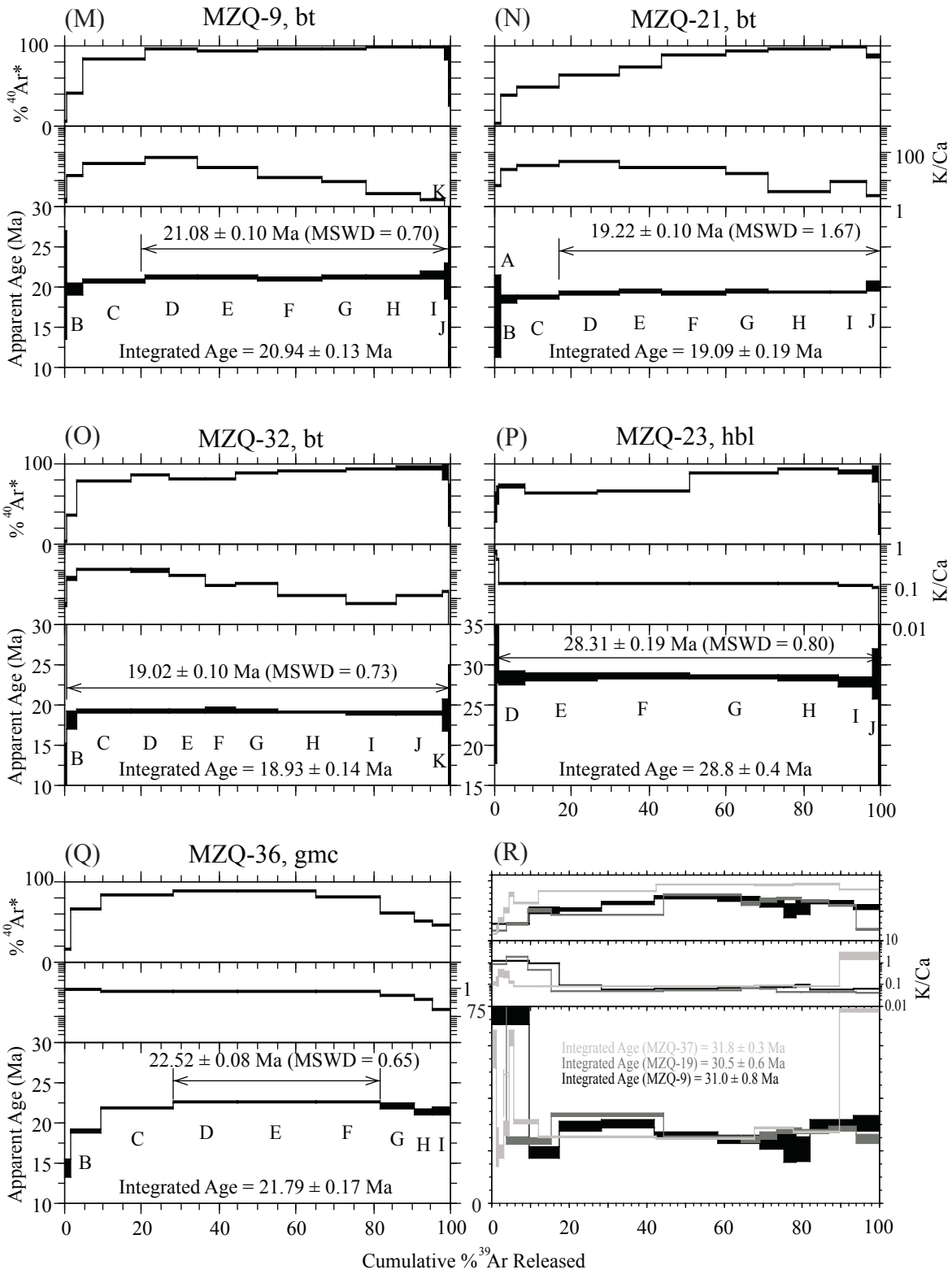

Figure 5 continued

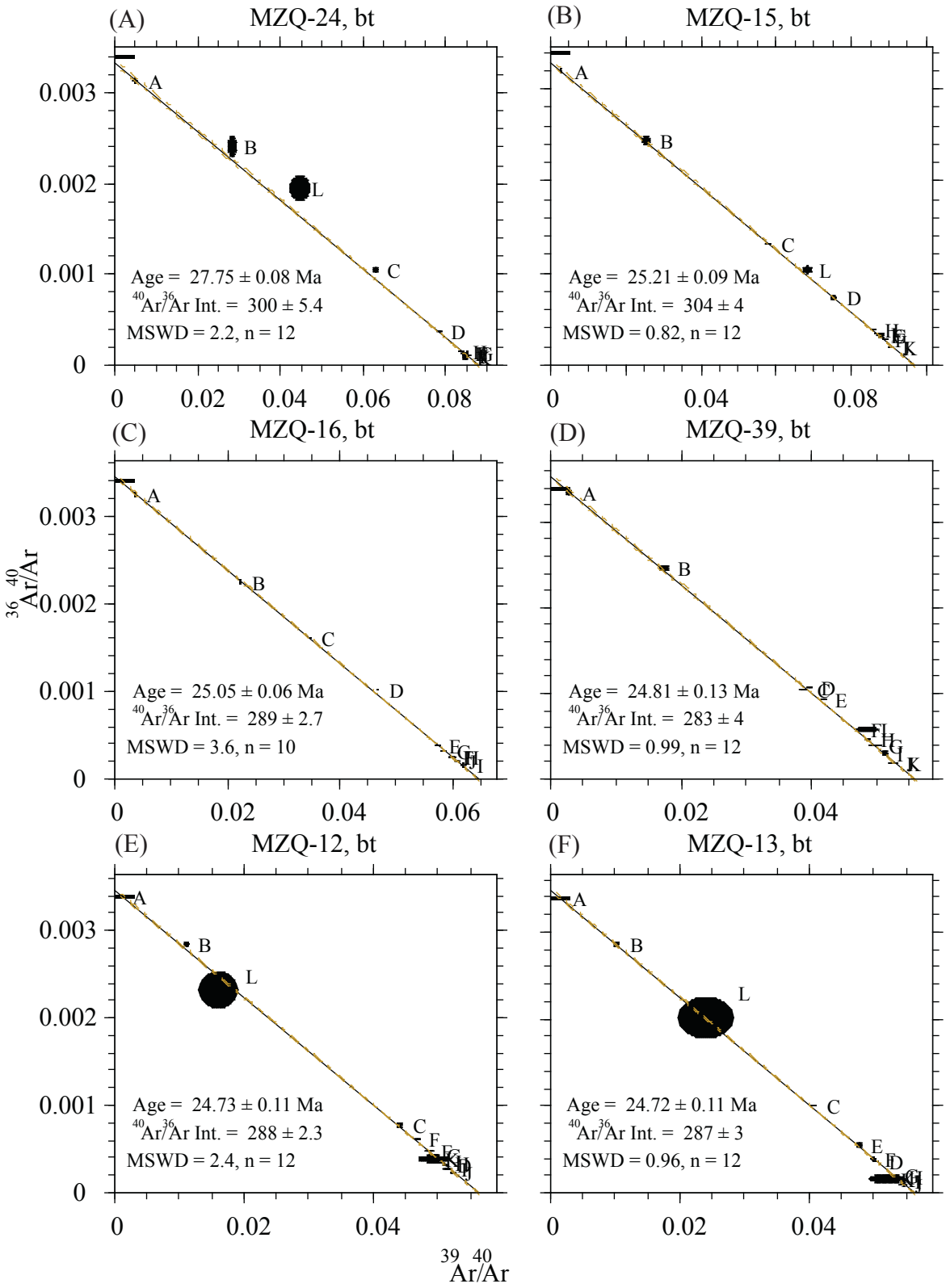

Figure 6 - Inverse isochron plots for biotite (A-O), hornblende (P), and groundmass concentrate (Q) mineral separates. All errors are reported at two sigma. The line on the y-axis is the reciprocal 40/36 value of air (295.5)

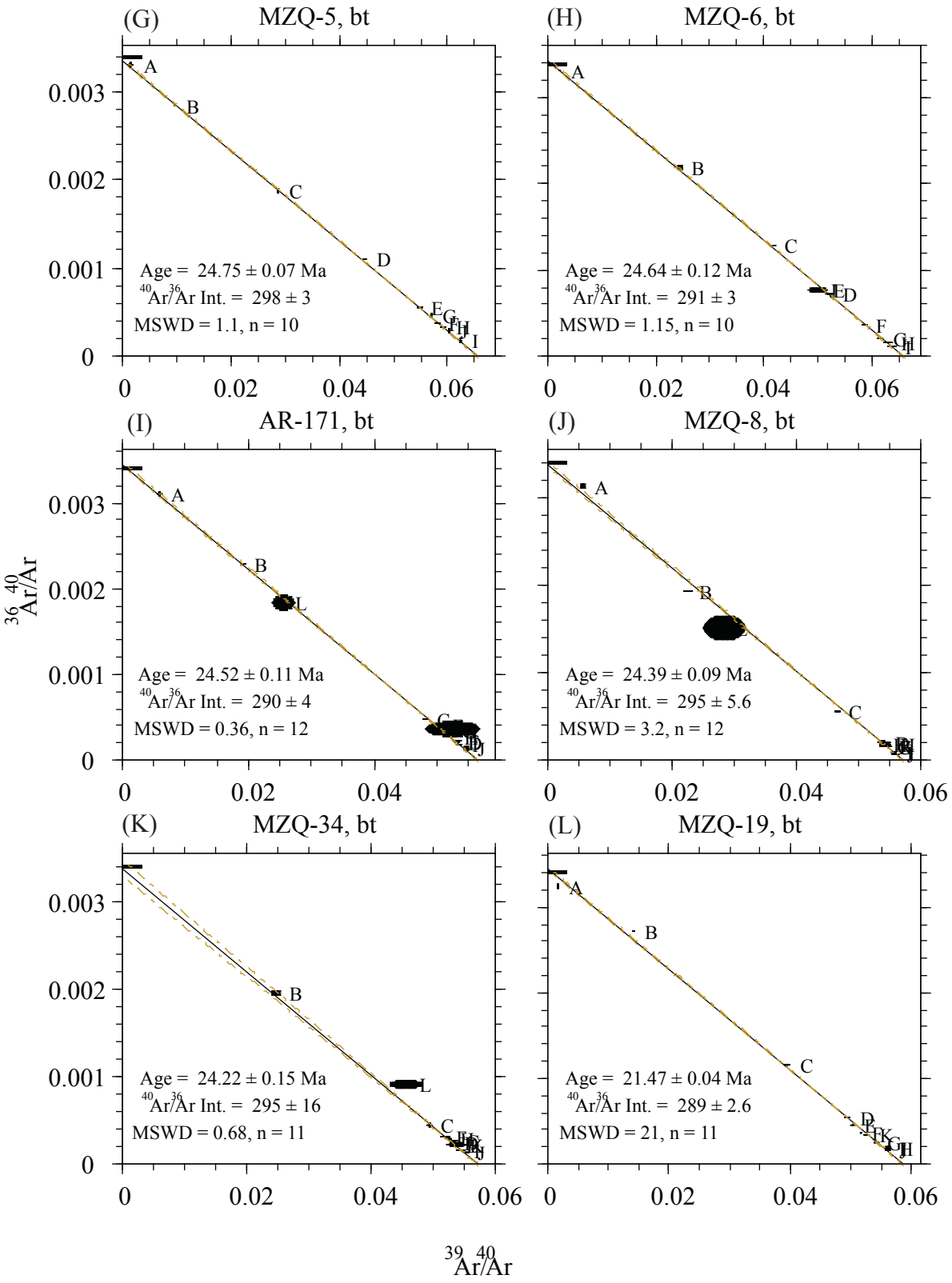

Figure 6 continued.

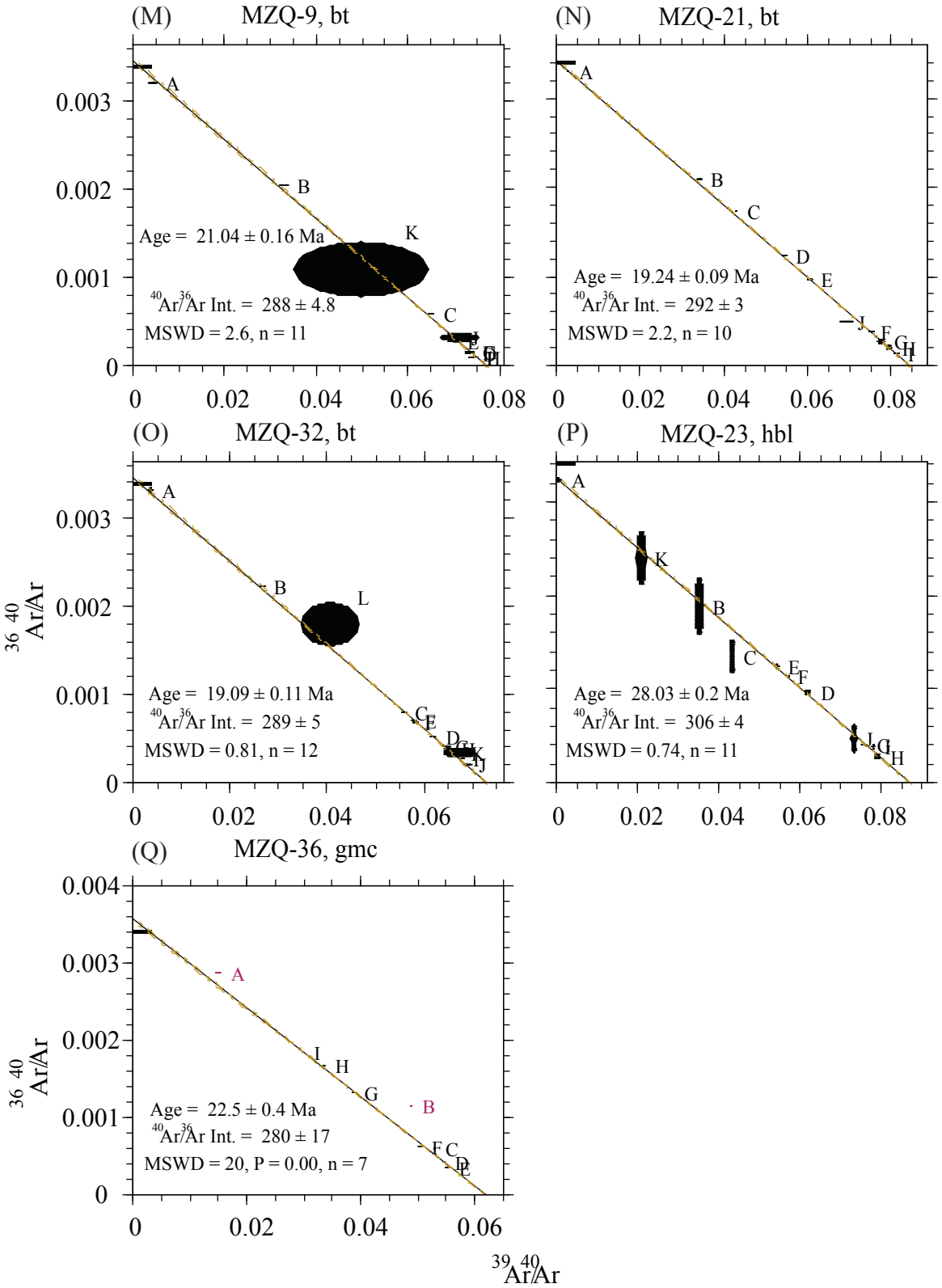

Figure 6 continued.

presence of apatite inclusions (Fig. 7). Radiogenic yields are initially 25% and in all samples increase to values nearing 100% during the analysis. The initially low $^{40}Ar^*$ values are due to atmospheric argon degassing at low temperatures. The combination of high radiogenic yields and 8-10 wt% K_2O obtained from the electron microprobe indicate pristine, unaltered biotites. Though inverse isochron plots (Fig. 6) for the biotite, hornblende, and groundmass samples do not all have $^{40}Ar/^{36}Ar$ intercepts of 295.5 within 2σ error, the ages determined from the inverse isochron are within 2σ error of the age calculated from the age spectrum. This indicates that if excess argon is present, the effect on sample age is minimal.

In general, biotite age spectra are uncomplicated and ages were determined by the plateau age. For the spectra with a plateau, plateaus comprise between ~80% to 97% of the ^{39}Ar released. Of these spectra, the first one or two steps were anomalously older or younger, have large errors, and low radiogenic yields. Degassing atmospheric argon on the grain surface at low temperature would result in the imprecise ages. Small amounts of excess argon or alteration at the grains surface would produce old or young ages, respectively. The small percentage of the total ^{39}Ar released associated with fusion step indicates complete ^{39}Ar degassing of the biotite separates. Plateau ages had 2σ errors between ± 0.05 and ± 0.16, averaging ± 0.10, and MSWDs ranging from 0.56 to 1.75, averaging 0.95. The small percent error and the MSWD values near unity imply a single population of ages for each analysis.

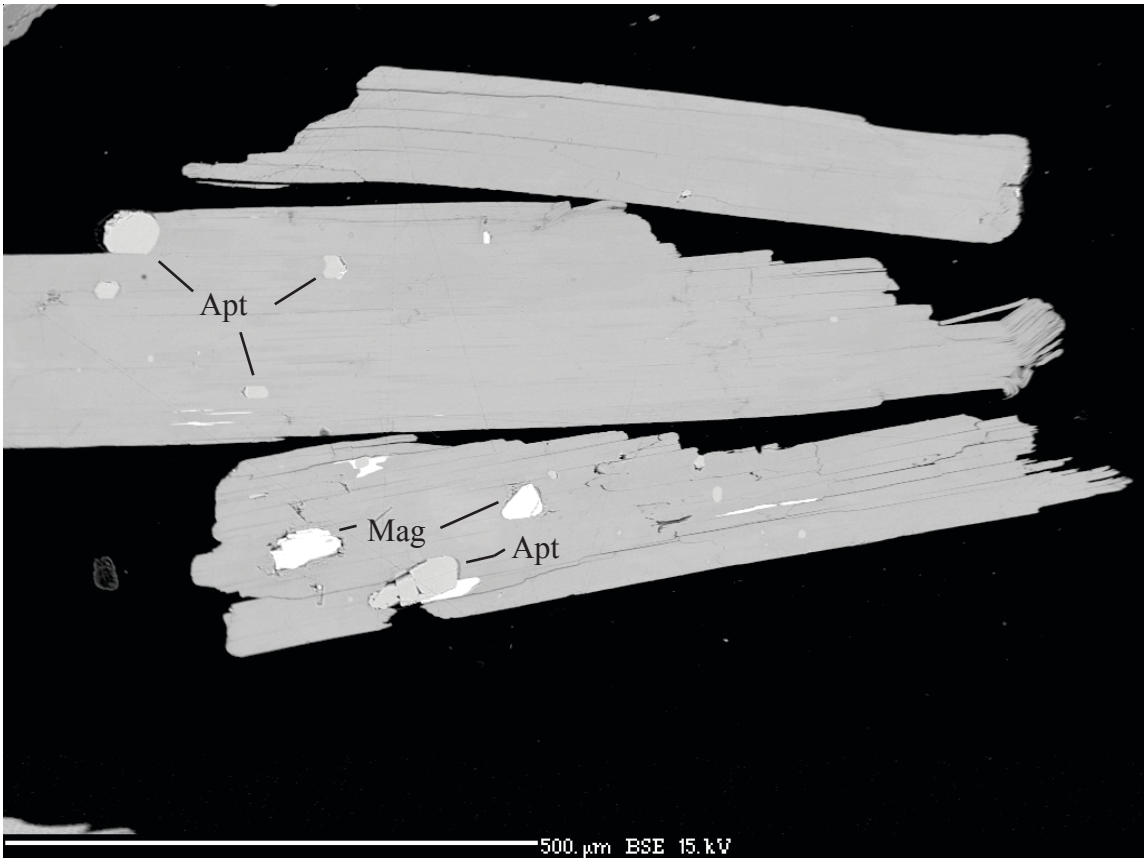

Figure 7 – Backscatter electron microprobe image of MZQ-21 biotite crystals. The top crystal has no inclusions, the middle crystal has apatite (apt) inclusions, and the bottom crystal has both apatite and magnetite (mag) inclusions. The high-Ca apatite inclusions degas at high temperatures and decrease the K/Ca values at the end of the analysis. Apatite inclusions were observed in all biotite separates. The scale is located at the bottom.

Sample	Unit	mineral	n	$\%^{39}Ar$	MSWD	K/Ca	Age(Ma)	2s
MZQ-24	Precaldera quartz latite	bt	10	99.4	2.0	37.8	27.77	0.10
MZQ-15	Canada Pinabete	bt	11	99.8	1.0	11.1	25.28	0.08
MZQ-16	Rito del Medio	bt	6	86.2	0.7	76.3	25.03	0.05
MZQ-39	Rito del Medio	bt	10	97.8	2.4	155.7	24.66	0.17
MZQ-12	Cabresto Lake	bt	10	95.6	1.6	54.4	24.65	0.13
MZQ-13	Cabresto Lake	bt	9	86.8	0.6	45.5	24.68	0.11
MZQ-5	Red River	bt	8	98.5	0.7	142.5	24.78	0.06
MZQ-6	Sulfur Gulch	bt	8	95.7	1.7	17.8	24.57	0.14
AR-171	Sulfur Gulch	bt	11	98.7	0.6	46.7	24.48	0.10
MZQ-8	Bear Canyon	bt	10	97.6	1.9	23.1	24.38	0.12
MZQ-34	Bear Canyon	bt	11	100.0	0.7	51.6	24.22	0.10
MZQ-19	Rio Hondo	bt	0	0.0	0.0	0.0	0.00	0.00
MZQ-9	Rio Hondo	bt	8	78.7	0.7	19.7	21.08	0.10
MZQ-21	Lucero Peak	bt	7	83.2	1.7	21.7	19.22	0.10
MZQ-32	Lucero Peak	bt	11	99.4	0.7	42.8	19.02	0.10
MZQ-23	Precaldera andesite	hbl	10	99.6	0.8	0.1	28.31	0.19
MZQ-36	Brushy Mountain Andesite	gmc	3	53.8	0.7	0.9	22.52	0.08

Table 3 – Summary of biotite, hornblende, and groundmass samples.

MZQ-19 is the only biotite analysis that did not yield a plateau. Ages of the first several steps are ~17 Ma, then they increase to 22 Ma, then decreased to 21 Ma and finally increase 22 Ma. Overall, the ^{39}Ar release profile crudely outlines a hump during the analysis. Lo and Onstott concluded that geologically meaningful ages could be obtained from disturbed biotite spectra using the total gas age. During irradiation, neutrons interacting with ^{39}K atoms can recoil the newly formed ^{39}Ar atoms into the adjacent chloritized layers or in severe cases of alteration completely eject ^{39}Ar from the biotite grains. For MZQ-19, wt% K_2O is 8.67 and 9.45 calculated from the argon and microprobe analysis, respectively. Because both values are well within the expected range of pristine biotite, alteration, if present, is in negligible amounts. The preferred age is 21.37 ± 0.09 Ma, calculated from the total gas released.

Only one of the four hornblende analyses yielded statistically robust results. The plateau for the MZQ-23 analysis is comprised of steps D through J corresponding to ~98% of the spectrum. K/Ca values of 0.1 and radiogenic yields approaching 100% are typical of pristine hornblendes. The age of 28.31 ± 0.09 (MSWD = 0.80) from the hornblende bearing andesite is interpreted as an accurate eruption age.

MZQ-9, MZQ-19, and MZQ-37 hornblende age spectra displayed extreme discordance between steps throughout the spectra (Fig. 5R). The age spectra, though disturbed, are remarkably similar to each other. The overall "saddle" shape of the age spectra is common to samples containing excess ^{40}Ar. Inverse isochrons for the analyses do not display clear trends, so if excess ^{40}Ar is responsible for spectra discordance, it is not homogeneous. The most likely probability for the cause of scatter in the age spectra is small amounts of chloritic alteration, coupled with excess ^{40}Ar and ^{39}Ar recoil.

Analysis of a groundmass separate from a precaldera andesite on Brushy Mountain yielded an age of 22.52 ± 0.08 (MSWD = 0.65). The initial 30% of the $^{39}Ar_K$ released (steps A-C) displays a monotonic increase in ages, from 14.2 to 21.72 Ma, a plateau from steps D-F with an age of 22.52 ± 0.08 (MSWD = 0.65), and the remaining 20% of the spectrum decreases in age to 21.4 ± 0.4 Ma. Argon loss is the most likely explanation for the initial age gradient within the sample. Though the last three steps display decreasing ages, the addition of those steps to the age calculation only changes the plateau age from 22.52 ± 0.08 to 22.4 ± 0.3 Ma.

K-feldspar age spectra and MDD cooling histories

Eighteen plutonic K-feldspars were step-heated to determine the 300-150ºC cooling history of the plutons. Additionally, eleven of these K-feldspars were modeled using MDD thermal modeling method of Lovera et al., (1989, 1991). Age spectra, inverse isochron and results of MDD thermal modeling can be found in figures 8-11. A summary of results is in table 4 with complete analytical data in table 3 in Appendix B. Supplementary MDD plots are in Appendix C. The MDD thermal modeling method of K-feldspar $^{40}Ar/^{39}Ar$ analyses is within Appendix RD2 of Sanders et al., (2006).

Sample	Unit	Analysis	n	$\%^{39}Ar$	MSWD	K/Ca	Age(Ma)	2s
MZQ-1	Virgin Canyon	TGA	0	0.0	0.0	0.0	29.53	0.24
MZQ-2	Virgin Canyon	plateau	8	74.6	1.0	126.6	26.50	0.09
MZQ-38	Virgin Canyon	plateau	10	76.0	1.9	422.3	25.78	0.07
MZQ-15	Canada Pinabete	TGA	0	0.0	0.0	0.0	29.19	0.27
MZQ-16	Rito del Medio	plateau	9	53.7	2.0	32.9	25.06	0.15
MZQ-39	Rito del Medio	Plateau	17	58.5	1.8	59.8	24.65	0.08
MZQ-12	Cabresto Lake	isochron	4	52.4	2.8	48.2	24.68	0.09
MZQ-13	Cabresto Lake	plateau	10		2.9	40.0	25.51	0.33
MZQ-5	Red River	TGA	0	0.0	0.0	0.0	24.36	0.21
MZQ-6	Sulfur Gulch	plateau	6	69.1	2.1	74.9	26.50	0.12
MZQ-8	Bear Canyon	plateau	6	57.2	3.1	80.0	23.56	0.18
MZQ-34	Bear Canyon	plateau	12	51.3	2.1	84.1	22.21	0.11
MZQ-9	Rio Hondo	TGA	0	0.0	0.0	0.0	21.73	0.12
MZQ-33	Rio Hondo	TGA	0	0.0	0.0	0.0	21.96	0.13
MZQ-10	Rio Hondo Dike	plateau	21	81.2	1.2	175.8	16.50	0.16
MZQ-19	Rio Hondo	plateau	0	0.0	0.0	0.0	21.27	0.08
MZQ-21	Lucero Peak	TGA	0	0.0	0.0	0.0	18.59	0.11
MZQ-32	Lucero Peak	TGA	0	0.0	0.0	0.0	19.27	0.09

Table 4 – Summary of K-feldspar analyses. If the analysis did not yield a plateau, the integrated or total gas age (TGA) is reported. One sample, MZQ-12 contained excess argon, so inverse isochron age is reported. "n" corresponds to the number of steps used for the age calculation.

Radiogenic yields for the analyzed samples have similar trends. Radiogenic yields begin at approximately 50%, climb to values nearing 90-100%, then decrease to

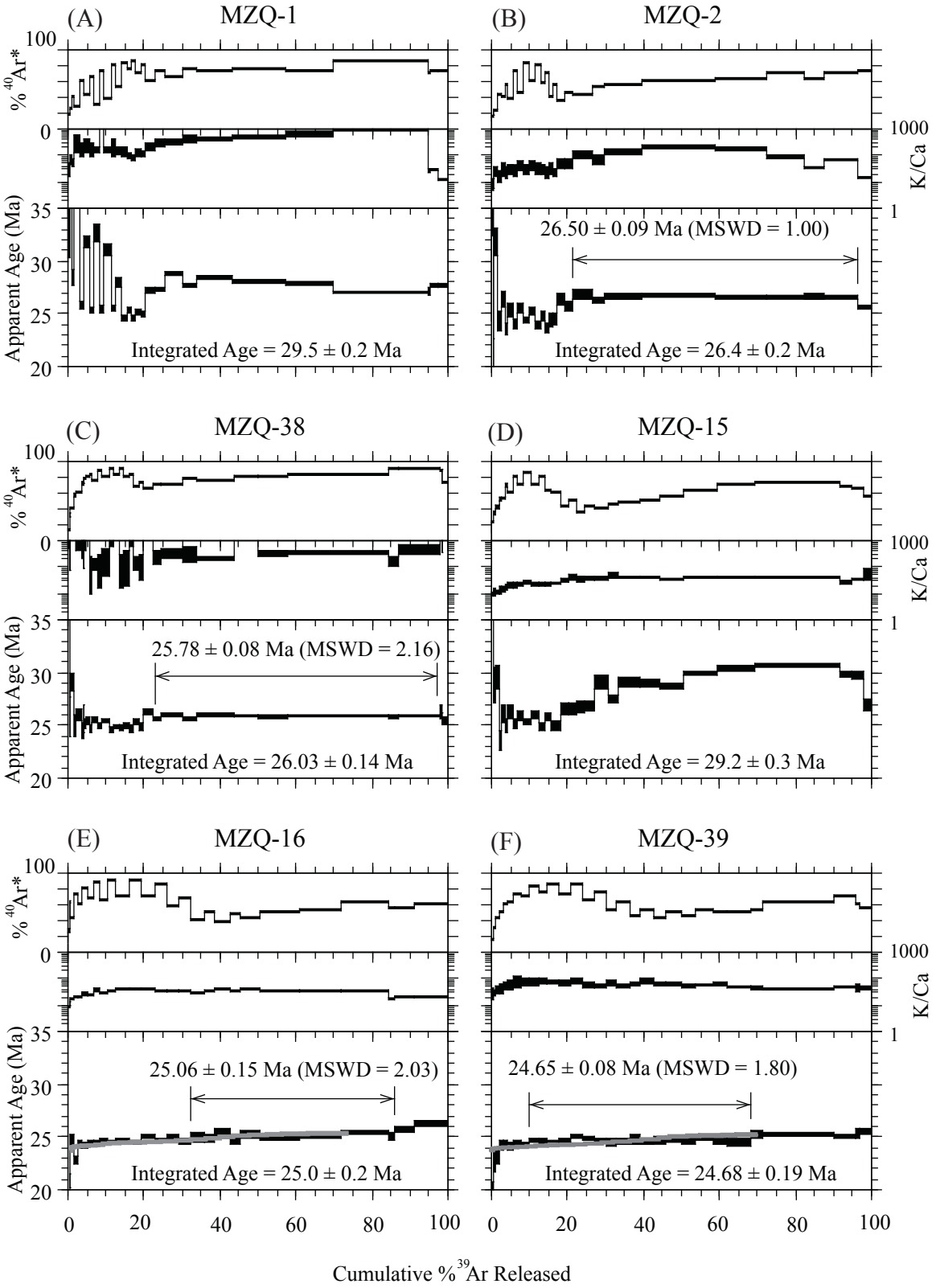

Figure 8 - K-feldspar age spectra along with K/Ca and radiogenic yield auxiliary plots. All errors are reported at two sigma. Modeled age spectra used to model MDD cooling histories are shown in gray.

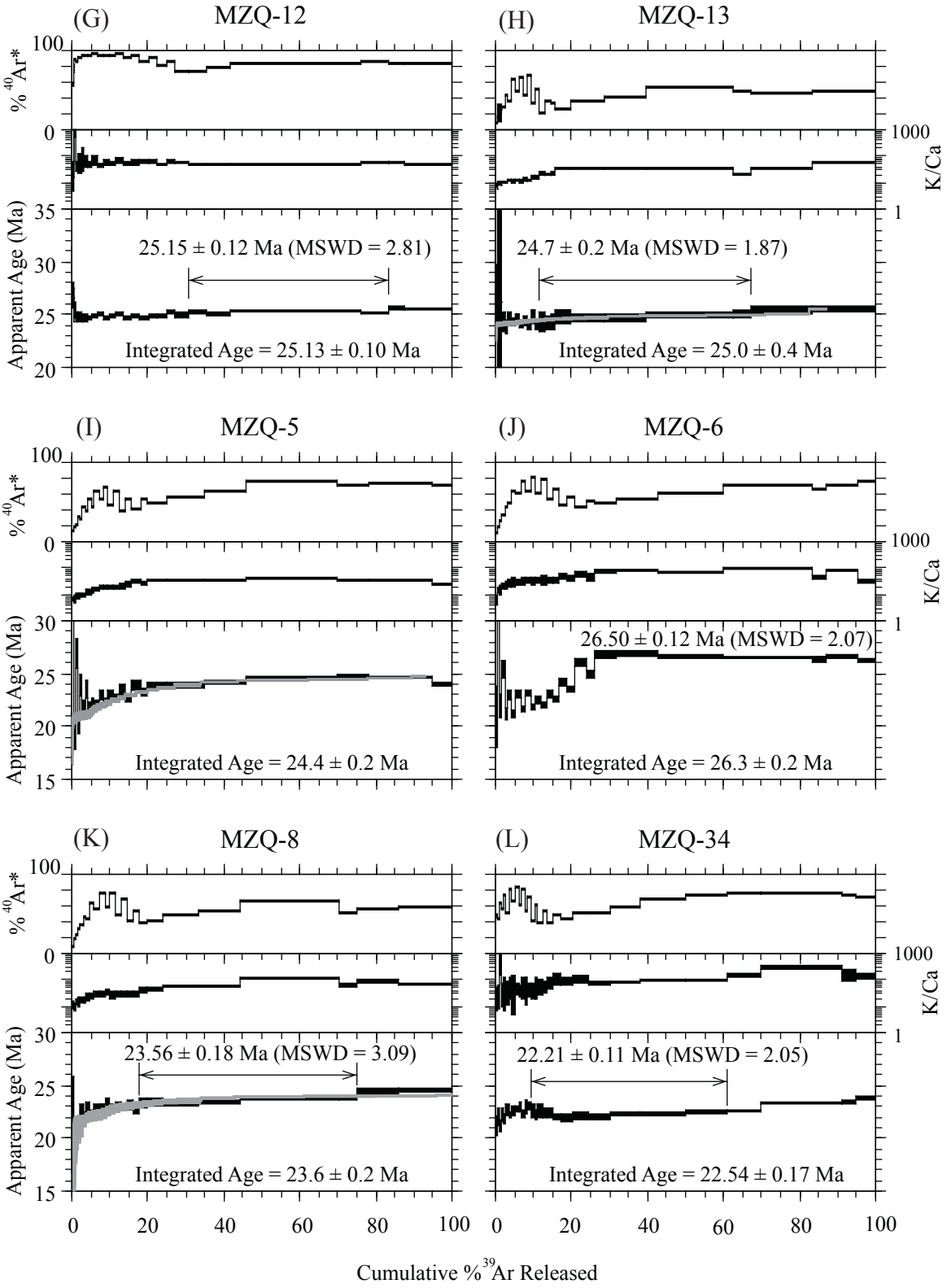

Figure 8 continued

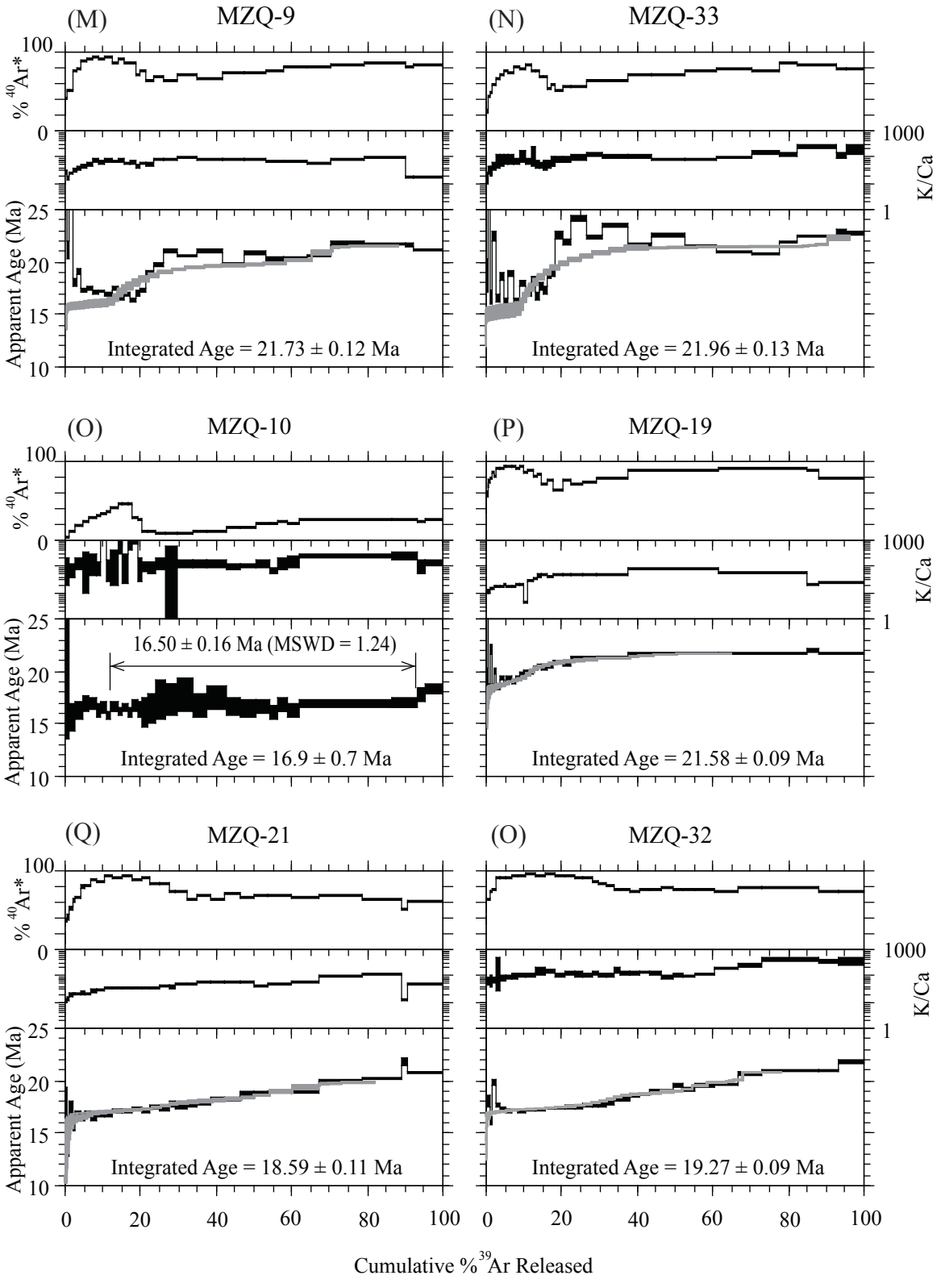

Figure 8 continued

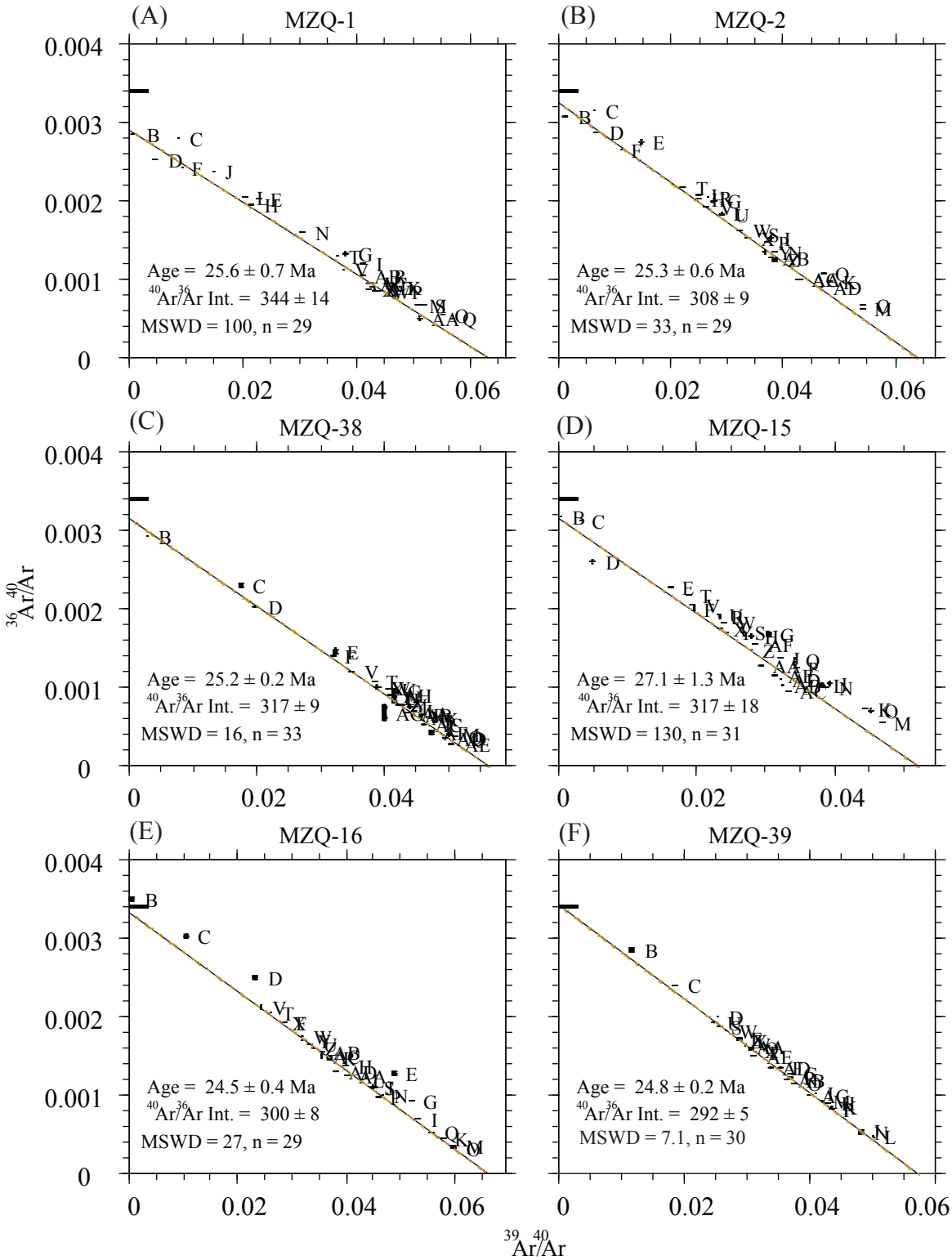

Figure 9 - Inverse isochron plots of the plutonic K-feldspar analyses. All errors are reported at two sigma. Line on the y-axis is the reciprocal 40/36 value of air (295.5).

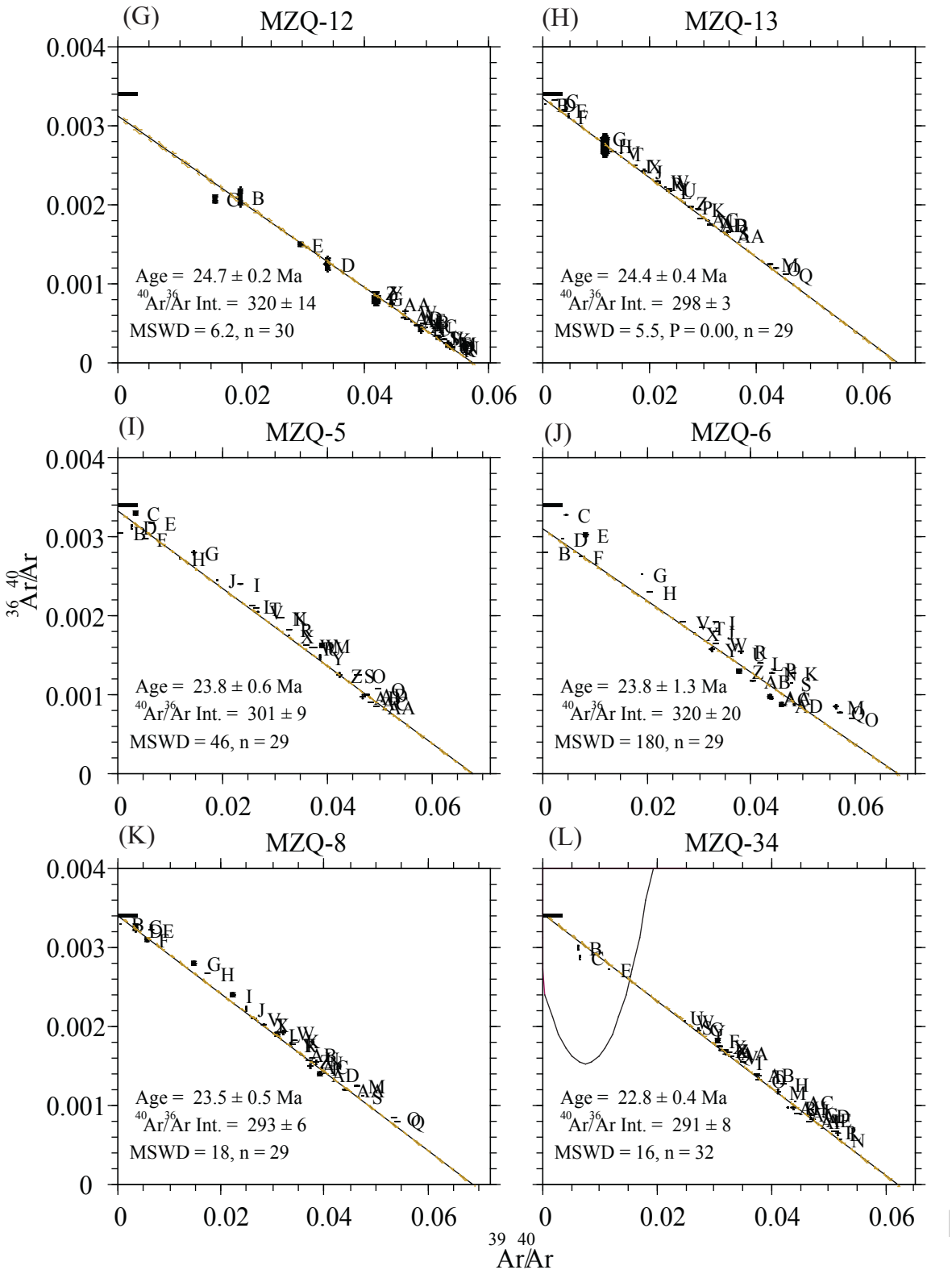

Figure 9 continued

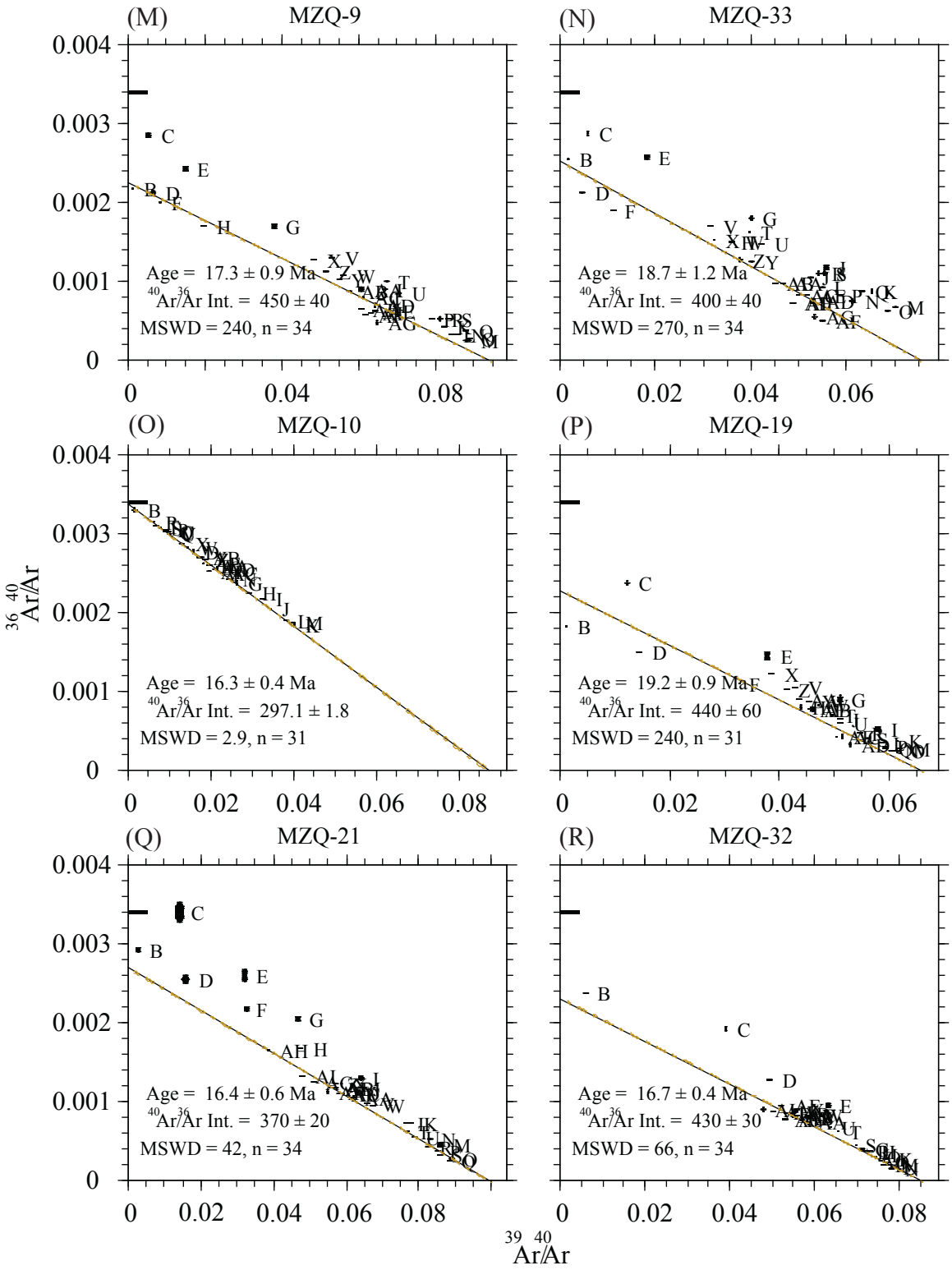

Figure 9 continued

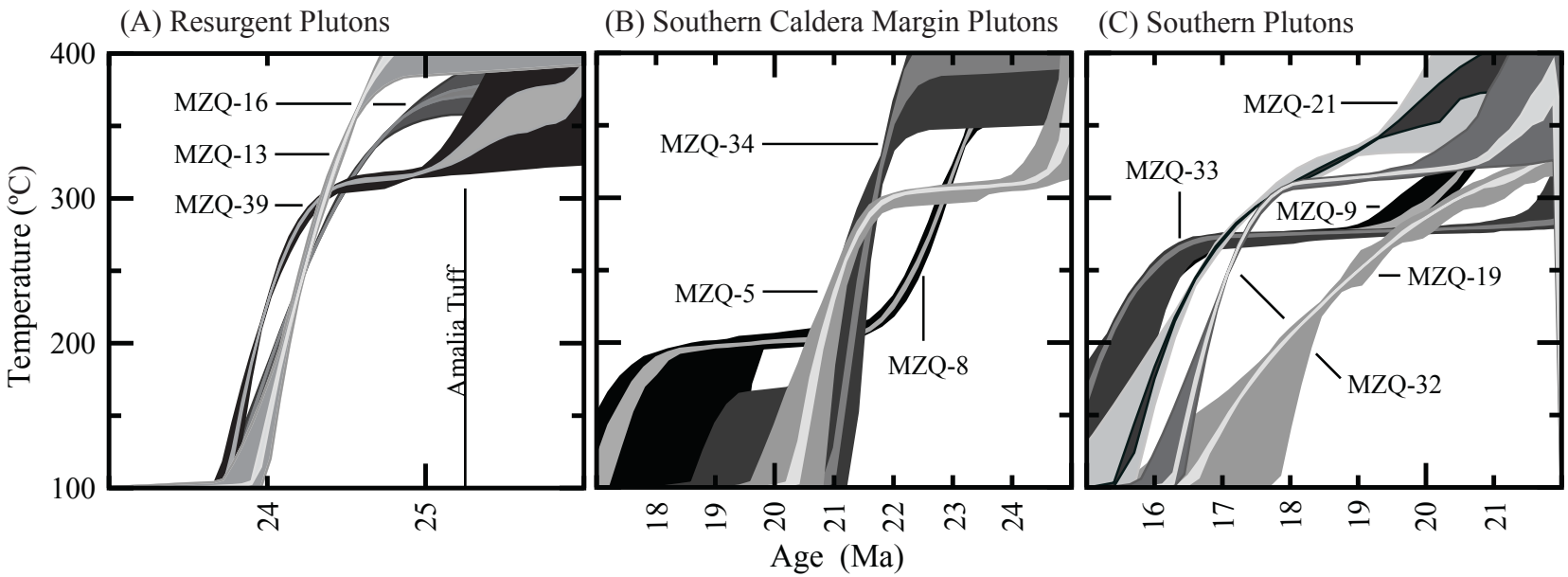

Figure 10 - Monotonic cooling histories from the exposed plutons of the Latir Volcanic Field. The ages on the x-axis change for the three subdivisions of plutons. A temperature range of 400 to 100 ºC is given, though the K-feldspars are only accurate between ~300 and 150 ºC. A) Resurgent plutons. MZQ-16 and 39 are from Rito del Medio and MZQ-13 is from Cabresto Lake. The line labeled Amalia tuff corresponds the age reported in this study of 25.23 ± 0.05 Ma. B) Southern caldera margin plutons. MZQ-8 and 34 correspond to the Bear Canyon pluton and MZQ-5 is from the Red River pluton. C) Southern plutons. MZQ-9, 19, and 33 are from the Rio Hondo pluton and MZQ-21 and 32 are from Lucero Peak. MZQ-9 and 33 follow the same cooling trend from 19 to 15 Ma and the cooling history of MZQ-9 is covered by that of MZQ-33.

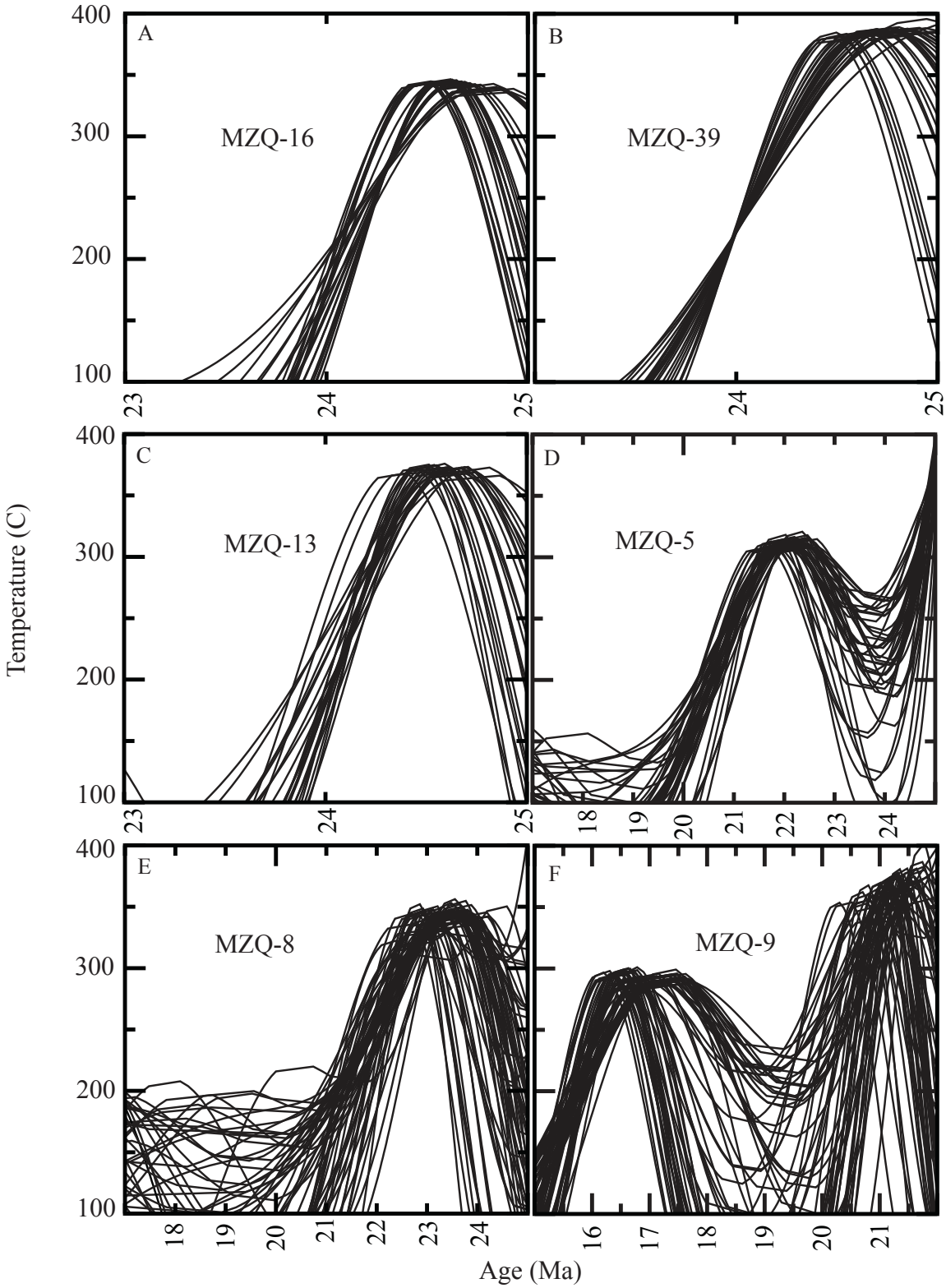

Figure 11 (A-J) – MDD unconstrained cooling models for plutonic K-feldspar. Note the scale along the x-axis changes amongst samples.

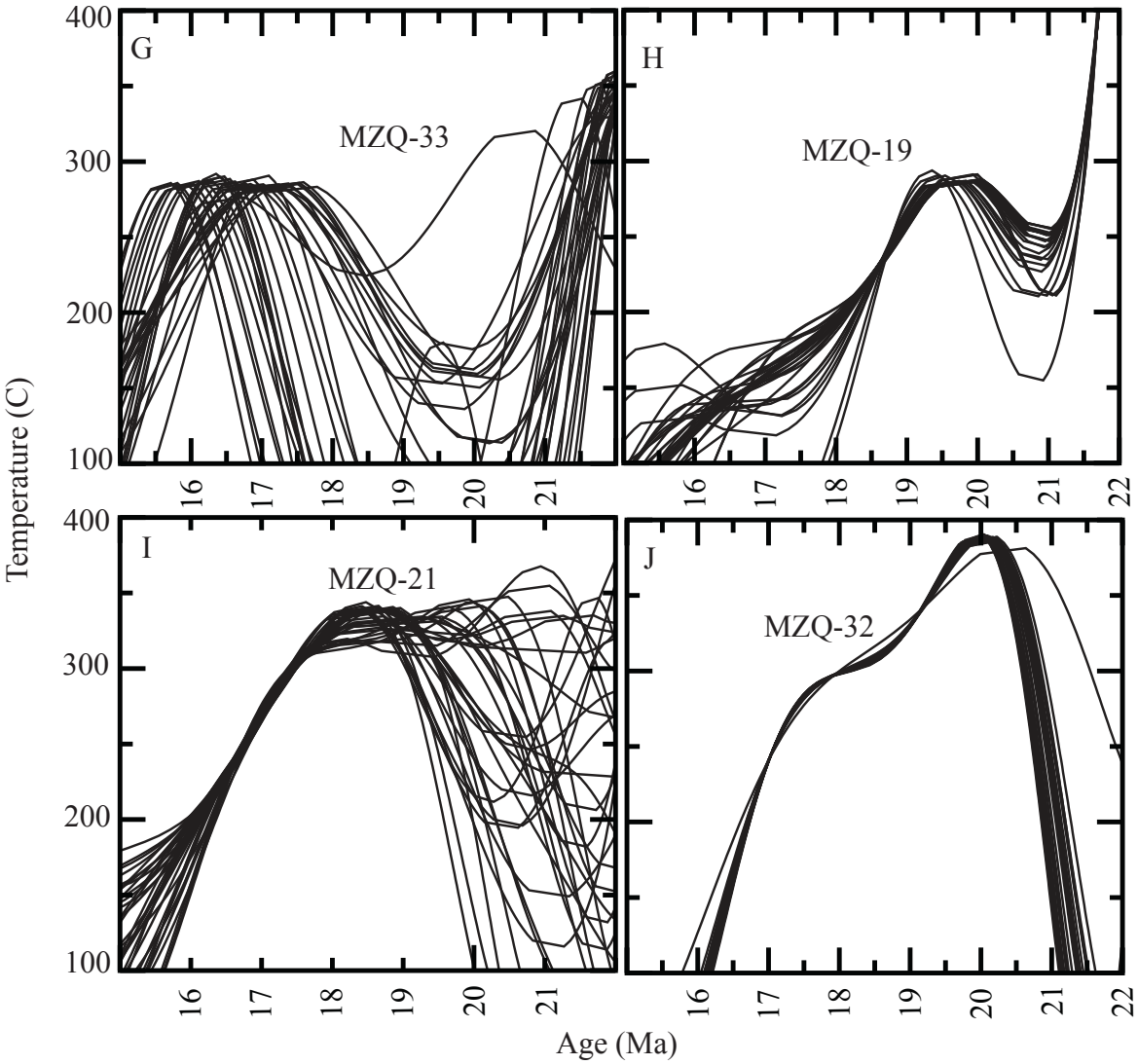

Figure 11 continued.

values of 40-60% $^{40}Ar^{*}$ all within the initial 10-30% ^{39}Ar released. Following this initial peak, radiogenic yields steadily increase, ending in values of 90-100%. In the most extreme examples, radiogenic yields began at 5-10% and never exceed 50% radiogenic (e.g. MZQ-10). The saw-tooth oscillation observed in the radiogenic yield, as well as the K/Ca in some samples, is interpreted to be the result of the isothermal duplicate step heating. The first step decrepitates fluid inclusions, which host excess argon and potassium rich fluids. The second duplicate step is more characteristic of degassing from K-feldspar crystal. The reason radiogenic yields of most samples are so low is not completely understood. Fluid inclusions are known to host excess argon and perhaps pluton emplacement into a shallow crustal environment incorporates a large amount of atmospheric argon into the fluid inclusions as well.

K/Ca trends are variable from sample to sample. Some K/Ca trends are constant throughout the analysis, others are vastly discordant (e.g. MZQ-10), and others have initial increasing gradients and that become constant. Weight percent K_2O determined from the $^{40}Ar/^{39}Ar$ analyses is variable among samples, ranging from 8.86 to 15.74. Interestingly, the initial peak in radiogenic yields correlates with the increasing gradient of the K/Ca auxiliary plot. Furthermore, once the K/Ca trend becomes constant, the radiogenic yields increase to 100%. This suggests that the same phenomenon controlling the trends in radiogenic yields is also controlling K/Ca trends. Electron microprobe BSE images show that all K-feldspar samples display perthitic microtextures, which are common in plutonic K-feldspars.

Overall, the age spectra display a variety of complexities, resulting from excess argon and moderate (~ 1 Ma) to long (1-5 Ma) cooling histories. Results of K-feldspar

age spectra will be discussed in terms of the resurgent, southern caldera margin, or southern plutons, because K-feldspar analyses from each these three groups display similarities in age and thermal histories. Though some age spectra are discordant and are not geological meaningful, the age spectra are briefly discussed.

K-feldspar age spectra from the resurgent plutons display evidence for rapid cooling or are discordant due to alteration and/or excess argon. Of the seven dated samples, four age spectra, all from the Virgin Canyon and Canada Pinabete plutons (MZQ-1, 2, 15, and 38; Fig. 8A, B, D, and C), yielded geologically meaningless results. Both analyses from the metaluminous phases of the Virgin Canyon pluton (MZQ 2 and 38) have plateaus significantly older than the age of the caldera, 25.23 ± 0.05 Ma. The oscillation of the steps observed in the initial 20-30% of the spectrum is because of the isothermal duplicate step heating. All cooling histories were modeled using the second of the isothermal duplicate steps to avoid erroneous results. Samples analyzed from the peralkaline region of the Virgin Canyon and Canada Pinabete (MZQ-1 and MZQ-15, respectively) did not yield plateaus and the majority of the steps are also older than the Amalia Tuff.

Inverse isochron plots for these four samples (Fig. 9A – D) are discordant and individual steps do not plot along a trend, indicated by the elevated MSWD values. The first of the isothermal duplicate steps plot to the left and below of the second corresponding isothermal duplicate step on an inverse isochron, confirming the presence of excess argon. K-feldspar analyses of MZQ-2 and 38 (Fig. 9 B and C) have the lowest MSWD values (33 and 16, respectively), $^{40}Ar/^{36}Ar$ intercepts indicative of slight excess argon contamination, and isochron ages within error of the age of the Amalia Tuff. The

anomalously old ages observed in K-feldspar age spectra, typically from gas released at higher temperature, is interpreted to be due to excess argon trapped within the largest domains upon cooling (Foster et al., 1990). Because of the elevated MSWD values, the isochron ages of the two samples should not be used alone in constructing the plutonic history. Because these two samples are similar to the composition of the Amalia Tuff (Johnson and Lipman, 1988; Johnson et al., 1989), the age of the pluton is probably similar to that of the tuff.

Samples from the Rito del Medio and Cabresto Lake pluton provide the most information concerning the 300-150ºC cooling history of the resurgent plutons. K-feldspar from the Rito del Medio pluton (MZQ-16 and 39; Fig. 8E and F) are characterized by monotonically increasing steps from ~15 to 24 Ma during the initial 5% of the spectrum, followed by a plateau comprised of the next 60 to 70% of the ^{39}Ar released, and finally ending in an increase in ages over the last 20-30% of the spectrum. The initial age gradient is most likely the result of low radiogenic yields. For sample MZQ-39, the plateau age is age 24.65 ± 0.08 Ma (MSWD = 1.80). If the first of the isothermal duplicate steps are removed, the new plateau age becomes 24.68 ± 0.13 Ma (MSWD = 2.80), which statistically similar. Because of the elevated MSWD resulting from the removal of the first isothermal steps, the preferred age is 24.64 ± 0.08 Ma. The plateau age of MZQ-16 is 25.06 ± 0.15 (MSWD = 2.03) and similar to MZQ-39, the removal of the first isothermal steps yields an indistinguishable age of 25.13 ± 0.19 (MSWD = 1.99). $^{40}Ar/^{36}Ar$ intercepts for the Rito del Medio analyses indicate the samples that do not contain excess argon. (Fig. 9E and F). Monotonic cooling models indicate similar rapid cooling histories between 24 and 25 Ma, but permit MZQ-16 to

cool ~ 200 ka prior to MZQ-39 (Fig. 10A). Unconstrained cooling models allow reheating at ~25 Ma, followed by rapid cooling similar to the monotonic model.

K-feldspar spectra from the Cabresto Lake pluton (MZQ-12 and 13, Fig 8G and H) are similar to the Rito del Medio K-feldspar. Unlike the Rito del Medio samples, which show slight age gradients in the initial 10% of the spectra, MZQ-12 and 13 age spectra display virtually no age gradients. During the first 15% of the ^{39}Ar released from MZQ-13, the characteristic age oscillation is observed, indicative of excess argon released from fluid inclusions. Both analyses yield plateaus with ages of 25.15 ± 0.12 Ma (MSWD = 2.81) and 24.7 ± 0.2 (MSWD = 1.87) for MZQ-12 and 13, respectively. Inverse isochron plots (Fig. 9 G and H) indicate that MZQ-13 has an atmospheric ^{40}Ar trapped component. However, the inverse isochron plot for MZQ-12 has a $^{40}Ar/^{36}Ar$ intercept of 309 ± 7, suggesting slight excess argon contamination. The preferred age is 24.62 ± 0.12 Ma, calculated from inverse isochron plot. This age is preferred because agrees with the plateau age from MZQ-12 and the corresponding biotite age of 24.64 ± 0.13 Ma. The cooling history of MZQ-13 is similar to those of the Rito del Medio, indicating rapid cooling (400ºC/Ma) at ~24.5 Ma (Fig. 10A). In summary, the ages of the resurgent plutons are similar to the age of Amalia Tuff, suggesting the plutons are closely related to the tuff. The relationship between the two is described in detail in the discussion.

In general, K-feldspar age spectra from the southern caldera margin plutons are more complex than those of the resurgent plutons, displaying trends compatible with rapid to slow cooling from 300 to150ºC. (Fig. 10B). Age and cooling histories are

different between each of the plutons and in some circumstance, vary within individual plutons.

K-feldspar analysis from the Red River pluton yielded monotonically increasing ages throughout the entire analysis. Ages of the first steps increase from 16 to 22 Ma within the first 5% of the spectrum (Fig. 8I). The steep age gradient and large errors associated with the low temperature steps makes modeling the cooling history from the smallest domains of the K-feldspar difficult. This is reflected in the large errors at ~150ºC in the cooling history of the Red River Pluton (Fig. 10B). Following the initially steep age profile, ages of steps gradually increase in age from 22.5 to 25 Ma. The monotonic cooling models indicate cooling to 300ºC by 24 Ma. Between 24 and 22 Ma monotonic models suggest the sampled remained at 300ºC. At 22 Ma, cooling rates increase to 100ºC/Ma, though the exact cooling rate is uncertain due to the large errors associated with the smallest domains. Alternatively, unconstrained models allow for rapid cooling at ~ 25 Ma and subsequent reheating to 300ºC at ~22 Ma, followed by another period of rapid cooling to below 150ºC by 20 Ma.

K-feldspar age spectra from the Bear Canyon pluton, MZQ-8 and 34 (Fig. 8K and L), yield plateau ages of 23.56 ± 0.18 Ma (MSWD = 3.09) and 22.21 ± 0.11 Ma (MSWD = 2.05), respectively. In addition to plateaus, both age spectra have small age gradients during the analysis. Monotonic cooling model results (Fig. 10B) are variable with respect to timing and trends of cooling, though the two samples are only separated by less than two kilometers. MZQ-34 cooled through the K-feldspar closure temperature in roughly 1 Ma, although errors associated with closure of the smallest domains allow for the possibility of a range of ages between 19.5 and 17 Ma at 150ºC. MZQ-8 monotonic

thermal models indicate that cooling from 300 to 200ºC occured 23 and 21.5 Ma and require a period of prolonged temperatures of 200ºC, until 20 Ma. The timing of cooling between 200 and 150ºC is highly uncertain. The unconstrained model of MZQ-8 allows for possible reheating to 300ºC between 22 and 24 Ma and rapid cooling thereafter. Numerous unconstrained models permit thermal perturbations up to 200ºC, as young as 17 Ma. The prolonged cooling and numerous thermal events younger than 22 Ma corresponds to the initial ~10% of the spectrum and this segment of the cooling history may be inaccurate because of the low radiogenic yields and large uncertainties. An unknown problem occurred during unconstrained thermal modeling of MZQ-34, thus no cooling history is presented.

Only one K-feldspar separate, MZQ-6 of the Sulfur Gulch pluton, produced anomalous results (Fig. 8J). Like the Virgin Canyon and Canada Pinabete plutons, the age spectra exhibits monotonically increasing ages from 21 Ma to 26.5 Ma during the first 30% of the spectrum and ends with a plateau older than the age of the caldera.

Age spectra and MDD cooling models of the Rio Hondo and Lucero Peak plutons support an idea of long thermal histories (Fig. 10C). In general, age spectra are complex, due to a combination of excess argon and protracted cooling. Monotonic cooling models are well constrained between 300 and 200ºC with errors as little as 10ºC. However, cooling from 200 to 150ºC is not well constrained. Unconstrained models are variable and allow for multiple reheating events from 22 to 16 Ma.

Samples from the deepest exposed section of the Rio Hondo pluton (MZQ-9, and 33; Fig. 6M and N) are the most complex and disturbed. Excess argon is present through the majority of age spectra, indicated by the oscillation of the ages common to isothermal

duplicate step heating. Excess argon is severe in the low temperature steps, present in the first isothermal duplicate step, and appears to even contaminate the second isothermal duplicate step. Excess argon degassed at the low temperature steps complicates determining the ages of the smallest domains. Both samples show climbing ages until 20% ^{39}Ar released. At this point during both analyses, ages of steps increase abruptly and the remaining age spectrum is characterized by discordant steps decreasing in age.

For both samples, age spectra were modeled using a straight line through the 'hump' portion of the spectrum. Monotonic cooling models (Fig. 10C) agree and show good correlation between 19 Ma and 16 Ma, depicting isothermal conditions at ~260ºC. At temperatures between 250 and 150ºC both samples have the same cooling trends but errors are larger. Models suggest differences in cooling above 260ºC, though due to the poor fit of the modeled age spectra to the actual data, this difference in cooling from 22 to 19 Ma is not statistically robust. Unconstrained cooling models are also similar to one another, depicting rapid cooling to 150ºC or below at ~20 to 21 Ma and reheating to 300ºC as early as 18 Ma or as late as 16 Ma.

Sample MZQ-10 (Fig. 6O) is from a rhyolitic dike that intruded into the main granodiorite phase of the Rio Hondo pluton. The age spectrum is characterized by an initial age gradient from 15 to 17 Ma, followed by a plateau age of 16.50 ± 0.16 Ma (MSWD = 1.24) composed of ~70% of the ^{39}Ar released. Radiogenic yields are enigmatic. During the analysis, radiogenic yields are as low as 10% and exceed 50%. The radiogenic yield does not have the typical oscillation pattern of isothermal duplicate step heating that characterizes excess argon degassing from fluid inclusions. An inverse isochron plot of the sample indicates a ^{40}Ar/^{36}Ar intercept of (297.1 ± 1.8 Ma), consistent

with an absence of excess argon. When ages obtained from argon analysis are younger than expected two explanations are generally called upon, argon loss or alteration. Argon loss is not expected from this sample because as a dike it should have cooled rapidly (consistent with a 'flat' age spectra). However, because there is an initial age gradient is common characteristic of argon loss, the age of the dike should be considered a minimum age. Weight percent K_2O from microprobe analyses averaged 14.4 wt% (n=9) and BSE images indicate no alteration, but shows a large population of fluid inclusions. The low radiogenic yields are probably because of atmospheric bearing, excess argon lacking fluid inclusions that degassed throughout the entire analysis.

Age spectra from the upper region of the main granodiorite phase of the Rio Hondo pluton (MZQ-19; Fig. 8P) and the Lucero Peak pluton (MZQ-21 and 32; Fig. 8Q and R)) suggest slow cooling. These analyses do not behave anomalously like the previously discussed Rio Hondo samples. All three analyses exhibit age gradients throughout the spectra. Also observed are short, flat segments containing between 10-30% of the spectrum (e.g. from 20-40% ^{39}Ar released for sample MZQ-19). The monotonic cooling history of MZQ-19 indicates a near constant cooling rate of 40ºC /Ma from 21.5 to 16 Ma, though due to the error the cooling rate may be as fast as 100°C/Ma. Lucero Peak monotonic cooling models are similar to each other. From 21 to 18 Ma, cooling rates are low, between 33ºC/Ma to near isothermal conditions. Between 17 and 18 Ma, cooling rates change to as fast as 100°C/Ma, though the change in cooling is more pronounced in MZQ-32. Though there is considerable agreement between the samples, models indicate that MZQ-32 may have cooled through the smallest domain closure temperatures as much as 1 Ma prior to MZQ-21.

Unconstrained cooling models are variable from sample to sample. MZQ-19 unconstrained models allow for cooling to between 150 and 250ºC at ~21 Ma, reheating to 300ºC between 19 and 20 Ma, and variable cooling rates between 19 and 15 Ma. All unconstrained cooling models indicate that at 18.6 Ma, the sample was 225ºC. Unconstrained cooling models of MZQ-21 do not generate common cooling trends between 22 and 20 Ma, but allow for various amounts of cooling and subsequent reheating. All models converge at 300 to 325ºC at 19 Ma. Similar cooling styles and rates occur between 300 and 150°C. Unconstrained cooling models of MZQ-32 are the only models where all the possible results are alike. All MZQ-32 cooling trends indicate heating from 100 to 375ºC between 21 and 20 Ma and suggest cooling without reheating until 16 Ma.

DISCUSSION

$^{40}Ar/^{39}Ar$ geochronology and thermochronology of the Latir volcanic field, summarized in figure 12, offers insight into volcanic-plutonic relationships related to shallow crustal (≤ 5km) caldera magmatism. In general, age determinations from this study, along with previous work, support the idea that caldera related magmatism is a dynamic process, characterized by repeated intrusions of small volumes of melt over long (> 10 Ma) periods, and document emplacement of a short-lived ignimbrite magma chamber accompanied and followed by continual growth of a postcaldera subvolcanic batholith. The volcanic record provides point-in-time information regarding the spatial-temporal-compositional changes in the Latir magmatic system, whereas the plutonic record provides a more continuous clock recording the magmatic evolution.

It should be stated briefly that because of the low closure temperature of the minerals used for argon thermochronology (hbl, 550-500°C; bt, 350-300°C; kspar, 300-150°C) compared to the emplacement temperature of granites (800-1000°C), the $^{40}Ar/^{39}Ar$ ages represent cooling, not emplacement. However, $^{40}Ar/^{39}Ar$ cooling ages are inherently related to the emplacement age and in cases of rapid cooling, constitute a good approximation of the emplacement age. The usefulness of $^{40}Ar/^{39}Ar$ thermochronology

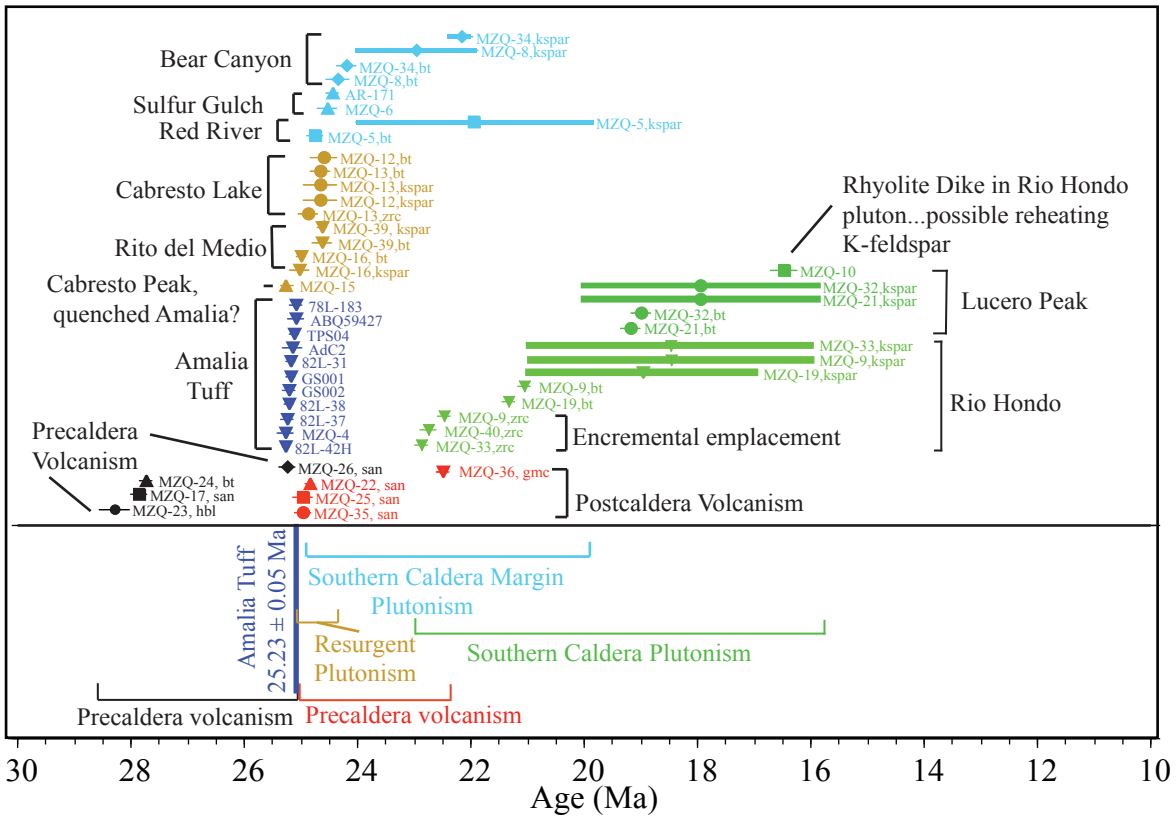

Figure 12 - Latir volcanic field geochronology summary. Ages are reported at 2 sigma error and include the mineral that was analyzed (hbl-hornblende, bt-biotite, kspar-Kfeldspar, zrc-zircon). Zircon ages are from Tappa (Ms thesis in progress). K-feldspar with long, bold horizontal lines correspond to MDD monotonic cooling histories (Fig. 10). The bottom panels shows an interpretation of the magmatic history of the Latir volcanic field based on geochronology summary.

to understanding the emplacement of magma and the construction of subvolcanic batholiths will be discussed later.

Precaldera volcanism and implications for caldera magmatism (28.31 ± 0.19 to 25.23 ± 0.19 Ma)

$^{40}Ar/^{39}Ar$ age determinations of precaldera volcanic rocks suggest that the earliest caldera magmatism is characterized of emplacement of numerous, short-lived, compositionally diverse magma chambers (Fig. 13A). Ages are interpreted as the timing of eruption and provide important constraints on the temporal-spatial evolution of initial caldera-related magmatism.

Precaldera volcanism began in the Latir volcanic field at 28.31 ± 0.19 Ma, with the eruption of an alkalic hornblende bearing andesite (MZQ-25). At 27.89 ± 0.06 the calc-alkaline rhyolite tuff of Tetilla peak (MZQ-17) erupted, now preserved as small outcrops throughout the northern region of the field. Beginning at 27.77 ± 0.09, large volumes of alkalic quartz latite were erupted as lava flows and emplaced as shallow magma bodies throughout the northeastern portion of the field. Between the emplacement of the voluminous quartz latite and the eruption of the Amalia Tuff at 25.23 ± 0.05 Ma, alkalic volcanism continued, yet the majority of the volcanic rocks erupted during this interval has not yet been dated largely because alteration. The last known volcanic eruption prior to the Amalia Tuff was the calc-alkaline rhyolite of Cordova Creek at 25.27 ± 0.06 Ma, which is now preserved as faulted remnants of three rhyolitic domes north of the caldera. The duration of precaldera volcanism was 3.08 ± 0.24 Ma,

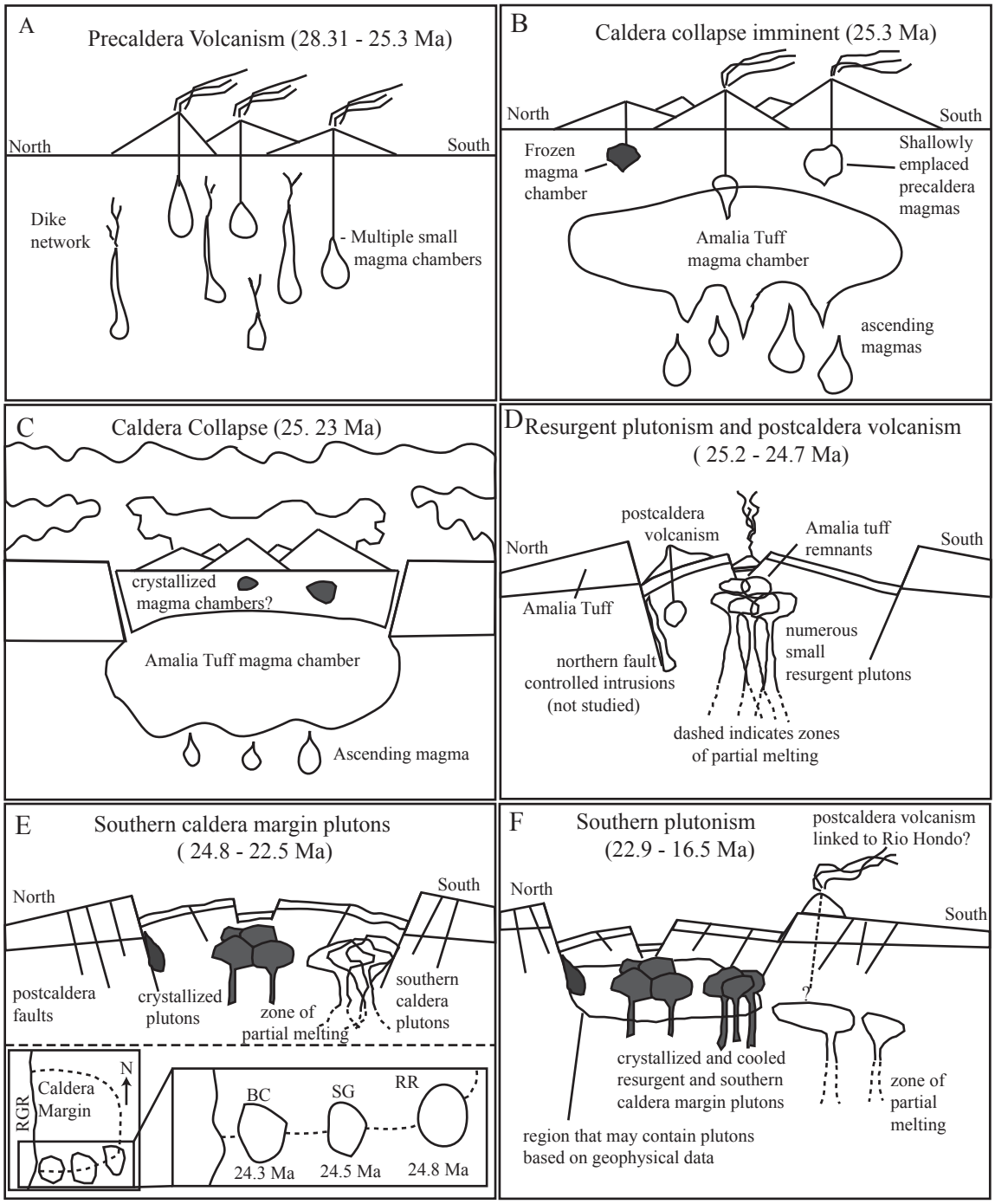

Figure 13 – Schematic diagram illustrating the magmatic evolution of the Latir volcanic field. Crystallized magma chambers shown in dark gray. Diagram is not to scale. A – Precaldera volcanism characterized by multiple small magma chambers. B – Immediately prior to caldera collapse smaller magma chambers exist above the Amalia tuff magma chamber. C – Caldera collapse. D – Resurgent plutonism characterized by the emplacement of small plutons. Magma ascent occurs along the main caldera-related faults. E – Resurgent plutons have crystallized and are cooling as a composite intrusion. Southern caldera plutons are incrementally emplaced, indicated by biotite ages shown in the inset. F – Resurgent and southern caldera margin plutons have crystallized and have cooled. Southern pluton are emplaced at deeper levels compared to the other plutons. Also shown is the region of gravity low from from (Cordell et al., 1986).

from 28.31 ± 0.19 Ma to 25.23 ± 0.05 Ma, much shorter than that suggested by previously published studies (Lipman et al., 1986; Lipman, 2007).

Defining the duration of precaldera volcanism is important because it provides time constraints for the necessary physical and compositional changes to the crust prior to a caldera eruption (Lipman, 2007). Because the only physical evidence for precaldera magmatism in the Latir field is the fragmented precaldera volcanic record, theoretical models are used to better describe the processes leading to caldera formation. Jellinek et al. (2003) presents a simple, theoretical caldera-forming model, which seems to fit the Latir volcanic field well. According to this model, geothermal gradients are low (~20°C/km) at the onset of magmatism, the crust is brittle, and magma is emplaced primarily as small dikes, sills, and stocks. Geothermal gradients increase with continued magmatism, fracture networks develop, and wall rock metamorphism occurs. Each or these processes decrease the effective viscosity of the country rocks and allow small magma chambers to be emplaced (Jellinek et al., 2003). Additionally, ductile extension can provide room in the crust for magma to accumulate, culminating in the formation of caldera. Because the previous geochronology of the Latir volcanic field suggested a duration of at least 5 Ma (Lipman et al., 1986; Lipman, 2007), the new age determinations indicate more rapid rates for physical and compositional changes of the crust prior to caldera eruption.

Determining the duration of precaldera volcanism from other regional volcanic fields is complicated by spatial-temporal overlap of multiple calderas. Table 1 of Lipman (2007), indicates that precaldera volcanism in the SRMVF can range from ~ 1 Ma to more than 6 Ma. The range in durations of precaldera volcanism may be related to

caldera size (a larger eruption requires more magma which may take longer to emplace) or tectonic setting. Many of these durations are based on the now antiquated K-Ar dating method, which can be inaccurate. Assessing $^{40}Ar/^{39}Ar$ geochronology of precaldera volcanism at other caldera centers will be important for determining if previously published durations of precaldera volcanism are accurate.

The timing of compositional changes during precaldera volcanism provides information concerning the temporal-spatial assembly of magma prior to caldera eruption. The previous studies suggested the earliest magma erupted was calc-alkaline, then compositions transitioned to alkaline, climaxing with the eruption of the peralkaline Amalia Tuff (Lipman, 1984; Lipman et al., 1986). The compositional evolution was explained by a single source evolving though time. Periodic 'tapping' of this source chamber produced the compositional evolution of the precaldera volcanism. The new stratigraphy indicates eruptions of compositionally oscillating magmas, fluctuating between alkaline and calc-alkaline magmas. The rapid, oscillating change from alkaline to calc-alkaline is explained by the presence of multiple small magma chambers (Fig. 13A). The most evident period of multiple magma chambers is immediately before caldera eruption. At 25.27 ± 0.06 Ma the calc-alkaline rhyolite of Cordova Creek erupted and at 25.23 ± 0.05 Ma the peralkaline Amalia Tuff erupted (Fig. 13C). Without multiple magma chambers, the compositional oscillation would require a proto-Amalia Tuff magma chamber changing composition from calc-alkaline to alkaline in 50 ka or a peralkaline Amalia Tuff magma chamber with a calc-alkaline cap that could be tapped for the eruption of the rhyolite of Cordova Creek. The preferred interpretation is that the source for the Cordova Creek rhyolite was located at a shallow level in the crust and that

the Amalia Tuff magma chamber was rapidly emplaced at a deeper crustal level (Fig. 13B). This magma chamber configuration allows for two distinct magma compositions to be erupted at nearly the same time.

Eruption of the Amalia Tuff (25.23 ± 0.05 Ma)

The formation of the Questa Caldera occurred at 25.23 ± 0.05 Ma during the eruption of the Amalia Tuff (Fig. 13C). The eruption left a depression approximately 15 km in diameter inferred by northern ring-fault intrusions and the geometry of the intracaldera fill (Lipman et al., 1986; Lipman and Reed, 1989; Meyer and Foland, 1991). The erupted volume is approximately 500 km^3 (Lipman et al., 1986; Johnson et al., 1990) and outflow sheets are preserved as much as 45 km west of the caldera margin in the Tusas Mountains (Miggins et al., 2002). Though two younger ages were excluded from the age calculation of the Amalia Tuff (Fig. 4), the overlapping errors of all the Amalia Tuff ages support the idea that the Amalia Tuff was the only ignimbrite erupted from the Questa caldera.

Caldera magmatism (25.23 ± 0.05 to ~ 24.3)

Magmatism associated with the caldera will be discussed in terms of resurgent plutonism, the emplacement of the southern caldera margin plutons, and coeval volcanism. The caldera formed at 25.23 ± 0.05 Ma, which provides an upper age limit for the emplacement of resurgent plutons. Plutons were emplaced immediately following the caldera formation and emplacement continued for approximately 1 Ma after. Though

dates for postcaldera volcanism are sparse, the data set suggests that volcanism occurred throughout this period of plutonism.

Caldera magmatism: resurgent plutonism and postcaldera volcanism (25.28 – 24.7 Ma)

Immediately following the eruption of the Amalia Tuff and formation of the Questa caldera, four resurgent plutons were emplaced, crystallized, and cooled to 150ºC within 500 ka (Fig. 13D). Two plutons, the Virgin Canyon and Canada Pinabete, are interpreted to be the quenched remnants of the Amalia Tuff. The Rito del Medio and Cabresto lake plutons were emplaced as small plutons that rapidly cooled and record magma changing to lesser evolved compositions. Postcaldera volcanism began and continued throughout resurgence.

The similar composition of the Virgin Canyon and Canada Pinabete pluton to the Amalia Tuff led previous workers (Lipman et al., 1986; Johnson and Lipman, 1988; Johnson et al., 1989) to suggest these plutons were the quenched remnants of the tuff. A biotite analysis from the Canada Pinabete (Fig. 5B) yielded a plateau age of 25.28 ± 0.08 Ma, indistinguishable from the Amalia Tuff. Though the biotite age is slightly older, many previous geochronology studies have found biotite ages are systematically older than sanidine ages (Heizler, 2001). No age could be determined for the Virgin Canyon pluton because age spectra are disturbed (Fig. 6 A thru C) and inverse isochron ages (Fig 7 A thru C), though similar to the Amalia Tuff, are statically invalid because of elevated MSWD values. However, because of the similar composition to the Amalia Tuff and

Canada Pinabete pluton, the Virgin Canyon pluton is interpreted to be contemporaneously with the Canada Pinabete pluton.

The implications are vast for correctly identifying a pluton with a similar age and geochemistry to the Amalia Tuff. Recent studies have suggested that exposed plutons in the Cordilleran margin are not related to volcanism because 1) incremental emplacement does not permit large volumes of eruptible melt (Schmitz and Bowring, 2001; Coleman et al., 2004; Glazner et al., 2004) and 2) plutons are not compositionally linked to the volcanic rocks (Glazner et al., 2008). This study, combined with the existing geochemistry (Johnson and Lipman, 1988; Johnson et al., 1989), indicates that some plutons are directly related to ignimbrites and suggest that ignimbrite magma chambers may not completely drain during the caldera forming event(s). This study suggests that plutons most closely linked in time and composition to caldera-forming ignimbrites may be the remnants of magma chambers. This conclusion differs from an alternate view that plutons represent magma chambers that crystallized and cooled within the crust and never erupted (Glazner et al., 2004). Further investigation of other volcanic fields with exposed resurgent plutons would help to confirm this hypothesis.

Following the emplacement of the Virgin Canyon and Canada Pinabete plutons, magmatism continued with the emplacement of the Rito del Medio pluton. $^{40}Ar/^{39}Ar$ analysis yield two distinct ages populations for the Rito del Medio pluton. One sample yielded indistinguishable biotite and K-feldspar ages of ~25.0 Ma and another sample yield indistinguishable, but younger biotite and K-feldspar ages of ~ 24.65 Ma. Overlapping biotite and K-feldspar ages from a sample indicates rapid cooling. It is striking that the two samples, which are located less than 0.5 km from each other, yield

two distinct ages (~25.0 and ~ 24.65). Because biotite and K-feldspar ages from each sample are identical, the age variation is not interpreted to be the result of differential cooling, but support the ideal of rapid, incremental emplacement of the pluton.

Contrastingly, the Cabresto Lake pluton, which is a similar size to the Rito del Medio pluton, was emplaced as a single intrusion. Thermal histories of Cabresto Lake K-feldspar suggest rapid cooling without the possibility of reheating. Four age determinations, two biotite and two K-feldspar, are statistically similar ranging from 24.65 ± 0.13 to 24.7 ± 0.2 Ma. Ages from the Cabresto Lake pluton illustrate the potential importance of the newly calibrated U-Pb and $^{40}Ar/^{39}Ar$ dating methods. Prior to Kuiper et al. (2008), results from the two dating methods suggested a 200 ka period of cooling from emplacement at 24.9 Ma (U-Pb age from Tappa, Ms Thesis in progress) to the closure temperature of biotite and K-feldspar (350 - 150ºC) at 24.7 Ma. If the newly calibrated age for the FC-2 sanidine irradiation monitor (28.201 Ma) is correct, cooling from emplacement to 150ºC was effectively instantaneous at 24.9 Ma, demonstrating the importance of accurate intercalibration of the two dating methods for deciphering the intrusive and cooling history of a pluton. Further investigation of the U-Pb and $^{40}Ar/^{39}Ar$ ages from rapidly cooled plutons will help to determine if the new calibration of the two methods is correct.

Though the postcaldera volcanic record is fragmented, the ages from this study indicate postcaldera volcanism occurred during the emplacement and cooling of the resurgent plutons. Volcanism began within 200 ka of caldera formation with the eruption of rhyolitic lavas and tuffs. A rhyolite tuff at the base of the Brushy Mountain horst block has an age of 25.01 ± 0.05 Ma and the rhyolite lava from the northern region of the

field has an age of 25.00 ± 0.09 Ma. A rhyolite intrusion at Comanche point is 24.89 ± 0.05 Ma, similar to the U-Pb age from the Cabresto Lake pluton. Comparing the geochemistry of these three postcaldera volcanic rocks to the resurgent plutons is important for linking plutons to volcanic eruptions and determining the relationship between the two processes.

Caldera magmatism: Southern caldera margin plutonism (24.8 - 22 Ma)

Three plutons were emplaced along the southern caldera margin following the emplacement of the resurgent plutons (Fig. 13E). The plutons, which appear to be the cupolas of a larger-single intrusion based on gravity data (Cordell et al., 1986; Lipman et al., 1986), have younging east to west $^{40}Ar/^{39}Ar$ ages suggesting incremental emplacement during a 500 ka period. Unlike the resurgent plutons that cooled rapidly, MDD thermal modeling of southern caldera margin K-feldspar indicate cooling from 300 to 150ºC was variable, possibly involving reheating events.

The oldest southern caldera margin pluton is the Red River pluton. The biotite age indicates cooling to 350ºC at 24.78 ± 0.06 Ma, which is the best estimate for the age of emplacement. The K-feldspar age spectra is indicative of slow cooling and/or reheating. Monotonic MDD thermal models require the pluton to remain at 300°C between 24 and 21 Ma, which can be explained by a locally elevated geothermal gradient. The preferred thermal history is the unconstrained model, which suggests rapid cooling at 24 Ma and reheating at 22 Ma. This model is preferred because 1) numerous dikes and smaller intrusive bodies, not yet dated, are present in the pluton, 2) the pluton is the oldest part of a larger intrusion (Cordell et al., 1986; Lipman et al., 1986), and 3) the

Rio Hondo Pluton to the south has U-Pb ages between 22 and 23 Ma, similar to the age of reheating event.

Ages from two biotite analyses from the Sulfur Gulch pluton are 24.57 ± 0.14 and 24.48 ± 0.10 Ma, suggesting that the pluton was emplaced and cooled as single intrusive unit, after the emplacement of the Red River pluton. K-feldspar did not yield geologically meaningful ages. Because of the lack of U-Pb ages, the biotite ages are the best approximation for the emplacement age. The overlapping ages suggest that the pluton was emplaced and cooled as a single intrusive unit.

The Bear Canyon pluton is the youngest pluton and has the most complicated cooling history of the southern caldera margin plutons. Two samples collected less than 2 km away from each other along the northern margin of the pluton have similar biotite plateau ages, 24.38 ± 0.12 and 24.22 ± 0.10 Ma, but the ages and cooling histories of the K-feldspar are radically different. The plateau ages for the two K-feldspar samples differ by more than 1 Ma and the differences between the biotite and K-feldspar ages for the two samples are 0.80 Ma and 2 Ma. The similar ages for the two biotites indicate that the pluton experienced a similar cooling history at 350ºC, followed by heterogeneous cooling at lower temperatures. The close proximity of the two samples to each other would suggest that difference in age between the two samples is not related to different geothermal gradients of the country rock. The similar biotite ages, combined with the absence of changes in texture or composition within the pluton, suggest the difference in K-feldspar cooling histories is the not result of incremental emplacement. The preferred explanation is reheating to, but not exceeding 350ºC. Small-scale dikes could result in localized partial argon degassing to produce the younger ages, but the absence of dikes in

the pluton, makes this an unlikely possibility. Thus the reheating event is not completely understood at this time and should be further investigated.

There is no evidence for postcaldera volcanism coeval with southern caldera margin plutonism. Lipman et al. (1986) proposed that the postcaldera volcanic rocks located on Brushy and Timber Mountain had similar ages and compositions to the southern caldera margin plutons, but this study has determined that the volcanic rocks on Brushy Mountain are most likely linked to the resurgent plutons and the southern plutons (discussed later). The absence of volcanic rocks with ages similar to the southern caldera margin plutons might indicate that the lull in volcanism during this period is due to a lack of eruptible melt because of incremental emplacement. This is only speculation. Not all the postcaldera volcanic rocks have been dated. Additionally, volcanic rocks linked to the southern caldera margin plutons may have been removed by erosion. Further investigation of the volcanic rocks located on Timber Mountain might identify rocks coeval with southern caldera margin plutons.

Postcaldera magmatism: Southern caldera plutons and coeval volcanism (22.9 – 16.5 Ma)

The Rio Hondo and Lucero Peak plutons are the youngest plutons in the field and have the longest thermal histories (Fig. 13 F). U-Pb ages suggest rapid incremental assembly of the Rio Hondo pluton and $^{40}Ar/^{39}Ar$ thermochronology of both plutons indicates protracted thermal histories. Unconstrained MDD cooling histories for the deepest exposed section of the Rio Hondo pluton indicate a thermal perturbation at 16.5 Ma, which potentially corresponds to a 16.5 Ma rhyolitic dike within the Rio Hondo

pluton. The Lucero Peak pluton also has a prolonged thermal history with the possibility of younger, but as of yet, unidentified reheating events.

Preliminary U-Pb zircon ages indicate the Rio Hondo pluton was incrementally emplaced during a 500 ka period. U-Pb ages from the main granodiorite body are 22.8 ± 0.10 and 22.5 ± 0.10 and the upper granitic unit is 22.9 ± 0.10 Ma. A biotite age from the deepest exposed granodiorite body is 21.37 ± 0.18 and a biotite from the highest exposure of the granodiorite body is 21.08 ± 0.2 Ma. The overlapping biotite ages indicate that following incremental emplacement, the pluton cooled as one unit, from 900 to 350ºC over a 1.5 to 2.0 Ma interval.

Particularly interesting in the cooling history of the Rio Hondo pluton is the divergence is cooling histories recorded by the K-feldspars. MDD monotonic cooling histories from the deepest exposed sections of the Rio Hondo pluton suggest isothermal cooling at 275°C between 21 and 16.5 Ma. This, however, is believed to be the result of later reheating caused by dike emplacement at 16.5 Ma. The cooling history determined from one sample in the upper part of the Rio Hondo granodiorite is significantly different. The extended thermal history is thought to be the result of a younger reheating based on interpretation of the other Rio Hondo pluton samples. The unconstrained cooling history suggests a thermal perturbation between 19 and 20 Ma, which may reflect another period of Rio Hondo related dike emplacement. Dating more dikes in the Rio Hondo pluton would be useful for testing this hypothesis.

The last known volcanic eruption in the Latir volcanic field was an eruption of a pyroxene andesite at 22.52 ± 0.08 Ma on Brushy Mountain. This age is important for two reasons. First, it constrains the duration of postcaldera volcanism to 2.71 ± 0.13 Ma,

shorter than the previous conclusions of Lipman et al. (1986), which determined postcaldera volcanism lasted from 26 to 22 Ma. Recall the duration of precaldera volcanism was 3.08 ± 0.24 Ma, which suggests that in a 'simple' one-caldera system the durations of pre- and postcaldera volcanism are similar. Second, though the andesite of Brushy Mountain has not been geochemically linked to the Rio Hondo pluton, it indicates postcaldera volcanism is coeval and volcanism occurred throughout pluton emplacement. One of the cruxes regarding linking plutons to volcanoes according to incremental emplacement, is that if a pluton is assembled at a slow rate, there may not be enough melt available for an eruption. Coeval volcanism with the Rio Hondo pluton indicates that incremental emplacement over ~ 500 ka may be able to sustain volcanic activity. It is interesting that the andesite of Brushy Mountain is a similar age to the youngest Rio Hondo pluton increment. This suggests that a large steady-state magma chamber may form after a period of prolonged incremental emplacement, when conditions exist for a magma chamber to be thermally sustained (Hansen and Glazner, 1995; Glazner et al., 2004).

For two Lucero Peak pluton samples, biotite ages and K-feldspar cooling histories are similar, though one sample is from the margin and the other is from the interior. Biotite ages from these samples are 19.22 ± 0.10 (interior) and 19.02 ± 0.10 (margin). Although the ages narrowly overlap at the 2σ-confidence level, they suggest that the interior of the pluton may have cooled slightly faster than the margin. K-feldspar monotonic cooling models are very similar, both indicating a period of slow cooling, followed by a more rapid cooling. During classic batch emplacement of plutons, the margins of the pluton cool first and more rapidly than the later, slowly cooled interior

(Glazner et al., 2004). However, the results from the Lucero Peak pluton are not supportive of this model and instead invoke a more complicated intrusive history. Dalrymple et al. (1999) suggested that spatially disorganized assembly of a pluton could cause resetting to produce results that do not match cooling of a single magma chamber. It is possible that younger, unexposed plutons are located beneath the Lucero Peak pluton, as well as beneath the Rio Hondo pluton. These could be a thermal source for reheating or causing an elevated local geothermal gradient necessary for slow cooling. However, no reheating events where generated in the unconstrained cooling models for the interior sample and a lack of a common trend for reheating events from the marginal sample suggest that reheating, if any, was minimal. The emplacement history is interpreted to be more complex than can be explained by batch emplacement. Change from slow to rapid cooling occurred at ~ 17.5 Ma for both samples, although the change in cooling is more pronounced in the interior sample. The change in cooling history may be associated uplift related to Rio Grande rifting.

Incremental emplacement and argon thermochronology

Incremental emplacement of plutons is becoming a widely accepted mechanism for intruding magma into the crust. This and numerous previous studies invoke the incremental emplacement hypothesis to explain age variations, both large (> 5 Ma) (Coleman et al., 2004; Matzel et al., 2006) and small (< 100 ka) (Michel et al., 2008), within composite batholiths, zoned intrusive suites, and individual plutons. The following paragraphs are intended to clarify certain details of the incremental

emplacement process and discuss the importance and suitability of the argon dating method for correctly identifying this process.

Assigning a single age to a pluton breeds the misconception that batch-emplaced plutons are episodic and instantaneously emplaced into the crust. Alternatively, assigning multiple ages to a pluton, in the framework of incremental emplacement, implies a prolonged intrusive history. However, it is important to remember all plutons, even those emplaced by large tank processes, such as assimilation and stopping, require some amount of time to emplace a large volume of magma into the crust. Thus, the difference between incremental emplacement and batch emplacement is not that one process is instantaneous and the other is a protracted process. Both styles of emplacement require some amount of time, be it short or long. Instead, incremental emplacement is a process defined by multiple events and batch emplacement is only one event. The multiple events that characterize incremental emplacement may be discrete pulses of magma injection, such as repeated diking, and the pulses are separated by finite amounts of time. Incremental emplacement may also be a continuum of magma emplacement, similar to slowly filling a balloon with air.

The two emplacement styles are expected to have two different emplacement and cooling histories. Batch emplacement will have U-Pb ages that are statistically the same or can be explained by slow cooling. For incremental emplacement, U-Pb ages from various localities will be statistically different and will not be explained by slow-cooling models (Glazner et al., 2004). Recognizing incremental emplacement using radiometric dating is also dependent on the ability to resolve the ages of individual increments, which is intimately related to the precision of the dating technique. Incremental emplacement

may not be recognized in rapidly emplaced magma and thus detailed field observations of emplacement mechanisms should always be combined with geochronology.

Determining emplacement histories using argon thermochronology is difficult because of the low closure temperature of the commonly used minerals. The $^{40}Ar/^{39}Ar$ data can be explained by the style of emplacement and in certain circumstances will approximate the age of emplacement. If a pluton is emplaced and cools rapidly, regardless of incremental or batch emplacement, the $^{40}Ar/^{39}Ar$ ages from various minerals and from different localities will be similar with little or no variation. In the absence of U-Pb ages, $^{40}Ar/^{39}Ar$ ages from rapidly cooled plutons are the best approximation for the emplacement age.

If slow cooling occurs, the $^{40}Ar/^{39}Ar$ ages will not approximate the emplacement age, but the style of cooling will be directly related to how the pluton was emplaced. For example, it is assumed that for batch emplacement, the margins cool faster than the interior and the data will reflect this. During incremental emplacement, short-lived, disordered thermal regimes are created by multiple injections of magma and slow cooling may occur, but they will be more chaotic than batch emplacement cooling.

Lastly, other factors should be considered that might lead to erroneous interpretations. Depth of emplacement and temperature of the country rocks can result in thermal homogenization of an incrementally emplaced pluton. Subsequent uplift may produce a cooling history similar to that of a batch-emplaced pluton. Because of the low closure temperature of K-bearing minerals, reheating events are likely in the incremental emplacement scenario. Reheating can completely reset an incrementally emplaced magma chamber to mimic batch emplacement cooling or can reset a region of a batch-

emplaced pluton to mimic incremental emplacement. The increased probability for reheating suggests that argon thermochronology might only be suitable for detecting incremental emplacement in scenarios with a limited number of increments (reheating events) or on a large scale where regions of prior emplaced melt are thermally unaffected by younger magma emplacement. The $^{40}Ar/^{39}Ar$ dating method can be a useful tool for understanding caldera-related magmatism and incremental emplacement if detailed field observations are combined with detailed examination of the geochronology.

CONCLUSIONS

Hornblende, biotite, and sanidine $^{40}Ar/^{39}Ar$ analysis, combined with MDD thermal modeling of plutonic K-feldspar, provide an accurate and precise timing of magmatism associated with the Latir volcanic field. The ages of volcanic rocks were used to modify the pre-existing stratigraphy and understand the volcanic evolution of the field. The ages and cooling histories of the plutonic rocks provide a relatively continuous record of evolution of magmatism. Comparing the ages of the volcanic record to that of the plutonic record helps to understand the volcanic-plutonic relationship and highlights potentially important volcanic-plutonic rocks pairs for future research.

In general, the ages indicate a ~ 6 Ma period of magmatism associated with the Questa caldera and perhaps a 10 Ma period of magmatism for entire volcanic field. The duration of precaldera volcanism was similar to postcaldera volcanism and caldera eruption marked the most intense period of magmatism. Plutons within the caldera margin were emplaced and cooled within 1 Ma of caldera formation and plutons outside of the caldera have longer emplacement and thermal histories. The specific conclusions of this study are:

(1) Precaldera volcanism began at 28.31 Ma and ended with eruption of the Amalia Tuff and formation of the Questa caldera at 25.23 Ma. This period

of volcanism is characterized by the emplacement of numerous magma chambers.

(2) Though fragmented, the postcaldera volcanic record indicates that volcanism began at 25.0 Ma and at 22.52 Ma. Postcaldera volcanism was coeval with postcaldera pluton emplacement, though none of the postcaldera volcanic rocks have been geochemically matched to any specific pluton.

(3) Resurgent plutons were emplaced and rapidly cooled to 150°C within 500 ka of caldera eruption. The Canada Pinabete is interpreted to be non-erupted Amalia Tuff.

(4) Incremental emplacement of magma occurred along the southern caldera margin between 24.8 and 24.3 Ma. MDD cooling histories from two of the three exposed cupolas indicate that reheating by young intrusions was likely.

(5) Following rapid, incremental emplacement of the Rio Hondo pluton between 22.4 and 22.9 Ma, the pluton cooled as one unit until ~21 Ma. The large (~5 Ma) age gradient observed in the K-feldspar age spectra is explained by reheating at 16.5 Ma, as indicated by unconstrained cooling models and supported by the age of one rhyolite dike (16.5 Ma) intruding the lower region of the pluton. $^{40}Ar/^{39}Ar$ analysis of the Lucero Peak pluton indicates a protracted cooling history that does not support emplacement of a single intrusion, but instead indicates a more complicated emplacement and cooling history.

Future research in the Latir volcanic field should include: dating more pre- and postcaldera volcanic rocks to complete the volcanic geochronology and identify volcanism coeval with plutonism, geochemically matching coeval volcanic rocks to plutons, U-Pb dating of all datable plutons, and continued fieldwork to better characterize pluton emplacement. Continued study of pluton thermal histories will be important for characterizing the longevity of geothermal activity related to magmatism. Investigating volcanic-plutonic rocks pairs in other volcanic fields will be important for further exploring the relationship between the volcanic and plutonic record.

REFERENCES

Baldridge, W. S., and Olsen, K. H., 1989, The Rio Grande rift: American Scientist, v. 77, p. 240-247.

Baldridge, W. S., Keller, G. R., Haak, V., Wendlandt, E., Jiracek, G. R., and Olsen, K. H., 1995, The Rio Grande rift in Olsen, K. H. ed. Continental rifts: evolution, structure, and tectonics: Developments in geotectonics, v. 25, Elsevier, Amsterdam, p. 233-276.

Bartley, J.M., Glazner, A.F., and Coleman, D.S., 2005, Do large silicic eruptions leave behind even larger plutons?: Eos (Transactions, American Geophysical Union), v. 86, no. 18, p. 58.

Chapin, C. E, Wilks, M., and McIntosh, W. C., 2004, Space-time patters of Late Cretaceous to present magmatism in New Mexico-comparison with Andean volcanism and potential for future volcanism: New Mexico Bureau of Geology and Mineral Resources, Bulletin 160, p. 13-40.

Coleman, D. S., Gray, W., and Glazner, A. F., 2004, Rethinking the emplacement and evolution of zoned plutons: geochronological evidence for incremental assembly of the Tuolumne Intrusive Suite, California: Geology, v. 32, p. 433-436.

Colucci, M.T., Dungan, M. A., and Ferguson, K. M., 1991, Precaldera lavas of the southeast San Juan volcanic field: Parent magmas and crustal interactions: Journal of Geophysical Research, v. 96, p. 13,413-13,434.

Coney, P. J., and Reynolds, S. J., 1977, Cordilleran Benioff zones: Nature, v. 270, p. 403-407.

Cordell, L., Long, C. L., and Jones, D. W., 1986, Geophysical expression of the batholith beneath Questa caldera, New Mexico: Journal of Geophysical Research, v. 90, p. 11,263-11,274.

Czamanske, G.K., Foland, K.A., Hubacher, F.A., and Allen, J.C., 1990, The $^{40}Ar/^{39}Ar$ chronology of caldera formation, intrusive activity and Mo-Ore near Questa, New Mexico: New Mexico Geological Society, Field Conference, 41st Guidebook, p. 355-358.

Dalrymple, G. B., Grove, M., Lovera, O. M., Harrison, T. M., Hulen, J. B., and Lanphere, M. A., 1999, Age and thermal history of The Geysers plutonic complex (felsite unit), Geysers geothermal field, California: a 40Ar/39Ar and U-Pb study: Earth and Planetary Science Letters, v. 173, p. 285-298.

Dickenson, W. R., and Snyder, W. S., 1978, Plate tectonics of the Laramide orogeny: Geological Society of America, Memoir 151, p. 355-366.

Fleck, R.J., Sutter, J.F., and Elliot, D.H., 1977, Interpretation of discordant 40Ar/39Ar age-spectra of Mesozoic tholeiites from Antarctica. Geochimica Cosmochimica. Acta, v. 41, p. 15- 32.

Foster, D.A., Harrison, T.M., Copeland, P., and Heizler, M.T., 1990, Effects of excess argon within large diffusion domains on K-feldspar age: Geochimica Cosmochimica. Acta, v. 54, p. 1699-1708

Glazner, A. F.,Bartley, J. M., Coleman, D. S., Gray, W. M. and Taylor, R. Z., 2004, Are plutons assembled over millions of years by amalgamation from small magma chambers?: Geological Society of America Today, v. 14, no. 4/5, p. 4-11.

Glazner, A. F., Bartley, J. M., 2006, Is stopping a volumetrically significant pluton emplacement process?: Geological Society of America Bulletin, v. 118, p. 1185-1195.

Glazner, A. F., Coleman, D. S., and Bartley, J. M., 2008, The tenuous connection between high-silica rhyolites and granodiorite plutons: Geology, v. 36, p. 183-186.

Hagstrum, J. T., Lipman, P. W., and Elston, D. P., 1982, Paleomagnetic evidence bearing on the structural development of the Latir Volcanic Field near Questa, New Mexico: Journal of Geophysical Research, v. 87, p. 7833-7842.

Hanson, R. B., and Glazner, A. F., 1995, Thermal requirements for extensional emplacement of granitoids: Geology, v. 23, p. 213-216.

Heizler, M. T., Lux, D. R., and Decker, E. R., 1988, The age and cooling history of The Chain of Ponds and Big Island plutons and the Spider Lake Granite, west-central Maine and Quebec: American Journal of Science, v. 288, p. 925-952.

Heizler, M. T., 2001, ^{39}Ar recoil distance and implantation efficiency: Eos Transactions, AGU, Fall meeting supplementary abstracts, abstract v22C-1060.

Jellinek, A.M., and DePaolo, D.J., 2003, A model for the origin of large silicic magma chambers: Precursors of caldera-forming eruptions: Bulletin of Volcanology, v. 65, p. 363–381.

Johnson, C. M., and Lipman, P. W., 1988, Origin of metaluminous and alkaline volcanic rocks of the Latir volcanic field, northern Rio Grande Rift, New Mexico: Contributions to Mineralogy and Petrology, v. 100, p. 107-128.

Johnson, C. M., Czamanske, G. K., and Lipman, P. W., 1989, Geochemistry of intrusive rocks associated with the Latir volcanic field, New Mexico, and contrasts between evolution of plutonic and volcanic rocks: Contributions to Mineralogy and Petrology, v. 103, p. 90-109.

Kuiper, K. F., Deino, A., Hilgen, F. J., Krijgsman, W., Renne, P. R., and Wijbrans, J. R., 2008, Synchronizing rock clocks of earth history: Science, v. 320, p. 500-504.

Lawton, T. F., and McMillan, N. J., 1999, Arc abandonment as a cause for passive continental rifting: Comparison of the Jurassic Mexican Borderland rift and the Cenozoic Rio Grande Rift: Geology, v. 27, p. 779-782.

Leonardson, R. W., Dunlop, G., Starquist, V. L., Bratton, G. P., Meyer, J. W., and Osborne, L. W. Jr., 1983, Preliminary geology and molybdenum deposits at Questa, New Mexico; in Babcock, J. W., The genesis of Rocky Mountain ore deposits; changes with time and tectonics: Denver Region Exploration Geologists Society, p. 151-155.

Lipman, P. W., 1984, Evolution of the Oligocene-Miocene Questa magmatic system, Rio Grande rift, northern New Mexico. eds. Dungan, M. A., Grove, T. L., and Hildreth, L., in Proceedings of the ISEM field conference on open magmatic systems.

Lipman, P. W. 2007, Incremental assembly and prolonged consolidation of Cordilleran magma chambers; evidence from the Southern Rocky Mountain volcanic field: Geosphere, v. 3, p. 42-70.

Lipman, P. W., Mehnert, H. H., Naeser, C. W., and Keller, G. R., 1986, Evolution of the Latir volcanic field, northern New Mexico, and its relation to the Rio Grande Rift, as indicated by potassium-argon and fission track dating: Journal of Geophysical Research, v. 91, p. 6329-6345.

Lipman, P.W and Reed, J.C. Jr., 1989, Geologic map of the Latir volcanic field and adjacent areas, northern New Mexico: U.S. Geological Survey, Miscellaneous Map 1 1907, scale 1:48,000.

Lo, C., and Onstott, T.C., 1989, ^{39}Ar recoil artifacts in chloritized biotite: Geochimica Cosmochimica Acta, v.53, p. 2967-2711.

Lovera, O.M., Richter, F.M., and Harrison, T.M., 1989, ^{40}Ar/^{39}Ar thermochronology for slowly cooled samples having a distribution of domain sizes: Journal of Geophysical Research, v.94, p. 17,917-17,935.

Lovera, O.M., Richter, F.M., and Harrision, T.M., 1991, Diffusion domains determined by 39Ar Released during step heating, Journal of Geophysical Research., v. 96, p. 2057-2069.

Mahon, K.I., 1996, The new "York" regression: Application of an improved statistical method to geochemistry. International Geology Review, v.38, p. 293-303.

Matzel, J.E.P., Bowring, S.A., and Miller, R.B., 2006, Time scales of pluton construction at differing crustal levels: Examples from the Mount Stuart and Tenpeak Intrusions, North Cascades, Washington: Geological Society of America Bulletin, v. 118, p. 1412–1430.

McDougall, I., and Harrison, T.M., 1999, Geochronology and thermochronology by the $^{40}Ar/^{39}Ar$ method: New York, Oxford University Press, p. 269.

McIntosh, W. C., Sutter, J. F., Chapin, C. E., and Kedzie, L. L., 1990, High-precision 40Ar/39Ar sanidine geochronology of ignimbrites in the Mogollon-Datil volcanic field, southwestern New Mexico: Bulletin of Volcanology, v. 52, p. 584-601.

McIntosh, W. C., Chapin, C. E., Ratte, J. C., and Sutter, J. F., 1992, Time-stratigraphic framework of the Eocene-Oligocene Mogollon-Datil volcanic field, southwest New Mexico: Geological Society of America Bulletin, v. 104, p. 851-871.

McIntosh, W. C., and Chapin, C. E., 2004, Geochronology of the central Colorado volcanic field: New Mexico Bureau of Geology & Mineral Resources, Bulletin 160, p. 205-238.

Meyer, J., and Foland, K.A., 1991, Magmatic-tectonic interaction during early Rio Grande rift extension at Questa, New Mexico: Geological Society of America Bulletin, v. 103, p. 993-1006.

Michel, J., Baumgartner, L., Putlitz, B., Schaltegger, U., and Ovtcharova, M., 2008, Incremental growth of the Patagonian Torres del Paine laccolith over 90 k.y.: Geology, v. 36, p. 459-462.

Pillmore, C. L., Obradovich, J. D., Landreth, J. O., and Pugh, L. E., Mid-Tertiary volcanism in the Sangre de Cristo Mountains of northern New Mexico: Geological Society of America Abstracts with Programs, v. 5, p. 502.

Renne, P.R., Swisher, C.C., Deino, A.L., Karner, D.B., Owens, T.L., and DePaolo, D.J., 1998, Intercalibration of standards, absolute ages and uncertainties in $^{40}Ar/^{39}Ar$ dating, Chem. Geol., v. 145, p. 117-152.

Richter, F.M., Lovera, O.M., Harrison, T.M., and Copeland, P., 1991, Tibetan tectonics from $^{40}Ar/^{39}Ar$ analysis of a single K-feldspar sample, Earth and Planetary Science Letters, v. 105, p. 266-278.

Sanders, R.E, and Heizler, M.T., 2005, Extraction of MDD thermal histories from $^{40}Ar/^{39}Ar$ K-feldspar step heating data: New Mexico Bureau of Geology and Mineral Resources Open-File Report OF-AR 26, p. 11

Schmitz, M. D., and Bowring, S. A., 2001, U-Pb zircon and titanite systematics of the Fish Canyon Tuff; an assessment of high-precision U-Pb geochronology and its application to young volcanic rocks: Geochimica et Cosmochimica Acta, v. 65, p. 2571-2587.

Smith, G. A., Moore, J. D., and McIntosh, W. C., 2002, Assessing roles of volcanism and basin subsidence in causing Oligocene-lower Miocene sedimentation in the northern Rio Grande rift, New Mexico, USA.: Journal of Sedimentary Research, v. 72, p. 836-848.

Steiger, R.H., and Jager E., 1977, Subcommision on geochronology: Convention on the use of decay constants in geo- and cosmochronology. Earth Planet. Science Letters, v. 36, p. 359-362.

Thompson, R. A., Dungan, M. A., and Lipman, P. W., 1986, Multiple differentiation processes in the early-rift calc-alkaline volcanics, northern Rio Grande rift, New Mexico: Journal of Geophysical Research, v. 91, p. 6046-6058.

Tappa, M, Ms Thesis in Progress.

ANALYTICAL APPENDIX

Sample Preparation

Forty-one volcanic and plutonic samples were collected during the course of this study. Seven previously prepared samples were provided by Peter Lipman (those that don't begin with MZQ) and one by Ren Thompson (TPS04), of the USGS. Rock samples were crushed in a standard disk mill, sieved to between 250 to 850 μm, and washed in deionized water to remove any dust created by the crushing procedure. Volcanic samples received an additional cleaning in a 15% HF solution for 10-15 minutes to remove any glass and/or quartz adhered to the grains. All samples were then prepared by Frantz magnetic separation, density separated with lithium metatungstate heavy liquid, rinsed and dried. Samples were then handpicked to obtain monomineralic separates. Samples to be dated were analyzed using Cameca SX-100 electron microprobe at the New Mexico Bureau of Geology and Mineral Resources to accomplish two goals. First, BSE images obtained from the electron microprobe insure the highest quality of mineral separation. Second, geochemical characterization of samples prior to $^{40}Ar/^{39}Ar$ analysis allows for recognition of any geochemical variation within the samples, which may be the result of alteration or geochemical contamination that would degrade the quality of geochronology results.

Irradiations and Correction Factors

Between 20 and 35 mg of the samples selected for dating were placed into 20-hole machined aluminum disks. To monitor neutron fluxes, the interlabratory standard FC-2 (28.02 Ma) (Renne et al., 1998) was placed in every other hole. In addition to unknowns and monitors, CaF_2 and K-glass were irradiated to determine calcium and potassium correction factors. Samples were irradiated at either the USGS Triga reactor in the NM-202H position for 6 hrs or the Nuclear Science reactor at the Texas A & M University in the NM-192A and B position for 7 hrs, the NM-196K,L, and M position for 8.85 hrs, the NM-203H position for 7.03 hrs, or the NM-208 K,L, and M position for 7 hrs. Following irradiation, J-values were determined by fusing 5 to 6 single grains of FC-2 from each hole for each tray. J-values were then calculated by assigning mean ages for each hole, fitting a sine curve to the values, and then extrapolating the J-values to the unknowns. Potassium and calcium correction factors were determined by fusing 4 to 5 grains of the CaF_2 and K-glass and the weighted mean averages are: NM-192: $(^{36}Ar/^{37}Ar)_{Ca}$ = 0.00028±0.00001; $(^{39}Ar/^{37}Ar)_{Ca}$ = 0.0007±0.00002; $(^{38}Ar/^{39}Ar)_{K}$ = 0.126±4.00e-4; $(^{40}Ar/^{39}Ar)_{K}$ = 0.00±4.00e-4: NM-196: $(^{36}Ar/^{37}Ar)_{Ca}$ = 0.000277±2.00e-6; $(^{39}Ar/^{37}Ar)_{Ca}$ = 0.000676±4.00e-6; $(^{38}Ar/^{39}Ar)_{K}$ = 0.013±.0005; $(^{40}Ar/^{39}Ar)_{K}$ = 0.00±4.00e-4: NM-202: $(^{36}Ar/^{37}Ar)_{Ca}$ = 0.00028±0.00002; $(^{39}Ar/^{37}Ar)_{Ca}$ = 0.0007±0.00005; $(^{38}Ar/^{39}Ar)_{K}$ = 0.013±0.001; $(^{40}Ar/^{39}Ar)_{K}$ = 0.01±0.002: NM-203: $(^{36}Ar/^{37}Ar)_{Ca}$ = 0.00028±0.00001; $(^{39}Ar/^{37}Ar)_{Ca}$ = 0.00068±0.00002; $(^{38}Ar/^{39}Ar)_{K}$ =

0.0.013±0.001; $(^{40}Ar/^{39}Ar)_K$ = 0.00±4.00e-4: NM-208: $(^{36}Ar/^{37}Ar)_{Ca}$ = 0.00028±0.00001; $(^{39}Ar/^{37}Ar)_{Ca}$ = 0.00068±0.00002; $(^{38}Ar/^{39}Ar)_K$ = 0.013±0.0005; $(^{40}Ar/^{39}Ar)_K$ = 0.00±4.00e-4.

Extraction line and mass spectrometer

All $^{40}Ar/^{39}Ar$ dating was performed at New Mexico Institute of Mining and Technology in the New Mexico Geochronology Research Laboratory. Samples were either incrementally heated using a double-vacuum Molybdenum resistance furnace (hornblende, biotite, K-Feldspar) or fused using a Synrad 50W CO_2 laser (sanidine). Temperature control on the furnace was accomplished by melting Cu-foil for calibration. Following furnace-step heating, gas was expanded into a two-stage extraction line. The first stage contains a SAES GP-50 getter pump, operated at 450°C, where the gas was cleaned before being expanded into the second stage and isolated from the first stage. The second stage contains two SAES GP-50 getter pumps, one operated at room temperature and the other at 450°C, as well as a tungsten filament operated at 2000°C. Clean gas is then expanded into the mass spectrometer and isolated from the second stage. Extracted gas from the laser is expanded into the second stage, but first cleaned using a cold-finger operated at -140. Once in the second stage, the gas is treated similarly to the furnace gas as described above.

Isotopic ratios were measured on a MAP-215 50 mass spectrometer with an extended geometry and an effective radius of 30 cm. The mass spectrometer was equipped with a Nier type ion source and used both a Johnston electron multiplier and Faraday collectors, with the electron multiplier operating at 2.2 kV and a gain of

approximately 10,000 over the Faraday. Resolution for mass 40 was approximately 600 during the analysis. Air pipette analysis were conducted to determine the mass discrimination, which were 1.00297±0.00095 to 1.00323±0.00095 for NM192, 0.99582±0.00086 to 0.99720±0.00084 for NM-196, 1.00141±0.00070 to 1.00216±0.00065 for NM-202, 1.00141±0.00070 for NM-203, and 1.00449±0.00058 for NM-208. Sensitivities (mol/pA) of the furnace and laser, respectively, during the course of this project were 2.5100e-16 to 2.6500e-16 and 1.4400e-16 to1.5200e-16 for NM-192, 1.2299e-16 to 1.2700e-16 and 7.0600e-17 to 7.9200e-17 for NM-196, 8.7329e-17 to 8.9676e-17 and 5.0100e-17 to 5.1500e-17 for NM-202, 8.9676e-17 and 5.15e-17 for NM-203, and 8.7771e-17 and 6.4200e-17 for NM-208.

Single-Crystal Laser-Fusion

Single crystals of the monitors and unknown sanidine were loaded into a 221-hole laser tray and were fused by the CO_2 laser. The laser power was between 1.8-3.3 watts for 15 to 20 seconds. After examination of peak regression to determine if any cycles should be removed, blanks and background were averaged by taking the average ± standard deviation. Blanks and background for the CO_2 laser averaged 330, 8.10, 1.41, 4.29, 5.52, 29 x 10^{-18} at masses 40, 39, 38, 37, and 36 respectively for the duration of this study.

Furnace Step-Heating

Unknowns to be heated in the furnace were weighed and wrapped in high purity copper foil packets. Sample weights varied as follows: 5.4 to 9.8 mg for biotite, 12.75 to

15.15 mg for hornblende, and 9.03 to 19.2 mg for K-feldspar. Heating schedules varied for each phase. Biotite samples were heated using 11 steps, beginning at 650°C, increasing in 50 to 100°C step intervals, and ending with total fusion. Hornblende samples were also step heated using 11 increments, but began at higher temperature and had 20-30°C intervals for the bulk of the heating schedule.

K-feldspars were heated using two different heating schedules, both containing isothermal duplicate steps designed to decrepitate fluid inclusions known to host excess argon. The MZQ K-feldspars were intended to be thermally modeled, thus were heated using a more robust schedule designed to optimize the $\%^{39}Ar_K$ released before melting begins, ending volume diffusion (i.e. volume diffusion ends). In order to extract maximum $^{39}Ar_K$ prior to melting, heating schedules began at lower temperatures, involved isothermal duplicate steps throughout the entire analysis, contain as many as four 1100°C steps, and the time at temperature varied from as little as ten minutes to as much as 2 hours. A similar process of peak regression handling used for laser samples was applied to furnace samples. Blanks for biotite and hornblende were measured every three to four heating steps and in the case in which numerous samples were ran continuously, blanks corrects were calculated using average ± standard deviation. K-feldspar contained no blanks during the analysis, in an attempt to keep the furnace at temperature, and thus bracketing or preceding blanks were used. Total blanks + backgrounds for the furnace averaged 1290, 20.7, 3.63, 9.68, 7.29×10^{-18} at masses 40, 39, 38, 37, and 36 respectively during the course of this study.

Age assignments

Ages were calculated using the FC-2 flux monitor with an assigned age of 28.02 Ma (Renne et al., 1998) and a total ^{40}K decay constant of $5.543e^{-10}$ derived by Steiger and Jager (1977). Samples heated in the furnace are plotted on age spectra as $\%^{39}Ar$ released vs. apparent age. Additionally, the age spectra are plotted along with auxiliary K/Ca and radiogenic yield plots. A plateau age was assigned to samples that yielded three or more contiguous step that comprise 50% of more the spectrum and overlap at two sigma. The plateau age is calculated by weighting each of the steps by the inverse of the variance. For analyses not yielding a plateau, the total gas was used to approximate the age. The total gas age was calculated by summing all gas fractions from the steps. Because several of the K-feldspar age spectra yield complex, monotonically increasing ages without a plateau, no weighted mean age was assigned to these spectra.

Laser heated samples are plotted on age probability diagram as apparent age vs. the summation of the normal probability distribution of the individual analysis. Radiogenic yields, K/Ca, and ^{39}Ar mole auxiliary plots are included with the age probability diagrams. After removal of any xenocrystic or problematic ages, the age was calculated by using the inverse variance of the age for each analysis. Errors for both the furnace and laser analysis were calculated using the methods of Taylor (1982). Isochron ages, MSWD, and errors where the MSWD values are $\leq$ 1are calculated using method of York (1969). When the MSWD is > 1, the error is multiplied by the square root of the MSWD.

Analytical parameter summary

	NM-192	NM-196	NM-202	NM-203	NM-208
Location	Texas A&M	Texas A&M	USGS Triga	Texas A&M	Texas A&M
Time (hrs)	7	8.85	6	7.03	7
$(^{36}Ar/^{37}Ar)_{Ca}$	$2.80e^{-4}\pm1e^{-5}$	$2.77e^{-4}\pm2e^{-6}$	$2.80e^{-4}\pm2e^{-5}$	$2.80e^{-4}\pm1e^{-5}$	$2.80e^{-4}\pm1e^{-5}$
$(^{39}Ar/^{37}Ar)_{Ca}$	$7.00e^{-4}\pm2e^{-5}$	$6.76e^{-4}\pm4e^{-4}$	$7.00e^{-4}\pm5e^{-5}$	$6.80e^{-4}\pm2e^{-5}$	$6.80e^{-4}\pm2e^{-5}$
$(^{38}Ar/^{39}Ar)_{K}$	$1.26e^{-1}\pm4e^{-4}$	$1.30e^{-2}\pm5e^{-4}$	$1.30e^{-2}\pm1e^{-3}$	$1.30e^{-2}\pm1e^{-3}$	$1.30e^{-2}\pm5e^{-4}$
$(^{40}Ar/^{39}Ar)_{K}$	$0.00\pm4e^{-4}$	$0.00\pm4e^{-4}$	$1.00e^{-2}\pm2e^{-3}$	$0.00\pm4e^{-4}$	$0.00\pm4e^{-4}$
Discrimination	$1.00297\pm9.5e^{-4}$ - $1.00323\pm9.5e^{-4}$	$0.99583\pm8.6e^{-4}$ - $0.9972\pm8.4e^{-4}$	$1.00141\pm7.0e^{-4}$ - $1.00216\pm6.5e^{-4}$	$1.00141\pm7.0e^{-4}$	$1.00449\pm5.8e^{-4}$
Furnace Sensitivity (mol/pA)	$2.51e^{-16}$ - $2.65e^{-16}$	$1.23e^{-16}$ - $1.26e^{-16}$	$8.73e^{-17}$ - $8.97e^{-17}$	$8.97e^{-17}$	$8.78e^{-17}$
Laser Sensitivity (mol/pA)	$1.44e^{-16}$ - $1.52e^{-16}$	$7.06e^{-17}$ - $7.92e^{-17}$	$5.01e^{-17}$ - $5.15e^{-17}$	$5.15e^{-17}$	$6.64e^{-17}$

Table 1- Summary of the irradiation parameters, discrimination, and sensitivity for each of the five irradiations used in this study.

APPENDIX B

Appendix B contains the data tables for all the analyses of this study. Table 1 contains the single-crystal laser-fusion analyses, table 2 contains the biotite, hornblende, and groundmass concentrate analyses, and table 3 contains the K-feldspar analyses.

Table 2. Sanidine $^{40}Ar/^{39}Ar$ analytical data.

	ID	$^{40}Ar/^{39}Ar$	$^{37}Ar/^{39}Ar$	$^{36}Ar/^{39}Ar$ (x 10^{-3})	$^{39}Ar_K$ (x 10^{-15} mol)	K/Ca	$^{40}Ar^*$ (%)	Age (Ma)	±1σ (Ma)
	79L-64, Sanidine, J=0.0007386±0.05%, D=1.003±0.001, NM-192A, Lab#=55916								
x	22	18.97	0.0130	0.5696	3.799	39.3	99.1	24.886	0.082
	16	19.01	0.0138	0.3301	8.642	37.1	99.5	25.022	0.054
	18	18.97	0.0133	0.1428	7.582	38.5	99.8	25.052	0.062
	25	19.05	0.0175	0.3965	8.107	29.1	99.4	25.053	0.060
	23	19.02	0.0141	0.2063	10.165	36.3	99.7	25.091	0.043
	20	19.08	0.0166	0.3154	5.615	30.7	99.5	25.123	0.062
	19	19.09	0.0140	0.3327	10.212	36.4	99.5	25.127	0.049
	21	19.04	0.0140	0.1550	7.151	36.5	99.8	25.130	0.058
	24	19.08	0.0157	0.2715	6.060	32.5	99.6	25.138	0.064
	17	19.12	0.0132	0.3743	6.379	38.8	99.4	25.150	0.062
	Mean age ± 2σ	n=9	MSWD=0.63		35.1	±6.9		25.097	0.044
	83L-8, Sanidine, J=0.0007373±0.04%, D=1.003±0.001, NM-192A, Lab#=55915								
	18	19.24	0.0053	0.1408	7.790	96.5	99.8	25.361	0.059
	21	19.23	0.0052	0.1047	10.218	98.3	99.8	25.362	0.052
	16	19.24	0.0052	0.1044	7.530	98.5	99.8	25.378	0.061
	23	19.26	0.0045	0.1290	8.402	112.6	99.8	25.386	0.051
	17	19.38	0.0051	0.4987	5.825	100.4	99.2	25.406	0.072
	22	19.28	0.0051	0.1136	7.502	100.2	99.8	25.425	0.058
	20	19.28	0.0056	0.0779	8.743	90.6	99.9	25.432	0.049
	19	19.27	0.0053	0.0219	12.718	95.9	100.0	25.445	0.046
	Mean age ± 2σ	n=8	MSWD=0.39		99.1	±12.6		25.402	0.044
	82L-42H, Sanidine, J=0.0007363±0.04%, D=1.003±0.001, NM-192A, Lab#=55914								
	23	19.12	0.0100	0.1102	7.351	51.0	99.8	25.181	0.058
	24	19.17	0.0107	0.1160	11.610	47.7	99.8	25.244	0.048
	18	19.18	0.0107	0.0927	11.251	47.6	99.9	25.264	0.052
	17	19.19	0.0102	0.1366	9.240	49.8	99.8	25.265	0.048
	20	19.23	0.0107	0.2095	9.449	47.6	99.7	25.290	0.046
	16	19.22	0.0110	0.0986	9.416	46.3	99.9	25.315	0.056
	21	19.27	0.0107	0.2666	10.898	47.5	99.6	25.322	0.049
	22	19.34	0.0101	0.2749	7.772	50.7	99.6	25.403	0.067
	19	19.30	0.0098	0.0026	8.260	52.2	100.0	25.461	0.064
	Mean age ± 2σ	n=9	MSWD=1.95		48.9	±4.1		25.295	0.054
	82L-31, Sanidine, J=0.000736±0.04%, D=1.003±0.001, NM-192A, Lab#=55913								
x	17	19.77	0.0124	2.817	3.512	41.1	95.8	24.979	0.089
x	20	19.13	0.0126	0.5329	3.802	40.6	99.2	25.023	0.087
	16	19.14	0.0134	0.1813	5.532	38.2	99.7	25.168	0.070
	21	19.36	0.0147	0.8500	3.541	34.6	98.7	25.203	0.091
	22	19.43	0.0134	1.033	5.737	38.1	98.4	25.223	0.073
	18	19.23	0.0127	0.3131	5.435	40.3	99.5	25.235	0.063
	19	19.30	0.0141	0.4503	4.317	36.3	99.3	25.274	0.078
	Mean age ± 2σ	n=5	MSWD=0.28		37.5	±4.3		25.220	0.069
	82L-38, Sanidine, J=0.0007378±0.05%, D=1.003±0.001, NM-192A, Lab#=55911								
	18	19.31	0.0115	1.195	4.101	44.3	98.2	25.060	0.082
	22	19.48	0.0133	1.507	6.135	38.5	97.7	25.159	0.078
	24	19.48	0.0127	1.337	5.146	40.1	98.0	25.222	0.074

	17	19.36	0.0119	0.9208	5.916	42.8	98.6	25.233	0.071
	20	19.51	0.0122	1.350	4.045	41.7	98.0	25.264	0.081
	23	19.28	0.0125	0.5015	6.476	40.7	99.2	25.287	0.063
	25	19.40	0.0133	0.9054	7.060	38.3	98.6	25.287	0.066
	21	19.29	0.0129	0.5082	5.657	39.5	99.2	25.295	0.063
	19	19.33	0.0116	0.5751	5.309	44.0	99.1	25.326	0.066
	16	19.37	0.0117	0.6445	7.418	43.6	99.0	25.348	0.059
	Mean age ± 2σ	n=10	MSWD=1.33			41.3 ±4.5		25.262	0.055
	82L-37, Sanidine, J=0.0007365±0.05%, D=1.003±0.001, NM-192A, Lab#=55912								
	17	20.32	0.0103	4.056	4.725	49.7	94.1	25.231	0.080
	21	20.68	0.0133	5.133	4.592	38.3	92.7	25.282	0.095
	25	20.63	0.0119	4.942	5.113	42.8	92.9	25.290	0.088
	20	20.01	0.0119	2.866	3.388	43.0	95.8	25.29	0.10
x	22	22.84	0.0115	12.38	2.879	44.4	84.0	25.31	0.12
x	19	20.66	0.0127	4.644	6.462	40.2	93.4	25.453	0.073
x	24	20.37	0.0140	3.568	2.759	36.3	94.8	25.48	0.12
x	23	20.17	0.0125	2.881	3.551	40.8	95.8	25.490	0.092
x	16	21.11	0.0106	6.025	6.037	48.2	91.6	25.504	0.078
x	18	20.80	0.0130	4.415	4.543	39.4	93.7	25.726	0.084
	Mean age ± 2σ	n=4	MSWD=0.12			43.5 ±9.4		25.27	0.09
	78L-183, Sanidine, J=0.000739±0.05%, D=1.003±0.001, NM-192A, Lab#=55910								
	24	18.94	0.0019	0.4213	2.724	264.9	99.3	24.91	0.11
	18	18.93	0.0033	0.1172	3.424	156.9	99.8	25.014	0.094
	16	19.08	0.0029	0.6076	3.602	174.4	99.1	25.031	0.086
	21	19.05	0.0048	0.3055	3.257	105.8	99.5	25.103	0.089
	25	19.17	0.0034	0.6228	3.442	151.3	99.0	25.135	0.094
	22	19.12	0.0052	0.3946	2.911	98.2	99.4	25.16	0.10
	19	19.17	0.0035	0.4083	4.337	146.8	99.4	25.222	0.082
	20	19.10	0.0035	0.1838	3.014	144.0	99.7	25.222	0.098
	17	19.18	0.0054	0.2873	3.418	94.3	99.6	25.278	0.092
x	23	19.26	0.0031	-0.1042	4.215	162.4	100.2	25.545	0.084
	Mean age ± 2σ	n=9	MSWD=1.53			148.5 ±104.0		25.13	0.08
	TPS04, Sanidine, J=0.0009001±0.05%, D=1.002±0.001, NM-196K, Lab#=56274								
	09	15.66	0.0035	0.6321	10.089	146.3	98.8	24.948	0.065
	04	15.85	0.0033	1.010	4.169	154.7	98.1	25.08	0.13
	14	15.62	0.0044	0.2464	7.304	116.8	99.5	25.079	0.078
	15	15.64	0.0055	0.2129	16.564	92.7	99.6	25.116	0.053
	02	15.95	0.0053	1.235	3.246	95.5	97.7	25.13	0.17
	07	15.68	0.0024	0.2871	6.487	210.6	99.5	25.151	0.088
	08	15.66	0.0029	0.2169	5.777	175.4	99.6	25.154	0.096
	03	15.87	0.0037	0.9111	5.835	137.1	98.3	25.164	0.098
	10	15.66	0.0028	0.1261	9.041	181.3	99.8	25.188	0.068
	05	15.69	0.0022	0.2018	6.486	230.7	99.6	25.208	0.090
	11	15.78	0.0023	0.4854	3.676	219.7	99.1	25.22	0.14
	01	15.82	0.0033	0.5885	3.852	152.6	98.9	25.22	0.14
	13	15.73	0.0025	0.1550	9.388	201.7	99.7	25.297	0.064
	12	15.85	0.0024	0.4987	3.495	215.7	99.1	25.31	0.15
	06	15.86	0.0038	0.4147	5.682	134.2	99.2	25.379	0.098
	Mean age ± 2σ	n=15	MSWD=1.74			164.3 ±90.1		25.157	0.064
	MZQ-7, Sanidine, J=0.0009002±0.06%, D=1.002±0.001, NM-196K, Lab#=56276								
x	26	15.68	0.0112	1.278	3.513	45.6	97.6	24.679	0.059
x	14	15.84	0.0074	1.700	3.783	68.9	96.8	24.74	0.10
	25	15.68	0.0068	0.9713	5.592	75.5	98.2	24.822	0.054
	13	15.73	0.0053	1.105	6.336	95.9	97.9	24.844	0.072

	04	15.87	0.0105	1.530	5.616	48.4	97.2	24.870	0.084
	05	16.09	0.0057	2.199	8.990	89.5	96.0	24.901	0.062
	09	15.68	0.0043	0.7708	10.258	118.2	98.5	24.916	0.057
	10	15.69	0.0033	0.8058	10.780	153.0	98.5	24.926	0.060
	32	15.79	0.0064	1.110	5.073	79.5	97.9	24.942	0.051
	34	15.66	0.0064	0.6422	9.799	79.5	98.8	24.944	0.042
	08	15.90	0.0054	1.449	6.020	94.6	97.3	24.947	0.074
	27	15.68	0.0067	0.7054	6.994	75.8	98.7	24.956	0.044
	06	15.66	0.0041	0.6144	17.066	123.3	98.8	24.964	0.045
	15	15.83	0.0070	1.189	6.310	72.9	97.8	24.969	0.071
	24	15.62	0.0050	0.4188	11.767	101.8	99.2	24.989	0.038
	29	15.73	0.0062	0.7898	7.631	82.8	98.5	24.991	0.045
	30	15.66	0.0066	0.5600	10.519	77.1	98.9	24.998	0.045
	23	15.79	0.0070	0.9610	6.263	72.5	98.2	25.006	0.047
	03	15.76	0.0030	0.8464	13.675	170.1	98.4	25.009	0.051
	01	15.83	0.0054	1.094	8.273	94.0	98.0	25.013	0.060
	12	15.74	0.0023	0.7951	13.047	219.0	98.5	25.013	0.053
	11	15.95	0.0051	1.478	7.640	100.2	97.3	25.015	0.062
	07	15.73	0.0036	0.7110	13.558	142.8	98.7	25.024	0.051
	28	15.77	0.0051	0.8593	14.374	100.0	98.4	25.024	0.041
	02	15.73	0.0034	0.6994	18.021	149.2	98.7	25.029	0.045
	22	15.68	0.0035	0.5387	18.804	146.6	99.0	25.037	0.037
	35	16.04	0.0068	1.712	8.069	75.5	96.9	25.060	0.047
	31	15.90	0.0049	1.166	7.476	105.1	97.8	25.091	0.045
	33	15.99	0.0056	1.457	6.674	91.7	97.3	25.092	0.048
	Mean age ± 2σ	n=27	MSWD=1.54			105.0 ±74.8		24.990	0.038
	MZQ-25, Sanidine, J=0.0009017±0.09%, D=1.002±0.001, NM-196K, Lab#=56279								
x	06	16.11	0.0123	3.262	1.874	41.6	94.0	24.47	0.45
	13	16.03	0.0103	2.715	3.682	49.6	95.0	24.60	0.23
x	05	16.80	0.0086	5.204	3.063	59.3	90.9	24.67	0.28
	10	16.02	0.0144	2.205	2.437	35.4	95.9	24.83	0.35
	12	15.86	0.0080	1.678	4.327	63.7	96.9	24.83	0.20
	11	15.82	0.0064	1.359	7.291	79.9	97.5	24.90	0.12
	09	15.99	0.0083	1.840	4.301	61.3	96.6	24.96	0.20
	08	15.87	0.0073	1.413	4.681	69.9	97.4	24.97	0.18
	03	15.89	0.0076	1.468	5.118	67.4	97.3	24.97	0.17
	14	15.70	0.0075	0.7253	11.833	67.7	98.6	25.021	0.083
x	07	16.88	0.0122	4.711	1.715	41.9	91.8	25.02	0.49
	02	16.06	0.0083	1.892	4.808	61.6	96.5	25.05	0.18
	04	15.81	0.0061	1.027	10.311	83.9	98.1	25.054	0.094
	01	16.06	0.0062	1.865	7.903	82.6	96.6	25.06	0.11
	15	16.00	0.0049	1.646	11.424	103.9	97.0	25.063	0.086
	Mean age ± 2σ	n=12	MSWD=0.55			68.9 ±35.1		25.001	0.087
	MZQ-4, Sanidine, J=0.0008999±0.05%, D=1.002±0.001, NM-196K, Lab#=56275								
x	01	63.39	0.0112	162.2	14.975	45.6	24.4	24.93	0.36
x	13	76.50	0.0109	206.6	7.255	46.7	20.2	24.94	0.46
x	14	37.33	0.0154	73.59	11.590	33.2	41.8	25.13	0.19
	02	16.42	0.0115	2.746	3.994	44.3	95.1	25.17	0.14
x	03	28.74	0.0102	44.26	15.166	49.9	54.5	25.25	0.13
	06	15.85	0.0106	0.6221	6.769	48.1	98.8	25.260	0.086
x	12	27.59	0.0116	40.32	11.934	43.9	56.8	25.28	0.13
x	11	19.56	0.0112	13.13	6.617	45.7	80.2	25.29	0.11
	05	17.47	0.0132	5.927	4.970	38.8	90.0	25.34	0.12
	15	16.10	0.0109	1.272	3.032	46.9	97.7	25.35	0.17
x	08	22.31	0.0106	22.17	8.149	47.9	70.6	25.41	0.11
x	07	25.45	0.0113	32.57	7.131	45.1	62.2	25.51	0.15
x	09	20.17	0.0149	14.66	8.355	34.1	78.5	25.533	0.098

x	10	18.12	0.0101	7.725	8.134	50.7	87.4	25.534	0.088
	04	16.30	0.0102	1.201	2.430	50.0	97.8	25.70	0.22
	Mean age ± 2σ	n=5	MSWD=1.17			45.6 ±8.7		25.301	0.125
	MZQ-17, Sanidine, J=0.0009007±0.08%, D=1.002±0.001, NM-196K, Lab#=56277								
x	06	17.57	0.0076	1.549	4.028	67.4	97.4	27.59	0.10
x	11	18.25	0.0068	3.599	5.857	75.6	94.2	27.721	0.083
x	12	18.41	0.0075	4.045	15.369	67.8	93.5	27.768	0.054
	09	17.91	0.0082	2.335	10.220	62.3	96.2	27.769	0.064
x	05	18.90	0.0078	5.667	6.299	65.8	91.1	27.774	0.082
	13	17.91	0.0070	2.191	23.866	73.0	96.4	27.832	0.045
	04	17.68	0.0053	1.398	17.867	97.1	97.7	27.842	0.053
	07	17.59	0.0062	1.067	7.104	82.8	98.2	27.859	0.068
	15	17.83	0.0150	1.858	10.200	34.0	96.9	27.864	0.063
	08	17.78	0.0062	1.704	7.407	82.5	97.2	27.864	0.068
	10	17.86	0.0079	1.955	5.898	64.4	96.8	27.866	0.079
	03	18.07	0.0115	2.632	12.429	44.5	95.7	27.881	0.056
	02	17.69	0.0093	1.274	18.240	55.0	97.9	27.925	0.051
	14	17.58	0.0077	0.8843	9.476	66.2	98.5	27.927	0.056
	01	17.61	0.0111	0.7546	23.965	46.1	98.7	28.031	0.044
	Mean age ± 2σ	n=11	MSWD=1.80			64.3 ±37.8		27.890	0.062
	MZQ-26, Sanidine, J=0.0009019±0.08%, D=1.002±0.001, NM-196K, Lab#=56280								
	13	16.19	0.0072	2.260	10.320	71.2	95.9	25.088	0.093
	06	15.92	0.0085	1.253	7.971	59.7	97.7	25.13	0.11
	09	16.44	0.0096	2.992	13.155	53.3	94.6	25.130	0.081
	03	16.00	0.0076	1.456	14.677	67.4	97.3	25.151	0.071
	14	16.03	0.0066	1.538	15.910	77.0	97.2	25.172	0.071
	15	15.97	0.0067	1.324	7.343	75.6	97.6	25.17	0.12
	07	16.28	0.0060	2.177	21.142	84.6	96.1	25.261	0.060
	12	16.08	0.0059	1.482	19.916	85.8	97.3	25.267	0.059
	10	16.06	0.0057	1.413	26.981	89.4	97.4	25.281	0.049
	02	15.91	0.0083	0.8955	9.170	61.7	98.3	25.29	0.10
	05	16.32	0.0067	2.238	29.364	75.9	96.0	25.299	0.051
	04	16.11	0.0069	1.490	20.969	74.1	97.3	25.314	0.059
	08	16.50	0.0061	2.820	23.165	83.1	95.0	25.318	0.058
	11	16.12	0.0063	1.503	26.666	81.2	97.2	25.322	0.052
	01	15.99	0.0056	0.9424	29.617	91.4	98.3	25.393	0.047
	Mean age ± 2σ	n=15	MSWD=1.67			75.4 ±22.3		25.274	0.059
	MZQ-22, Sanidine, J=0.0009013±0.09%, D=1.002±0.001, NM-196K, Lab#=56278								
x	06	15.97	0.0181	2.550	3.743	28.2	95.3	24.57	0.11
x	16	15.84	0.0198	1.895	3.636	25.7	96.5	24.670	0.069
	03	15.85	0.0155	1.732	5.554	32.9	96.8	24.764	0.081
	12	15.82	0.0157	1.603	7.306	32.6	97.0	24.780	0.067
	05	15.69	0.0146	1.152	7.908	34.9	97.8	24.791	0.059
	22	15.72	0.0182	1.245	4.618	28.1	97.7	24.798	0.056
	18	15.59	0.0154	0.7464	10.691	33.1	98.6	24.813	0.045
	26	15.67	0.0153	1.041	9.794	33.4	98.0	24.813	0.043
	07	15.85	0.0136	1.624	12.129	37.5	97.0	24.820	0.055
	09	15.80	0.0149	1.431	5.942	34.3	97.3	24.828	0.079
	02	15.71	0.0175	1.132	9.241	29.2	97.9	24.831	0.055
	14	15.80	0.0129	1.439	12.524	39.5	97.3	24.837	0.054
	13	15.75	0.0163	1.226	7.688	31.3	97.7	24.856	0.063
	27	15.62	0.0176	0.7665	7.559	29.0	98.6	24.857	0.040
	17	15.76	0.0169	1.190	8.067	30.1	97.8	24.879	0.043
	04	15.88	0.0119	1.590	13.091	42.8	97.0	24.880	0.049
	15	15.67	0.0158	0.8915	11.465	32.3	98.3	24.888	0.055

19	15.91	0.0169	1.671	5.316	30.1	96.9	24.895	0.056
10	15.78	0.0158	1.241	11.482	32.3	97.7	24.896	0.051
20	15.83	0.0192	1.400	6.289	26.5	97.4	24.903	0.050
28	15.65	0.0140	0.7668	7.005	36.5	98.6	24.904	0.044
25	15.60	0.0137	0.5409	10.607	37.1	99.0	24.931	0.045
08	15.70	0.0128	0.8828	23.426	39.9	98.3	24.939	0.047
21	15.73	0.0173	0.8892	7.233	29.5	98.3	24.974	0.048
01	15.67	0.0205	0.6876	13.634	24.9	98.7	24.983	0.050
24	15.87	0.0231	1.334	8.621	22.1	97.5	24.988	0.045
23	15.94	0.0152	1.551	9.355	33.5	97.1	24.996	0.040
Mean age ± 2σ		n=25	MSWD=1.76		32.5 ±9.6		24.885	0.051

MZQ-35, Sanidine, J=0.0007927±0.04%, D=1.0068±0.0015, NM-208L, Lab#=57184

14	17.64	0.0099	0.4045	2.764	51.7	99.3	24.881	0.064
13	17.72	0.0143	0.5639	1.753	35.6	99.1	24.934	0.084
05	17.61	0.0103	0.1784	6.975	49.4	99.7	24.938	0.051
06	17.72	0.0126	0.4100	1.891	40.5	99.3	24.990	0.080
07	17.66	0.0118	0.2131	2.862	43.1	99.6	24.994	0.063
12	17.73	0.0117	0.4382	2.284	43.8	99.3	25.002	0.069
09	17.87	0.0130	0.8449	2.372	39.3	98.6	25.023	0.066
17	17.69	0.0100	0.1956	2.791	51.0	99.7	25.043	0.062
10	17.84	0.0078	0.7047	2.252	65.4	98.8	25.044	0.068
16	17.72	0.0100	0.3026	2.333	51.0	99.5	25.044	0.071
08	17.74	0.0081	0.2932	2.548	63.1	99.5	25.073	0.065
15	17.72	0.0091	0.2094	2.650	56.2	99.7	25.074	0.070
11	17.73	0.0119	0.1137	4.142	42.9	99.8	25.139	0.058
Mean age ± 2σ		n=13	MSWD=1.21		48.7 ±18.0		25.014	0.045

Notes:

Isotopic ratios corrected for blank, radioactive decay, and mass discrimination, not corrected for interfering reactions.
Errors quoted for individual analyses include analytical error only, without interfering reaction or J uncertainties.
Mean age is weighted mean age of Taylor (1982). Mean age error is weighted error of the mean (Taylor, 1982), multiplied by the root of the MSWD where MSWD>1, and also incorporates uncertainty in J factors and irradiation correction uncertainties.
Decay constants and isotopic abundances after Steiger and Jäger (1977).
symbol preceding sample ID denotes analyses excluded from mean age calculations.
Ages calculated relative to FC-2 Fish Canyon Tuff sanidine interlaboratory standard at 28.02 Ma
Decay Constant (LambdaK (total)) = 5.543e-10/a
Correction factors:

$(^{39}Ar/^{37}Ar)_{Ca}$ = 0.00068 ± 2e-05
$(^{36}Ar/^{37}Ar)_{Ca}$ = 0.00028 ± 1e-05
$(^{38}Ar/^{39}Ar)_{K}$ = 0.013
$(^{40}Ar/^{39}Ar)_{K}$ = 0 ± 0.0004

Table 3. Biotite, hornblende, and groundmass $^{40}Ar/^{39}Ar$ analytical data.

	ID	Temp (°C)	$^{40}Ar/^{39}Ar$	$^{37}Ar/^{39}Ar$	$^{36}Ar/^{39}Ar$ (x 10^{-3})	$^{39}Ar_K$ (x 10^{-15} mol)	K/Ca	$^{40}Ar^*$ (%)	^{39}Ar (%)	Age (Ma)	±1σ (Ma)
	MZQ-24, Biotite, 7.33 mg, J=0.0013622±0.07%, D=1.002±0.001, NM-202H, Lab#=56745-01										
X	A	650	199.0	0.2005	621.4	0.327	2.5	7.8	0.3	37.5	4.3
	B	750	35.14	0.0473	84.22	0.305	10.8	29.2	0.6	25.0	3.4
	C	850	15.89	0.0164	16.55	2.62	31.2	69.2	3.0	26.82	0.42
	D	920	12.76	0.0106	4.672	9.41	48.2	89.2	11.5	27.74	0.12
	E	1000	11.88	0.0063	1.426	20.3	80.5	96.5	30.0	27.931	0.068
	F	1075	11.76	0.0088	1.306	22.2	57.7	96.7	50.2	27.723	0.066
	G	1110	11.80	0.0138	1.553	8.05	36.9	96.1	57.5	27.63	0.14
	H	1180	11.94	0.0461	1.845	10.58	11.1	95.5	67.2	27.79	0.11
	I	1210	11.78	0.0553	1.284	11.17	9.2	96.8	77.3	27.79	0.10
	J	1250	11.69	0.0714	1.155	19.1	7.1	97.1	94.8	27.663	0.068
	K	1300	11.81	0.1299	1.047	5.43	3.9	97.5	99.7	28.05	0.20
X	L	1720	21.87	19.02	47.50	0.335	0.027	43.0	100.0	23.3	3.1
	Integrated age ± 2σ			n=12	MSWD=2.27	109.8	5.4		K2O=4.23%	27.76	0.11
	Plateau ± 2σ	steps B-K		n=10	MSWD=1.96	109.2	37.8 ±51.9		99.4	27.765	0.096
	Isochron±2σ	steps A-L		n=12	MSWD=2.25		$^{40}Ar/^{36}Ar$=	299.5±5.4		27.750	0.077
	MZQ-15, Biotite, 6.96 mg, J=0.0013622±0.07%, D=1.002±0.001, NM-202H, Lab#=56743-01										
X	A	650	349.5	1.266	1114.2	0.237	0.40	5.8	0.2	49.4	6.4
	B	750	38.59	0.3260	94.00	0.589	1.6	28.1	0.9	26.4	1.9
	C	850	17.23	0.0242	22.42	4.09	21.1	61.5	5.1	25.85	0.29
	D	920	13.23	0.0179	9.716	7.12	28.6	78.3	12.5	25.26	0.16
	E	1000	11.44	0.0190	3.615	8.44	26.8	90.7	21.3	25.30	0.13
	F	1075	11.25	0.0435	2.961	5.44	11.7	92.3	26.9	25.30	0.20
	G	1110	11.37	0.0521	3.629	4.26	9.8	90.6	31.3	25.11	0.25
	H	1180	11.65	0.0984	4.320	9.27	5.2	89.1	41.0	25.31	0.12
	I	1210	11.47	0.1520	3.942	14.73	3.4	89.9	56.3	25.149	0.086
	J	1250	10.99	0.0613	2.135	32.9	8.3	94.3	90.5	25.282	0.052
	K	1300	11.04	0.0499	2.022	7.42	10.2	94.6	98.2	25.46	0.15
	L	1720	14.52	5.007	16.32	1.71	0.10	69.6	100.0	24.75	0.62
	Integrated age ± 2σ			n=12	MSWD=2.17	96.2	3.2		K2O=3.90%	25.35	0.13
	Plateau ± 2σ	steps B-L		n=11	MSWD=0.95	96.0	11.1 ±19.7		99.8	25.277	0.079
	Isochron±2σ	steps A-L		n=12	MSWD=0.82		$^{40}Ar/^{36}Ar$=	303.7±4.3		25.21	0.09
	MZQ-16, Biotite, 8.1 mg, J=0.0009044±0.06%, D=1.002±0.001, NM-196M, Lab#=56294-01										
X	A	650	272.2	0.0460	881.1	0.836	11.1	4.3	0.5	19.2	2.6
X	B	750	44.74	0.0347	99.99	1.79	14.7	34.0	1.5	24.63	0.58
X	C	850	28.83	0.0110	46.23	7.45	46.2	52.6	5.8	24.58	0.19
X	D	920	21.40	0.0096	21.70	13.77	53.1	70.0	13.8	24.30	0.11
	E	1000	17.37	0.0100	6.479	15.5	51.1	89.0	22.8	25.039	0.064
	F	1075	16.65	0.0139	4.038	14.05	36.8	92.8	30.9	25.049	0.067
	G	1110	17.08	0.0037	5.303	12.72	136.4	90.8	38.3	25.129	0.071
	H	1180	16.59	0.0128	3.998	35.0	39.8	92.9	58.5	24.971	0.054
	I	1210	16.11	0.0041	2.267	41.6	124.7	95.8	82.6	25.024	0.043
	J	1720	16.40	0.0088	3.288	30.1	58.1	94.1	100.0	25.001	0.052
	Integrated age ± 2σ			n=10	MSWD=6.01	172.8	55.2		K2O=9.06%	24.91	0.11
	Plateau ± 2σ	steps E-J		n=6	MSWD=0.71	149.0	76.3 ±88.5		86.2	25.026	0.055
	Isochron±2σ	steps A-J		n=10	MSWD=3.63		$^{40}Ar/^{36}Ar$=	289.2±2.7		25.05	0.06
	MZQ-39, Biotite, 7.89 mg, J=0.0007729±0.07%, D=1.004±0.001, NM-208M, Lab#=57199-01										

X	A	650	347.5	0.0265	1158.2	0.749	19.3	1.5	0.5	7.4	3.8
X	B	750	56.65	0.0042	139.0	2.290	120.2	27.5	2.2	21.6	1.1
	C	850	25.63	0.0020	26.63	12.66	250.7	69.3	11.4	24.59	0.21
	D	920	25.14	0.0021	26.37	12.29	240.7	69.0	20.3	24.03	0.22
	E	1000	23.86	0.0030	21.79	9.31	168.8	73.0	27.1	24.13	0.27
	F	1075	21.06	0.0053	12.14	6.93	96.8	83.0	32.1	24.21	0.34
	G	1110	20.01	0.0045	7.568	7.15	112.5	88.8	37.3	24.61	0.33
	H	1180	20.56	0.0049	9.415	19.69	103.2	86.5	51.6	24.62	0.14
	I	1210	19.47	0.0163	5.453	18.82	31.2	91.7	65.2	24.73	0.14
	J	1250	18.86	0.0042	3.227	27.5	120.7	94.9	85.2	24.794	0.096
	K	1300	18.96	0.0015	3.268	17.41	336.7	94.9	97.8	24.91	0.14
	L	1650	20.48	0.1370	11.61	3.06	3.7	83.3	100.0	23.64	0.77
	Integrated age ± 2σ			n=12	MSWD=4.50	137.9	61.4	K2O=8.69%		24.43	0.17
	Plateau ± 2σ	steps C-L		n=10	MSWD=2.36	134.8	155.7	±206.8	97.8	24.66	0.17
	Isochron±2σ	steps A-L		n=12	MSWD=0.99		$^{40}Ar/^{36}Ar$=	282.7±4.2		24.81	0.13

MZQ-12, Biotite, 8.97 mg, J=0.0007777±0.08%, D=1.004±0.001, NM-208M, Lab#=57195-01

X	A	650	1083.5	0.0826	3656.0	1.116	6.2	0.3	0.7	4.4	7.1
X	B	750	89.11	0.0196	253.5	5.92	26.0	15.9	4.4	19.81	0.72
	C	850	22.56	0.0054	16.96	30.6	93.7	77.8	23.5	24.46	0.11
	D	920	19.52	0.0044	5.900	25.5	115.8	91.1	39.5	24.77	0.11
	E	1000	20.43	0.0073	9.684	18.76	69.5	86.0	51.2	24.48	0.14
	F	1075	21.28	0.0139	12.79	17.89	36.7	82.3	62.4	24.39	0.15
	G	1110	20.21	0.0188	8.464	12.91	27.1	87.6	70.4	24.67	0.20
	H	1180	19.74	0.0620	6.524	16.61	8.2	90.3	80.8	24.83	0.15
	I	1210	19.34	0.2380	5.104	15.55	2.1	92.3	90.5	24.88	0.16
	J	1250	19.05	0.5024	4.157	12.94	1.0	93.8	98.6	24.90	0.19
	K	1300	20.23	0.2139	7.751	1.935	2.4	88.8	99.8	25.0	1.2
	L	1650	61.92	3.181	144.2	0.279	0.16	31.6	100.0	27.3	8.6
	Integrated age ± 2σ			n=12	MSWD=6.11	160.0	6.0	K2O=8.81%		24.34	0.23
	Plateau ± 2σ	steps C-L		n=10	MSWD=1.55	153.0	54.4	±85.5	95.6	24.65	0.13
	Isochron±2σ	steps A-L		n=12	MSWD=2.44		$^{40}Ar/^{36}Ar$=	288.3±2.3		24.73	0.11

MZQ-13, Biotite, 9.16 mg, J=0.0007768±0.07%, D=1.004±0.001, NM-208M, Lab#=57196-01

X	A	650	671.9	0.1529	2270.7	0.994	3.3	0.1	0.6	1.2	4.8
X	B	750	96.46	0.0194	275.8	3.03	26.3	15.5	2.5	20.9	1.0
X	C	850	24.46	0.0059	24.33	16.96	86.8	70.6	13.2	24.04	0.17
	D	920	19.85	0.0038	7.215	25.3	134.7	89.3	29.1	24.66	0.11
	E	1000	20.87	0.0078	11.00	27.7	65.0	84.4	46.6	24.53	0.10
	F	1075	20.02	0.0190	7.400	20.60	26.9	89.1	59.5	24.82	0.13
	G	1110	18.93	0.0241	3.888	13.64	21.1	93.9	68.1	24.75	0.18
	H	1180	18.69	0.0629	3.096	16.51	8.1	95.1	78.5	24.75	0.15
	I	1210	18.32	0.1363	2.179	18.34	3.7	96.5	90.1	24.62	0.14
	J	1250	18.31	0.4015	1.754	13.62	1.3	97.4	98.7	24.82	0.18
	K	1300	19.13	0.2820	3.077	1.819	1.8	95.4	99.8	25.4	1.3
	L	1650	41.36	3.173	83.55	0.320	0.16	40.9	100.0	23.6	7.2
	Integrated age ± 2σ			n=12	MSWD=5.02	158.8	6.8	K2O=8.57%		24.41	0.18
	Plateau ± 2σ	steps D-L		n=9	MSWD=0.61	137.8	45.5	±89.3	86.8	24.68	0.11
	Isochron±2σ	steps A-L		n=12	MSWD=0.96		$^{40}Ar/^{36}Ar$=	286.8±2.6		24.72	0.11

MZQ-5, Biotite, 5.4 mg, J=0.0009051±0.05%, D=1.002±0.001, NM-196L, Lab#=56290-01

X	A	650	608.1	0.0491	2005.7	0.320	10.4	2.5	0.3	25.1	6.0
X	B	750	103.1	0.0056	290.4	1.153	90.9	16.7	1.5	27.9	1.1
	C	850	34.77	0.0036	65.05	5.36	141.0	44.7	7.0	25.21	0.25
	D	920	22.35	0.0016	24.14	7.54	319.7	68.1	14.7	24.68	0.15
	E	1000	18.13	0.0033	9.854	8.53	156.0	83.9	23.4	24.687	0.099
	F	1075	17.13	0.0032	6.119	8.70	158.9	89.4	32.2	24.856	0.096

	G	1110	17.54	0.0027	7.750	7.25	187.3	86.9	39.6	24.739	0.097
	H	1180	16.85	0.0064	5.322	20.6	80.2	90.7	60.7	24.776	0.056
	I	1210	16.03	0.0030	2.527	27.8	169.2	95.3	89.0	24.783	0.055
	J	1720	16.59	0.0345	4.426	10.74	14.8	92.1	100.0	24.797	0.072
	Integrated age ± 2σ			n=10	MSWD=1.54	98.0	70.0	K2O=7.70%		24.83	0.14
	Plateau ± 2σ	steps C-J		n=8	MSWD=0.73	96.6	142.5 ±175.3		98.5	24.779	0.063
	Isochron±2σ	steps A-J		n=10	MSWD=1.12		$^{40}Ar/^{36}Ar$=	298.1±2.5		24.752	0.070
	MZQ-6, Biotite, 7.5 mg, J=0.000905±0.06%, D=1.002±0.001, NM-196L, Lab#=56291-01										
X	A	650	458.8	0.1486	1516.5	1.071	3.4	2.3	0.7	17.4	4.1
X	B	750	40.61	0.0281	88.72	5.17	18.2	35.4	4.3	23.35	0.54
	C	850	23.94	0.0154	30.63	18.5	33.1	62.2	16.9	24.15	0.17
	D	920	19.04	0.0166	13.59	22.1	30.7	78.9	32.0	24.37	0.13
	E	1000	19.66	0.0300	15.07	21.7	17.0	77.4	46.8	24.66	0.14
	F	1075	17.00	0.0302	5.879	20.3	16.9	89.8	60.6	24.76	0.13
	G	1110	16.19	0.0291	3.278	20.9	17.5	94.0	74.9	24.68	0.13
	H	1180	15.80	0.2107	2.295	20.9	2.4	95.8	89.1	24.55	0.13
	I	1210	15.64	0.0864	1.532	13.43	5.9	97.2	98.3	24.64	0.19
	J	1720	19.96	0.2953	15.05	2.52	1.7	77.8	100.0	25.19	0.97
	Integrated age ± 2σ			n=10	MSWD=2.24	146.5	8.2	K2O=8.29%		24.46	0.18
	Plateau ± 2σ	steps C-J		n=8	MSWD=1.74	140.3	17.8 ±23.9		95.7	24.57	0.14
	Isochron±2σ	steps A-J		n=10	MSWD=1.15		$^{40}Ar/^{36}Ar$=	290.9±3.0		24.64	0.12
	AR-171, Biotite, 8.24 mg, J=0.0007723±0.07%, D=1.004±0.001, NM-208M, Lab#=57200-01										
X	A	650	169.2	0.0556	524.3	1.816	9.2	8.4	1.3	19.7	1.8
	B	750	51.79	0.0364	117.6	6.14	14.0	32.9	5.7	23.58	0.49
	C	850	20.69	0.0048	9.836	20.19	105.7	86.0	20.1	24.61	0.13
	D	920	18.81	0.0039	3.704	21.08	131.4	94.2	35.2	24.52	0.12
	E	1000	18.78	0.0183	3.869	9.37	27.8	93.9	41.9	24.41	0.26
	F	1075	19.71	0.1088	7.770	3.71	4.7	88.4	44.5	24.12	0.63
	G	1110	19.19	0.0962	6.486	3.08	5.3	90.1	46.7	23.92	0.75
	H	1180	19.08	0.1229	5.060	9.13	4.2	92.2	53.2	24.35	0.26
	I	1210	18.63	0.0894	3.189	38.1	5.7	95.0	80.4	24.486	0.076
	J	1250	18.28	0.0143	2.107	25.3	35.7	96.6	98.5	24.44	0.11
	K	1300	19.03	0.1384	6.928	1.098	3.7	89.3	99.3	23.5	2.1
	L	1650	38.73	0.5935	71.22	0.977	0.86	45.8	100.0	24.5	2.4
	Integrated age ± 2σ			n=12	MSWD=1.21	140.0	10.2	K2O=8.45%		24.36	0.16
	Plateau ± 2σ	steps B-L		n=11	MSWD=0.61	138.2	46.7 ±90.2		98.7	24.48	0.10
	Isochron±2σ	steps A-L		n=12	MSWD=0.36		$^{40}Ar/^{36}Ar$=	289.5±4.0		24.52	0.11
	MZQ-8, Biotite, 9.85 mg, J=0.0007782±0.08%, D=1.004±0.001, NM-208M, Lab#=57194-01										
X	A	650	177.1	0.4616	555.8	1.197	1.1	7.3	0.7	18.0	2.3
X	B	750	44.03	0.0294	84.40	3.30	17.3	43.4	2.4	26.61	0.80
	C	850	21.40	0.0075	11.74	14.31	68.2	83.8	10.2	25.00	0.18
	D	920	18.50	0.0091	3.343	20.21	55.9	94.7	21.2	24.42	0.15
	E	1000	18.28	0.0230	2.564	15.37	22.2	95.9	29.6	24.43	0.16
	F	1075	18.46	0.0460	2.938	10.60	11.1	95.3	35.4	24.54	0.23
	G	1110	18.38	0.0440	2.642	11.11	11.6	95.8	41.4	24.55	0.22
	H	1180	18.23	0.0652	2.886	29.1	7.8	95.4	57.3	24.239	0.092
	I	1210	17.91	0.1217	1.521	31.0	4.2	97.5	74.2	24.357	0.087
	J	1250	17.77	0.0232	1.160	38.9	22.0	98.1	95.3	24.302	0.078
	K	1300	18.31	0.0170	2.460	8.07	30.0	96.0	99.7	24.51	0.30
	L	1650	34.94	1.531	53.12	0.537	0.33	55.4	100.0	27.0	4.4
	Integrated age ± 2σ			n=12	MSWD=2.97	183.7	9.6	K2O=9.21%		24.43	0.13
	Plateau ± 2σ	steps C-L		n=10	MSWD=1.90	179.2	23.1 ±45.0		97.6	24.377	0.120
	Isochron±2σ	steps A-L		n=12	MSWD=3.23		$^{40}Ar/^{36}Ar$=	294.8±5.6		24.39	0.09

MZQ-34, Biotite, 8.62 mg, J=0.0007737±0.07%, D=1.004±0.001, NM-208M, Lab#=57198-01

	B	750	40.01	0.0161	77.83	2.73	31.6	42.5	1.9	23.59	0.90
	C	850	20.17	0.0038	8.594	19.46	132.7	87.4	15.4	24.44	0.14
	D	920	18.77	0.0041	4.419	16.64	125.4	93.0	27.0	24.22	0.15
	E	1000	18.62	0.0123	3.804	10.68	41.4	94.0	34.4	24.26	0.22
	F	1075	19.17	0.0203	5.861	7.86	25.2	91.0	39.8	24.18	0.30
	G	1110	18.71	0.0160	4.710	10.41	31.8	92.6	47.1	24.02	0.23
	H	1180	18.98	0.0326	5.138	27.4	15.7	92.0	66.1	24.211	0.099
	I	1210	18.25	0.0405	2.737	25.2	12.6	95.6	83.6	24.19	0.10
	J	1250	18.03	0.0111	2.126	18.80	45.9	96.5	96.7	24.13	0.13
	K	1300	18.51	0.0182	3.815	3.25	28.0	93.9	98.9	24.10	0.72
	L	1650	21.72	0.3575	19.46	1.561	1.4	73.7	100.0	22.2	1.5
	Integrated age ± 2σ			n=11	MSWD=0.65	144.0	21.7		K2O=8.29%	24.18	0.13
	Plateau ± 2σ	steps B-L		n=11	MSWD=0.65	144.0	51.6	±87.2	100.0	24.22	0.10
	Isochron±2σ	steps B-L		n=11	MSWD=0.68		$^{40}Ar/^{36}Ar$=	295.4±16.2		24.22	0.15

MZQ-19, Biotite, 9.69 mg, J=0.0007018±0.04%, D=1.002±0.001, NM-203H, Lab#=56825-01

X	A	650	606.9	-0.0050	1961.9	0.188	-	4.5	0.1	34.0	5.7
X	B	750	70.84	0.0919	192.2	2.25	5.6	19.8	1.6	17.71	0.46
X	C	850	25.17	0.0072	28.95	17.2	71.3	66.0	12.8	20.924	0.087
X	D	920	20.17	0.0091	10.79	13.09	56.0	84.2	21.3	21.376	0.068
X	E	1000	19.83	0.0110	8.689	16.3	46.2	87.1	31.9	21.723	0.059
X	F	1075	19.35	0.0227	6.959	24.0	22.5	89.4	47.6	21.761	0.050
X	G	1110	18.42	0.0307	4.422	13.25	16.6	92.9	56.2	21.537	0.050
X	H	1180	17.81	0.0353	3.195	29.4	14.5	94.7	75.4	21.228	0.038
X	I	1210	17.77	0.0628	2.881	19.6	8.1	95.2	88.2	21.297	0.045
X	J	1250	17.79	0.1382	2.623	14.54	3.7	95.7	97.6	21.435	0.048
X	K	1300	18.92	0.1961	6.244	3.64	2.6	90.3	100.0	21.51	0.14
	Integrated age ± 2σ			n=11	MSWD=21.32	153.5	11.9		K2O=8.67%	21.368	0.089
	Plateau ± 2σ	no plateau		n=0	MSWD=0.00	0.000	0.000±0.000		0.0	0.00	0.000
	Isochron±2σ	steps A-K		n=11	MSWD=20.77		$^{40}Ar/^{36}Ar$=	289.3±2.6		21.469	0.044

MZQ-9, Biotite, 7.4 mg, J=0.0009045±0.06%, D=1.002±0.001, NM-196L, Lab#=56292-01

X	A	650	216.6	0.3433	691.0	0.823	1.5	5.7	0.5	20.2	3.4
X	B	750	30.09	0.0380	61.03	7.14	13.4	40.1	5.2	19.58	0.37
X	C	850	15.33	0.0127	8.863	24.6	40.1	82.9	21.3	20.62	0.11
	D	920	13.55	0.0086	1.831	20.3	59.0	96.0	34.5	21.11	0.12
	E	1000	14.14	0.0196	3.643	24.2	26.0	92.4	50.4	21.20	0.11
	F	1075	13.52	0.0414	2.099	25.4	12.3	95.4	67.0	20.927	0.099
	G	1110	13.56	0.0593	2.053	17.8	8.6	95.6	78.6	21.03	0.14
	H	1180	13.38	0.1781	1.237	21.2	2.9	97.4	92.4	21.14	0.11
	I	1210	13.43	0.2858	1.139	9.41	1.8	97.7	98.6	21.28	0.24
	J	1250	13.95	0.6095	4.428	1.91	0.84	91.0	99.8	20.6	1.2
	K	1300	19.90	2.186	22.05	0.290	0.23	68.2	100.0	22.0	7.8
	Integrated age ± 2σ			n=11	MSWD=3.46	153.1	6.6		K2O=8.79%	20.94	0.13
	Plateau ± 2σ	steps D-K		n=8	MSWD=0.70	120.5	19.7	±40.3	78.7	21.08	0.10
	Isochron±2σ	steps A-K		n=11	MSWD=2.57		$^{40}Ar/^{36}Ar$=	288.3±4.8		21.04	0.10

MZQ-21, Biotite, 9.8 mg, J=0.0009044±0.07%, D=1.002±0.001, NM-196M, Lab#=56295-01

X	A	650	351.1	0.0953	1154.0	3.31	5.4	2.9	1.6	16.3	2.6
X	B	750	29.29	0.0228	60.79	9.08	22.4	38.7	6.2	18.38	0.31
X	C	850	23.30	0.0152	40.00	21.4	33.6	49.3	16.8	18.64	0.16
	D	920	18.33	0.0116	22.34	31.5	44.0	64.0	32.4	19.04	0.11
	E	1000	16.51	0.0185	15.68	22.1	27.6	71.9	43.4	19.27	0.12
	F	1075	13.28	0.0181	5.042	33.4	28.2	88.8	60.0	19.145	0.078

	G	1110	12.85	0.0283	3.221	22.8	18.1	92.6	71.3	19.31	0.10
	H	1180	12.56	0.1531	2.360	31.6	3.3	94.5	87.0	19.279	0.078
	I	1210	12.30	0.0615	1.497	19.8	8.3	96.4	96.8	19.25	0.12
	J	1720	14.36	0.2127	6.936	6.36	2.4	85.8	100.0	20.01	0.35
	Integrated age ± 2σ			n=10	MSWD=3.44	201.4	10.0		K2O=8.73%	19.09	0.19
	Plateau ± 2σ	steps D-J		n=7	MSWD=1.67	167.6	21.7 ±30.8		83.2	19.225	0.105
	Isochron±2σ	steps A-J		n=10	MSWD=2.25		$^{40}Ar/^{36}Ar$=	291.7±2.3		19.24	0.09

MZQ-32, Biotite, 8.69 mg, J=0.0007748±0.07%, D=1.004±0.001, NM-208M, Lab#=57197-01

X	A	650	273.9	0.0958	905.7	0.834	5.3	2.3	0.6	8.7	3.3
	B	750	37.35	0.0109	82.40	4.35	46.8	34.8	3.5	18.08	0.58
	C	850	17.92	0.0046	14.11	20.78	110.4	76.7	17.3	19.12	0.13
	D	920	16.16	0.0050	8.158	14.89	101.9	85.1	27.2	19.11	0.16
	E	1000	17.30	0.0086	11.92	14.35	59.0	79.6	36.8	19.15	0.17
	F	1075	17.18	0.0173	11.51	11.62	29.5	80.2	44.5	19.16	0.21
	G	1110	15.58	0.0166	6.354	16.09	30.7	88.0	55.2	19.05	0.15
	H	1180	15.32	0.0415	5.635	27.1	12.3	89.2	73.2	18.991	0.094
	I	1210	14.76	0.0788	3.995	19.79	6.5	92.0	86.4	18.90	0.12
	J	1250	14.47	0.0464	2.970	17.64	11.0	94.0	98.2	18.90	0.13
	K	1300	14.82	0.0332	4.985	2.250	15.4	90.1	99.7	18.57	0.99
	L	1650	24.53	1.205	44.30	0.496	0.42	47.0	100.0	16.1	4.4
	Integrated age ± 2σ			n=12	MSWD=1.57	150.1	15.1		K2O=8.57%	18.93	0.14
	Plateau ± 2σ	steps B-L		n=11	MSWD=0.73	149.3	42.8 ±75.5		99.4	19.016	0.099
	Isochron±2σ	steps A-L		n=12	MSWD=0.81		$^{40}Ar/^{36}Ar$=	288.7±4.7		19.09	0.11

MZQ-23, Hornblende, 15.15 mg, J=0.0013623±0.07%, D=1.002±0.001, NM-202H, Lab#=56744-01

X	A	800	1165.1	5.916	3757.5	0.104	0.086	4.7	0.4	131.4	17.3
	B	900	28.08	0.8817	52.76	0.096	0.58	44.7	0.8	30.6	6.5
	C	1000	22.97	1.308	31.12	0.203	0.39	60.4	1.6	33.8	3.1
	D	1100	16.05	5.059	16.69	1.69	0.10	71.9	8.1	28.23	0.42
	E	1130	18.31	5.177	24.05	4.80	0.099	63.5	26.7	28.44	0.26
	F	1160	17.45	4.845	21.04	6.24	0.11	66.7	50.9	28.44	0.19
	G	1190	13.12	4.696	6.484	5.85	0.11	88.4	73.5	28.35	0.16
	H	1220	12.55	5.132	4.900	4.05	0.099	91.9	89.2	28.19	0.21
	I	1250	12.77	5.491	6.362	2.31	0.093	88.8	98.1	27.75	0.35
	J	1300	13.57	6.390	7.972	0.414	0.080	86.5	99.7	28.7	1.6
	K	1650	44.17	80.16	127.5	0.072	0.006	29.7	100.0	33.9	10.4
	Integrated age ± 2σ			n=11	MSWD=4.26	25.8	0.098		K2O=0.48%	28.80	0.35
	Plateau ± 2σ	steps B-K		n=10	MSWD=0.80	25.7	0.11 ±0.35		99.6	28.31	0.19
	Isochron±2σ	steps A-K		n=11	MSWD=0.74		$^{40}Ar/^{36}Ar$=	306.3±3.8		28.03	0.21

MZQ-36, Groundmass Concentrate, 24.01 mg, J=0.0007792±0.08%, D=1.006±0.001, NM-208K, Lab#=57182-01

X	A	3	66.22	0.5791	190.0	4.63	0.88	15.3	7.5	14.19	0.57
X	B	3	20.48	0.5559	23.65	19.33	0.92	66.1	31.4	18.94	0.10
X	C	4	18.89	0.6332	11.50	47.8	0.81	82.3	63.4	21.723	0.067
	D	4	18.30	0.5806	7.679	42.29	0.88	87.9	78.2	22.473	0.062
	E	5	18.01	0.5893	6.466	50.8	0.87	89.7	89.1	22.565	0.056
	F	6	19.71	0.6358	12.42	42.80	0.80	81.7	95.3	22.498	0.071
X	G	8	25.85	0.8988	34.43	21.22	0.57	60.9	97.7	22.02	0.14
X	H	10	29.84	1.342	49.88	12.35	0.38	51.0	98.9	21.27	0.19
X	I	25	33.46	2.907	62.31	11.31	0.18	45.7	100.0	21.41	0.22
	Integrated age ± 2σ			n=9	MSWD=165.88	252.4	0.66		K2O=5.18%	21.79	0.17
	Plateau ± 2σ	steps D-F		n=3	MSWD=0.65	135.9	0.85 ±0.08		53.8	22.518	0.080
	Isochron±2σ	steps A-I		n=9	MSWD=130.55		$^{40}Ar/^{36}Ar$=	268.4±2.8		22.53	0.08

Notes:
Isotopic ratios corrected for blank, radioactive decay, and mass discrimination, not corrected for interfering reactions.
Errors quoted for individual analyses include analytical error only, without interfering reaction or J uncertainties.
Integrated age calculated by summing isotopic measurements of all steps.
Integrated age error calculated by quadratically combining errors of isotopic measurements of all steps.
Plateau age is inverse-variance-weighted mean of selected steps.
Plateau age error is inverse-variance-weighted mean error (Taylor, 1982) times root MSWD where MSWD>1.
Plateau error is weighted error of Taylor (1982).
Decay constants and isotopic abundances after Steiger and Jäger (1977).
symbol preceding sample ID denotes analyses excluded from plateau age calculations.
Weight percent K_2O calculated from ^{39}Ar signal, sample weight, and instrument sensitivity.
Ages calculated relative to FC-2 Fish Canyon Tuff sanidine interlaboratory standard at 28.02 Ma
Decay Constant (LambdaK (total)) = 5.543e-10/a
Correction factors:
$(^{39}Ar/^{37}Ar)_{Ca}$ = 0.00068 ± 2e-05
$(^{36}Ar/^{37}Ar)_{Ca}$ = 0.00028 ± 1e-05
$(^{38}Ar/^{39}Ar)_{K}$ = 0.013
$(^{40}Ar/^{39}Ar)_{K}$ = 0 ± 0.0004

Table 3. K-feldspar $^{40}Ar/^{39}Ar$ analytical data.

	ID	Temp (°C)	$^{40}Ar/^{39}Ar$	$^{37}Ar/^{39}Ar$	$^{36}Ar/^{39}Ar$ (x 10^{-3})	$^{39}Ar_K$ (x 10^{-15} mol)	K/Ca	$^{40}Ar^*$ (%)	^{39}Ar (%)	Age (Ma)	±1σ (Ma)
	MZQ-1, K-Feldspar, 16.5 mg, J=0.0009017±0.06%, D=1.002±0.001, NM-196K, Lab#=56281-01										
X	B	500	1068.5	0.0113	3023.6	2.98	45.3	16.4	0.5	264.4	5.7
X	C	500	115.5	0.0166	321.8	1.121	30.7	17.7	0.7	32.9	1.3
X	D	550	214.0	0.0076	537.4	3.12	66.8	25.8	1.2	87.6	1.3
X	E	550	43.25	0.0099	87.05	2.65	51.4	40.5	1.6	28.30	0.39
X	F	600	106.4	0.0016	256.7	10.83	309.8	28.7	3.4	48.98	0.60
X	G	600	26.11	0.0030	34.53	5.78	171.0	60.9	4.3	25.70	0.21
X	H	650	46.12	0.0022	89.42	9.06	234.3	42.7	5.8	31.76	0.29
X	I	650	24.16	0.0027	28.92	5.98	187.3	64.6	6.8	25.23	0.16
X	J	700	67.12	0.0034	158.8	11.38	150.2	30.1	8.7	32.57	0.39
X	K	700	21.34	0.0009	19.14	6.55	538.4	73.5	9.8	25.34	0.16
X	L	750	48.47	0.0032	99.11	12.04	161.9	39.6	11.7	30.93	0.27
X	M	750	19.61	0.0023	13.10	7.20	219.7	80.3	12.9	25.42	0.14
X	N	800	32.60	0.0036	51.87	10.07	140.5	53.0	14.6	27.88	0.20
X	O	800	18.06	0.0039	9.781	6.66	129.9	84.0	15.6	24.51	0.11
X	P	850	20.86	0.0058	17.65	7.35	87.2	75.0	16.9	25.27	0.12
X	Q	850	17.63	0.0070	8.418	6.51	72.9	85.9	17.9	24.46	0.12
X	R	900	22.39	0.0039	23.12	8.58	129.7	69.5	19.3	25.14	0.14
X	S	900	19.20	0.0045	12.86	8.34	114.3	80.2	20.7	24.87	0.11
X	T	950	27.22	0.0026	35.10	14.02	195.1	61.9	23.0	27.19	0.14
X	U	950	23.43	0.0018	22.12	16.0	289.0	72.1	25.6	27.27	0.11
X	V	1000	26.48	0.0016	29.51	31.1	328.5	67.1	30.7	28.66	0.10
X	W	1000	22.70	0.0013	19.08	20.0	385.3	75.2	34.0	27.544	0.098
X	X	1050	23.60	0.0013	20.53	56.4	391.2	74.3	43.3	28.302	0.081
X	Y	1100	23.02	0.0011	19.25	87.6	461.0	75.3	57.6	27.975	0.075
X	Z	1150	23.08	0.0008	19.75	75.9	610.4	74.7	70.1	27.834	0.076
X	AA	1250	19.47	0.0006	9.366	151.4	921.1	85.8	94.9	26.972	0.050
X	AB	1300	24.15	0.0214	24.95	5.24	23.9	69.5	95.7	27.08	0.20
X	AC	1400	23.65	0.0185	22.19	10.85	27.6	72.3	97.5	27.60	0.13
X	AD	1700	23.18	0.0445	20.70	15.14	11.5	73.6	100.0	27.55	0.11
	Integrated age ± 2σ		n=29	MSWD=326.16		609.8	160.4	K2O=15.74%		29.53	0.24
	Plateau ± 2σ no plateau		n=0	MSWD=0.00		0.000	0.000±0.000		0.0	0.00	0.000
	Isochron±2σ steps B-AD		n=29	MSWD=101.03			$^{40}Ar/^{36}Ar$=	344.1±1.4		25.552	0.074
	MZQ-2, K-Feldspar, 14.4 mg, J=0.0009011±0.06%, D=1.002±0.001, NM-196K, Lab#=56282-01										
X	B	500	742.9	0.0805	2273.7	0.870	6.3	9.6	0.2	111.9	5.1
X	C	500	157.5	0.1399	492.4	0.533	3.6	7.6	0.4	19.4	2.3
X	D	550	143.2	0.0628	410.5	1.045	8.1	15.3	0.7	35.3	1.4
X	E	550	67.69	0.0583	185.8	1.207	8.7	18.9	1.0	20.68	0.94
X	F	600	88.86	0.0226	234.2	3.55	22.6	22.1	2.1	31.69	0.68
X	G	600	36.02	0.0298	71.20	2.35	17.1	41.6	2.7	24.19	0.44
X	H	650	40.05	0.0172	80.28	3.54	29.6	40.8	3.7	26.35	0.37
X	I	650	26.33	0.0221	39.91	3.05	23.1	55.2	4.6	23.48	0.32
X	J	700	40.03	0.0189	82.66	4.28	27.0	39.0	5.8	25.20	0.34
X	K	700	20.61	0.0178	19.61	3.95	28.6	71.9	6.9	23.92	0.23
X	L	750	34.42	0.0131	63.15	5.92	39.0	45.8	8.6	25.44	0.25
X	M	750	18.42	0.0167	11.44	4.93	30.6	81.7	10.0	24.29	0.17
X	N	800	25.84	0.0122	34.79	6.22	41.8	60.2	11.8	25.13	0.20
X	O	800	18.37	0.0151	12.09	4.50	33.7	80.6	13.1	23.90	0.20
X	P	850	26.88	0.0185	39.14	4.46	27.6	57.0	14.3	24.72	0.25
X	Q	850	21.18	0.0223	22.28	3.22	22.9	68.9	15.3	23.58	0.26
X	R	900	37.60	0.0164	76.23	4.18	31.2	40.1	16.4	24.35	0.33

X	S	900	28.06	0.0227	43.80	3.58	22.5	53.9	17.5	24.41	0.30
X	T	950	44.73	0.0111	96.30	7.51	45.8	36.4	19.6	26.27	0.30
X	U	950	34.15	0.0107	62.02	7.96	47.7	46.3	21.9	25.54	0.24
	V	1000	37.80	0.0053	71.91	17.5	96.6	43.8	26.8	26.71	0.21
	W	1000	30.85	0.0074	49.50	11.56	69.3	52.6	30.1	26.19	0.17
	X	1050	29.61	0.0039	44.70	34.8	129.9	55.4	40.0	26.48	0.14
	Y	1100	27.15	0.0026	36.12	66.4	195.4	60.7	58.9	26.59	0.11
	Z	1150	25.78	0.0031	31.66	47.7	163.5	63.7	72.5	26.51	0.10
	AA	1250	23.28	0.0063	23.19	35.9	80.5	70.6	82.7	26.514	0.092
	AB	1300	26.42	0.0168	33.56	17.4	30.4	62.5	87.6	26.63	0.14
	AC	1400	23.11	0.0079	22.82	31.0	64.8	70.8	96.5	26.406	0.093
X	AD	1700	21.37	0.0394	18.81	12.46	12.9	74.0	100.0	25.53	0.11
	Integrated age ± 2σ			n=29	MSWD=42.49	351.6	53.1	K2O=10.41%		26.43	0.24
	Plateau ± 2σ steps V-AC			n=8	MSWD=1.00	262.3	126.6	±110.4	74.6	26.500	0.088
	Isochron±2σ steps B-AD			n=29	MSWD=32.27		$^{40}Ar/^{36}Ar$=	308.1±1.6		25.26	0.12

MZQ-38, K-Feldspar, 18.15 mg, J=0.0007896±0.06%, D=1.004±0.001, NM-208L, Lab#=57191-01

X	B	570	344.6	0.0034	1004.7	2.48	148.8	13.8	0.8	66.7	2.0
X	C	570	56.66	0.0157	130.2	0.951	32.4	32.1	1.0	25.74	0.95
X	D	620	50.48	-0.0005	101.3	3.38	-	40.7	2.1	29.05	0.40
X	E	620	30.79	0.0011	44.58	1.614	454.4	57.2	2.6	24.92	0.54
X	F	670	31.11	0.0033	43.20	3.89	153.5	59.0	3.7	25.94	0.26
X	G	670	23.96	0.0066	22.71	2.082	77.6	72.0	4.4	24.41	0.35
X	H	670	24.07	0.0169	20.36	0.468	30.2	75.0	4.5	25.55	0.68
X	I	670	22.71	0.0035	16.93	1.471	145.3	78.0	4.9	25.04	0.21
X	J	720	22.39	-0.0001	15.27	3.05	-	79.9	5.9	25.30	0.19
X	K	720	21.05	0.0045	12.26	2.135	113.0	82.8	6.5	24.66	0.19
X	L	770	24.25	0.0040	21.03	5.65	128.4	74.4	8.2	25.52	0.15
X	M	770	19.86	0.0034	7.874	3.31	151.7	88.3	9.2	24.81	0.15
X	N	820	21.93	0.0020	13.61	6.85	249.4	81.7	11.3	25.33	0.11
X	O	820	19.25	0.0021	6.626	3.66	243.0	89.8	12.4	24.46	0.15
X	P	870	20.85	0.0008	11.24	5.29	653.5	84.1	14.0	24.80	0.11
X	Q	870	19.55	0.0037	7.168	3.49	136.6	89.2	15.1	24.66	0.14
X	R	920	21.77	0.0027	14.10	5.10	191.2	80.9	16.6	24.91	0.12
X	S	920	20.99	0.0024	12.07	2.67	215.2	83.0	17.4	24.65	0.19
X	T	970	25.87	0.0034	27.31	5.17	148.2	68.8	19.0	25.18	0.15
X	U	970	24.55	0.0036	23.61	3.43	141.1	71.6	20.0	24.86	0.18
X	V	1020	28.56	0.0003	33.86	8.92	######	65.0	22.7	26.24	0.12
	W	1020	25.51	0.0022	25.19	7.00	234.1	70.8	24.8	25.55	0.12
	X	1070	25.72	0.0015	25.16	18.57	341.1	71.1	30.5	25.864	0.095
	Y	1070	23.34	0.0014	17.74	11.38	365.9	77.5	33.9	25.60	0.10
	Z	1120	23.68	0.0024	18.26	33.4	211.6	77.2	44.0	25.858	0.071
	AA	1120	22.79	0.0003	15.36	20.89	######	80.1	50.3	25.811	0.093
	AB	1120	22.42	0.0017	14.38	24.8	299.4	81.0	57.8	25.703	0.071
	AC	1170	21.64	0.0016	11.27	88.0	324.3	84.6	84.5	25.888	0.054
	AD	1220	20.13	0.0031	6.714	9.59	166.7	90.1	87.4	25.661	0.084
	AE	1320	19.77	0.0010	5.225	36.1	488.3	92.2	98.3	25.781	0.047
	AF	1370	21.08	0.0011	8.784	1.349	454.3	87.7	98.7	26.15	0.34
X	AG	1470	24.99	-0.0076	16.33	0.306	-	80.7	98.8	28.5	1.2
X	AH	1770	24.28	0.0014	21.50	3.89	376.8	73.8	100.0	25.36	0.16
	Integrated age ± 2σ			n=33	MSWD=29.51	330.4	282.3	K2O=8.86%		26.03	0.14
	Plateau ± 2σ steps W-AF			n=10	MSWD=1.87	251.2	422.3	±763.9	76.0	25.782	0.072
	Isochron±2σ steps B-AH			n=33	MSWD=16.00		$^{40}Ar/^{36}Ar$=	317.5±2.3		25.17	0.07

MZQ-15, K-Feldspar, 15.56 mg, J=0.0007889±0.04%, D=1.004±0.001, NM-208L, Lab#=57187-01

X	B	570	3104.8	0.1172	9834.2	0.294	4.4	6.4	0.1	262.8	16.7
X	C	570	317.0	0.0748	984.0	0.832	6.8	8.3	0.4	37.0	2.7
X	D	620	196.6	0.0631	511.2	2.034	8.1	23.2	1.0	63.7	1.1

X	E	620	60.90	0.0483	137.3	1.277	10.6	33.4	1.5	28.71	0.83
X	F	670	50.79	0.0478	101.3	2.255	10.7	41.1	2.2	29.45	0.57
X	G	670	32.73	0.0403	54.68	1.928	12.7	50.6	2.8	23.44	0.48
X	H	720	35.69	0.0368	58.54	2.85	13.9	51.5	3.8	25.99	0.38
X	I	720	25.45	0.0329	26.66	2.69	15.5	69.1	4.7	24.84	0.34
X	J	770	30.90	0.0259	41.79	3.76	19.7	60.0	5.9	26.21	0.30
X	K	770	22.47	0.0269	16.02	4.04	19.0	78.9	7.2	25.06	0.22
X	L	820	26.13	0.0231	26.67	4.69	22.0	69.8	8.8	25.79	0.25
X	M	820	21.23	0.0206	11.40	5.35	24.8	84.1	10.5	25.24	0.17
X	N	870	25.70	0.0244	25.12	6.25	21.0	71.1	12.6	25.83	0.19
X	O	870	22.03	0.0244	15.25	4.62	20.9	79.6	14.1	24.77	0.20
X	P	920	28.85	0.0254	36.01	5.99	20.1	63.1	16.1	25.74	0.19
X	Q	920	29.25	0.0227	39.46	6.87	22.5	60.1	18.3	24.87	0.21
X	R	970	42.76	0.0169	81.19	7.02	30.1	43.9	20.6	26.52	0.29
X	S	970	37.21	0.0127	62.61	5.68	40.2	50.3	22.5	26.44	0.27
X	T	1020	52.70	0.0151	114.4	7.54	33.7	35.9	25.0	26.69	0.31
X	U	1020	43.29	0.0142	82.40	6.93	36.0	43.7	27.3	26.75	0.25
X	V	1070	51.17	0.0138	103.7	10.56	37.0	40.1	30.7	29.00	0.29
X	W	1070	41.53	0.0115	74.91	9.23	44.4	46.7	33.8	27.39	0.23
X	X	1120	42.39	0.0132	74.08	16.08	38.6	48.4	39.1	28.95	0.22
X	Y	1120	40.86	0.0143	68.92	15.99	35.7	50.2	44.3	28.93	0.20
X	Z	1170	35.86	0.0149	52.53	20.24	34.1	56.7	51.0	28.71	0.14
X	AA	1170	33.91	0.0142	43.17	26.5	36.0	62.4	59.7	29.86	0.13
X	AB	1220	30.77	0.0140	31.40	29.4	36.6	69.8	69.4	30.33	0.11
X	AC	1320	29.91	0.0128	27.93	69.3	39.9	72.4	92.2	30.561	0.090
X	AD	1370	31.02	0.0197	33.62	8.21	25.9	68.0	94.9	29.77	0.17
X	AE	1470	31.67	0.0154	36.10	10.63	33.1	66.3	98.3	29.64	0.15
X	AF	1770	34.90	0.0098	53.81	5.02	51.9	54.4	100.0	26.85	0.25
	Integrated age ± 2σ			n=31	MSWD=153.33	304.0	30.4	K2O=9.51%		29.19	0.27
	Plateau ± 2σ no plateau			n=0	MSWD=0.00	0.000	0.000±0.000		0.0	0.00	0.000
	Isochron±2σ steps B-AF			n=31	MSWD=125.35		$^{40}Ar/^{36}Ar$=	317.1±1.6		27.15	0.12

MZQ-16, K-Feldspar, 19.2 mg, J=0.0009044±0.05%, D=1.002±0.001, NM-196L, Lab#=56288-03

X	B	500	1459.6	1.254	5098.8	0.035	0.41	-3.2	0.0	-78.4	31.4
X	C	500	93.66	0.0893	282.8	1.044	5.7	10.8	0.2	16.4	1.1
X	D	550	42.89	0.0661	106.8	1.301	7.7	26.4	0.5	18.41	0.64
X	E	550	20.41	0.0476	25.82	1.78	10.7	62.6	0.9	20.74	0.31
X	F	600	34.83	0.0308	66.83	4.45	16.6	43.3	1.9	24.45	0.33
X	G	600	19.17	0.0276	17.28	3.71	18.5	73.4	2.8	22.80	0.19
X	H	650	24.91	0.0260	33.83	5.95	19.6	59.9	4.1	24.17	0.20
X	I	650	18.69	0.0212	12.91	5.44	24.1	79.6	5.3	24.12	0.14
X	J	700	22.01	0.0236	23.85	7.68	21.7	68.0	7.0	24.25	0.14
X	K	700	17.26	0.0140	7.616	7.63	36.5	87.0	8.8	24.33	0.17
X	L	750	23.34	0.0190	27.68	8.71	26.8	65.0	10.7	24.57	0.13
X	M	750	16.70	0.0154	5.618	9.66	33.2	90.1	12.9	24.370	0.088
X	N	800	21.42	0.0143	21.12	16.2	35.8	70.9	16.5	24.59	0.10
X	O	800	16.66	0.0126	5.304	13.48	40.6	90.6	19.5	24.457	0.076
X	P	850	21.65	0.0134	21.10	15.9	38.0	71.2	23.1	24.98	0.11
X	Q	850	17.87	0.0145	9.140	13.50	35.3	84.9	26.1	24.590	0.079
X	R	900	26.84	0.0166	38.94	15.67	30.8	57.1	29.6	24.85	0.14
X	S	900	22.16	0.0173	23.90	13.20	29.6	68.1	32.6	24.47	0.12
	T	950	38.36	0.0172	77.81	15.51	29.6	40.1	36.1	24.90	0.22
	U	950	29.79	0.0150	49.12	12.93	33.9	51.3	39.0	24.75	0.18
	V	1000	41.21	0.0125	86.62	18.1	40.7	37.9	43.0	25.30	0.23
	W	1000	31.39	0.0155	54.72	10.53	32.9	48.5	45.4	24.66	0.19
	X	1050	35.77	0.0132	68.50	24.5	38.7	43.4	50.9	25.17	0.18
	Y	1100	30.80	0.0147	52.22	45.5	34.8	49.9	61.1	24.90	0.15
	Z	1150	29.30	0.0166	46.64	48.7	30.7	53.0	72.1	25.14	0.14

	AA	1250	24.73	0.0164	30.90	56.5	31.1	63.1	84.7	25.28	0.10
	AB	1300	28.09	0.0315	43.08	7.24	16.2	54.7	86.4	24.90	0.20
X	AC	1400	28.14	0.0271	41.55	22.7	18.8	56.4	91.4	25.69	0.14
X	AD	1700	26.11	0.0276	33.57	38.1	18.5	62.0	100.0	26.22	0.11
	Integrated age ± 2σ			n=29	MSWD=28.80	445.5	27.8	K2O=9.86%		24.96	0.21
	Plateau ± 2σ steps T-AB			n=9	MSWD=2.03	239.4	32.9 ±14.0		53.7	25.06	0.15
	Isochron±2σ steps B-AD			n=29	MSWD=26.63		$^{40}Ar/^{36}Ar$=	300.4±1.6		24.50	0.09

MZQ-39, K-Feldspar, 18.39 mg, J=0.0007913±0.05%, D=1.004±0.001, NM-208L, Lab#=57192-01

X	B	570	84.75	0.0176	241.4	1.852	29.0	15.8	0.5	19.07	0.82
X	C	620	53.51	0.0186	127.4	2.73	27.4	29.6	1.3	22.51	0.45
X	D	620	39.41	0.0136	78.18	2.91	37.4	41.4	2.2	23.14	0.35
X	E	670	34.44	0.0124	59.01	3.91	41.1	49.4	3.3	24.12	0.27
X	F	670	28.21	0.0096	37.62	4.62	53.4	60.6	4.7	24.24	0.22
X	G	720	26.90	0.0089	33.70	4.84	57.5	63.0	6.1	24.03	0.19
X	H	720	23.21	0.0063	20.49	6.05	81.5	73.9	7.8	24.32	0.14
X	I	770	24.40	0.0066	24.79	7.34	77.5	70.0	10.0	24.21	0.13
	J	770	20.63	0.0068	11.03	8.82	75.1	84.2	12.5	24.63	0.10
	K	820	22.99	0.0069	19.34	8.79	74.4	75.1	15.1	24.49	0.11
	L	820	19.99	0.0072	9.162	10.63	70.9	86.5	18.2	24.507	0.083
	M	870	23.86	0.0077	21.89	9.56	65.8	72.9	20.9	24.66	0.10
	N	870	20.68	0.0068	10.36	11.50	74.6	85.2	24.3	24.984	0.084
	O	920	26.45	0.0093	30.33	9.78	55.1	66.1	27.1	24.80	0.13
	P	920	22.87	0.0099	18.49	11.55	51.3	76.1	30.5	24.676	0.096
	Q	970	32.38	0.0076	51.20	9.52	67.3	53.3	33.2	24.46	0.18
	R	970	26.93	0.0105	32.59	11.47	48.4	64.2	36.6	24.53	0.12
	S	1020	38.80	0.0091	72.39	9.81	56.0	44.9	39.4	24.69	0.23
	T	1020	31.96	0.0070	49.46	12.41	72.4	54.3	43.0	24.59	0.14
	U	1070	40.26	0.0082	77.47	11.11	62.0	43.1	46.3	24.62	0.19
	V	1070	33.61	0.0081	54.87	14.06	63.0	51.8	50.3	24.67	0.16
	W	1120	37.50	0.0095	68.18	12.69	53.5	46.3	54.0	24.60	0.20
	X	1120	32.47	0.0093	50.51	15.00	54.7	54.0	58.4	24.88	0.17
	Y	1170	34.39	0.0094	57.87	13.77	54.5	50.3	62.4	24.52	0.15
	Z	1170	34.51	0.0121	58.44	21.02	42.2	50.0	68.5	24.45	0.16
X	AA	1220	33.64	0.0128	53.95	10.42	39.8	52.6	71.5	25.09	0.17
X	AB	1320	27.39	0.0126	32.86	64.1	40.4	64.6	90.1	25.069	0.094
X	AC	1370	24.85	0.0111	24.62	19.67	45.8	70.7	95.9	24.920	0.099
X	AD	1470	29.51	0.0114	39.53	3.57	44.9	60.4	96.9	25.28	0.25
X	AE	1770	32.02	0.0119	47.66	10.66	42.7	56.0	100.0	25.43	0.14
	Integrated age ± 2σ			n=30	MSWD=7.55	344.1	50.9	K2O=9.08%		24.68	0.19
	Plateau ± 2σ steps J-Z			n=17	MSWD=1.80	201.5	59.8 ±20.4		58.5	24.65	0.08
	Isochron±2σ steps B-AE			n=30	MSWD=7.11		$^{40}Ar/^{36}Ar$=	292.5±1.8		24.80	0.10

MZQ-12, K-Feldspar, 17.59 mg, J=0.0007922±0.04%, D=1.004±0.001, NM-208L, Lab#=57185-01

X	B	570	50.36	-0.0569	104.6	0.164	-	38.6	0.0	27.6	3.0
X	C	620	62.83	-0.0174	129.9	0.493	-	38.9	0.2	34.6	1.6
X	D	620	29.22	-0.0264	36.25	0.408	-	63.3	0.3	26.2	1.2
X	E	670	33.54	0.0157	49.53	0.878	32.4	56.4	0.5	26.82	0.61
X	F	670	23.75	-0.0284	18.83	0.588	-	76.6	0.7	25.80	0.79
X	G	720	23.72	0.0159	19.30	1.233	32.1	76.0	1.0	25.57	0.47
X	H	720	20.36	0.0034	8.596	1.450	148.2	87.5	1.4	25.29	0.36
X	I	770	20.23	0.0121	9.665	2.40	42.2	85.9	2.0	24.66	0.22
X	J	770	19.21	0.0078	6.042	2.261	65.3	90.7	2.7	24.74	0.23
X	K	820	18.87	0.0047	5.282	3.43	108.5	91.7	3.6	24.57	0.16
X	L	820	18.52	0.0079	4.021	3.37	64.2	93.6	4.5	24.60	0.15
X	M	870	18.72	0.0115	4.623	4.51	44.5	92.7	5.7	24.63	0.12
X	N	870	18.40	0.0075	3.225	4.56	68.2	94.8	6.9	24.77	0.13
X	O	920	18.67	0.0116	3.621	5.85	44.1	94.3	8.5	24.98	0.11

X	P	920	18.38	0.0091	3.618	5.96	56.3	94.2	10.1	24.57	0.11
X	Q	970	18.62	0.0106	3.812	6.92	48.0	94.0	12.0	24.823	0.094
X	R	970	18.47	0.0080	2.920	6.73	64.0	95.3	13.8	24.99	0.11
X	S	1020	19.17	0.0106	6.129	7.97	48.2	90.6	15.9	24.640	0.091
X	T	1020	18.65	0.0094	4.200	8.16	54.2	93.3	18.1	24.71	0.10
X	U	1070	19.98	0.0093	8.839	8.57	54.9	86.9	20.4	24.660	0.093
X	V	1070	19.27	0.0089	5.980	8.68	57.1	90.8	22.8	24.837	0.087
X	W	1120	21.37	0.0108	13.44	8.80	47.4	81.4	25.1	24.698	0.093
X	X	1120	20.53	0.0089	9.661	8.81	57.3	86.1	27.5	25.092	0.089
X	Y	1170	23.70	0.0104	20.92	12.93	49.2	73.9	31.0	24.87	0.11
	Z	1170	24.00	0.0105	21.46	16.81	48.5	73.6	35.5	25.065	0.094
	AA	1220	22.47	0.0109	16.41	24.3	46.7	78.4	42.1	25.004	0.082
	AB	1320	21.04	0.0108	10.98	126.3	47.2	84.6	76.1	25.255	0.052
	AC	1370	20.50	0.0095	9.498	27.4	53.8	86.3	83.4	25.109	0.066
X	AD	1470	21.57	0.0098	12.09	17.02	52.1	83.4	88.0	25.535	0.083
X	AE	1770	21.25	0.0108	11.44	44.5	47.5	84.1	100.0	25.363	0.056
	Integrated age ± 2σ			n=30	MSWD=9.10	371.4	50.5	K2O=10.24%		25.127	0.095
	Plateau ± 2σ steps Z-AC			n=4	MSWD=2.81	194.7	48.2 ±6.5		52.4	25.15	0.12
	Isochron±2σ steps B-AE			n=30	MSWD=6.21		$^{40}Ar/^{36}Ar$=	319.9±5.6		24.68	0.09

MZQ-13, K-Feldspar, 18.5 mg, J=0.0009039±0.05%, D=1.002±0.001, NM-196L, Lab#=56287-01

X	B	500	2057.9	0.4404	6689.2	0.201	1.2	3.9	0.0	127.9	17.4
X	C	500	423.5	0.2834	1398.4	0.357	1.8	2.4	0.1	16.8	4.5
X	D	550	635.4	0.1889	2069.9	0.574	2.7	3.7	0.2	38.4	5.5
X	E	550	237.0	0.1481	754.3	0.795	3.4	5.9	0.3	22.8	2.7
X	F	600	210.0	0.0728	655.8	2.39	7.0	7.7	0.7	26.2	1.7
X	G	600	91.65	0.0702	259.4	2.00	7.3	16.4	1.0	24.30	0.92
X	H	650	84.60	0.0585	231.5	3.47	8.7	19.1	1.6	26.2	7.7
X	I	650	58.43	0.0599	145.4	3.15	8.5	26.5	2.1	25.05	0.53
X	J	700	52.56	0.0539	127.4	4.51	9.5	28.4	2.8	24.18	0.44
X	K	700	34.19	0.0548	66.14	4.51	9.3	42.8	3.5	23.73	0.31
X	L	750	41.94	0.0471	90.86	6.31	10.8	36.0	4.5	24.45	0.31
X	M	750	23.49	0.0486	28.94	5.55	10.5	63.6	5.4	24.21	0.20
X	N	800	32.33	0.0433	58.10	7.38	11.8	46.9	6.6	24.57	0.23
X	O	800	22.93	0.0497	27.32	5.90	10.3	64.8	7.6	24.08	0.20
X	P	850	35.88	0.0405	70.62	7.08	12.6	41.9	8.7	24.33	0.26
X	Q	850	21.90	0.0456	24.42	5.72	11.2	67.1	9.6	23.78	0.19
X	R	900	45.94	0.0354	103.8	7.51	14.4	33.2	10.8	24.73	0.34
X	S	900	28.79	0.0359	47.45	6.30	14.2	51.3	11.8	23.93	0.24
	T	950	68.50	0.0250	181.3	9.77	20.4	21.8	13.4	24.18	0.45
	U	950	41.94	0.0269	91.56	8.18	18.9	35.5	14.7	24.12	0.29
	W	1000	46.23	0.0242	105.8	8.69	21.1	32.4	16.1	24.23	0.34
	X	1050	57.37	0.0166	142.4	24.0	30.7	26.6	20.0	24.76	0.33
	Y	1100	43.65	0.0154	96.36	54.8	33.1	34.8	28.8	24.59	0.23
	Z	1150	37.60	0.0144	75.74	70.1	35.4	40.5	40.0	24.65	0.19
	AA	1250	29.32	0.0144	47.16	140.6	35.4	52.5	62.6	24.91	0.12
	AB	1300	31.79	0.0269	55.39	30.4	19.0	48.5	67.5	24.97	0.16
X	AC	1400	33.65	0.0160	60.94	100.0	32.0	46.5	83.6	25.34	0.15
X	AD	1700	32.30	0.0094	56.20	102.1	54.1	48.6	100.0	25.41	0.14
	Integrated age ± 2s			n=28	MSWD=6.13	622.2	26.1	K2O=14.29%		24.96	0.36
	Plateau ± 2s steps T-AB			n=8	MSWD=1.87	346.5	32.1 ±15.1		55.7	24.74	0.20
	Isochron±2s steps A-AD			n=28	MSWD=5.50		$^{40}Ar/^{36}Ar$=	298.0±0.4		24.4	0.4

MZQ-5, K-Feldspar, 18.4 mg, J=0.0009006±0.05%, D=1.002±0.001, NM-196K, Lab#=56283-01

X	B	500	1452.3	0.1859	4416.8	0.523	2.7	10.1	0.1	224.5	9.6
X	C	500	281.7	0.2708	928.5	0.296	1.9	2.6	0.2	11.8	4.6
X	D	550	365.0	0.1541	1138.7	0.548	3.3	7.8	0.3	45.8	3.5
X	E	550	150.0	0.1475	472.8	0.618	3.5	6.9	0.5	16.6	2.1

X	F	600	180.0	0.0809	532.4	1.94	6.3	12.6	0.9	36.5	1.4
X	G	600	68.48	0.0766	191.2	1.408	6.7	17.5	1.3	19.36	0.87
X	H	650	84.11	0.0620	228.3	2.44	8.2	19.8	1.8	26.87	0.69
X	I	650	42.46	0.0624	101.4	2.14	8.2	29.5	2.3	20.22	0.51
X	J	700	52.61	0.0561	128.1	3.09	9.1	28.1	3.1	23.84	0.53
X	K	700	31.74	0.0577	62.17	2.62	8.8	42.1	3.7	21.59	0.41
X	L	750	38.53	0.0442	81.26	3.93	11.5	37.7	4.6	23.44	0.38
X	M	750	25.58	0.0428	41.45	2.67	11.9	52.1	5.2	21.53	0.35
X	N	800	32.10	0.0384	62.69	3.60	13.3	42.3	6.1	21.94	0.34
X	O	800	21.56	0.0336	26.69	5.20	15.2	63.4	7.3	22.08	0.19
X	P	850	26.73	0.0282	42.45	5.88	18.1	53.1	8.7	22.91	0.23
X	Q	850	20.02	0.0295	21.09	5.07	17.3	68.9	9.9	22.27	0.18
X	R	900	30.37	0.0288	54.83	6.54	17.7	46.7	11.4	22.89	0.24
X	S	900	22.06	0.0290	27.50	5.50	17.6	63.2	12.7	22.51	0.19
X	T	950	37.41	0.0259	77.70	5.89	19.7	38.6	14.1	23.33	0.28
X	U	950	26.34	0.0224	41.77	7.30	22.8	53.1	15.8	22.60	0.19
X	V	1000	37.32	0.0171	76.41	10.97	29.9	39.5	18.4	23.80	0.23
X	W	1000	27.49	0.0212	44.46	7.43	24.0	52.2	20.2	23.18	0.18
X	X	1050	30.48	0.0164	53.29	20.6	31.2	48.3	25.0	23.79	0.16
X	Y	1100	25.84	0.0149	37.48	42.0	34.2	57.1	34.9	23.83	0.11
X	Z	1150	23.50	0.0163	28.85	47.0	31.4	63.7	46.0	24.172	0.095
X	AA	1250	20.17	0.0136	16.86	102.9	37.6	75.3	70.2	24.513	0.066
X	AB	1300	21.27	0.0167	20.35	34.1	30.6	71.7	78.3	24.617	0.085
X	AC	1400	20.59	0.0158	18.21	71.3	32.3	73.9	95.1	24.547	0.071
X	AD	1700	20.88	0.0242	20.56	21.0	21.1	70.9	100.0	23.895	0.098
	Integrated age ± 2σ			n=29	MSWD=48.55	424.4	25.5	K2O=9.84%		24.36	0.21
	Plateau ± 2σ	no plateau		n=0	MSWD=0.00	0.000	0.000±0.000		0.0	0.00	0.000
	Isochron±2σ	steps B-AD		n=29	MSWD=46.40		$^{40}Ar/^{36}Ar$=	300.7±1.3		23.763	0.090

MZQ-6, K-Feldspar, 16.7 mg, J=0.0009035±0.06%, D=1.002±0.001, NM-196L, Lab#=56284-01

X	B	500	1561.9	0.1412	4346.2	0.566	3.6	17.8	0.1	403.8	9.7
X	C	500	217.7	0.1602	708.2	0.441	3.2	3.9	0.2	13.7	3.0
X	D	550	263.3	0.0893	779.0	0.812	5.7	12.6	0.4	53.2	2.3
X	E	550	119.1	0.0829	359.6	1.060	6.2	10.8	0.6	20.8	1.4
X	F	600	130.1	0.0366	355.5	3.17	13.9	19.2	1.3	40.34	0.95
X	G	600	52.44	0.0346	131.9	2.50	14.7	25.7	1.8	21.80	0.54
X	H	650	48.13	0.0254	109.9	4.17	20.0	32.5	2.6	25.34	0.44
X	I	650	29.96	0.0235	57.32	3.70	21.8	43.5	3.4	21.10	0.31
X	J	700	29.87	0.0206	53.34	5.07	24.8	47.2	4.5	22.86	0.25
X	K	700	20.76	0.0185	26.17	4.77	27.6	62.8	5.5	21.11	0.20
X	L	750	23.85	0.0178	32.88	6.35	28.7	59.3	6.8	22.89	0.19
X	M	750	17.72	0.0167	15.00	5.60	30.5	75.0	7.9	21.53	0.17
X	N	800	22.69	0.0163	28.61	7.42	31.4	62.7	9.5	23.06	0.17
X	O	800	16.83	0.0168	11.43	5.98	30.4	79.9	10.7	21.79	0.15
X	P	850	22.51	0.0160	29.42	7.23	31.9	61.4	12.2	22.38	0.17
X	Q	850	17.51	0.0152	13.36	6.41	33.6	77.5	13.6	21.97	0.15
X	R	900	26.08	0.0147	40.31	8.84	34.7	54.3	15.4	22.96	0.17
X	S	900	20.93	0.0152	23.94	7.57	33.7	66.2	17.0	22.46	0.15
X	T	950	32.51	0.0114	59.73	10.43	44.8	45.7	19.2	24.06	0.20
X	U	950	26.31	0.0126	39.97	9.49	40.3	55.1	21.1	23.48	0.17
X	V	1000	36.79	0.0098	70.32	15.41	52.2	43.5	24.3	25.91	0.20
X	W	1000	29.93	0.0118	49.31	10.15	43.2	51.3	26.4	24.87	0.19
	X	1050	34.32	0.0075	60.36	26.5	67.8	48.0	32.0	26.67	0.17
	Y	1100	30.56	0.0068	47.46	52.4	74.8	54.1	42.9	26.76	0.13
	Z	1150	26.32	0.0080	33.57	83.7	63.7	62.3	60.3	26.531	0.098
	AA	1250	22.77	0.0056	21.76	111.7	91.2	71.8	83.5	26.440	0.075
	AB	1300	24.69	0.0124	28.60	18.7	41.0	65.8	87.4	26.27	0.11
	AC	1400	22.71	0.0070	21.35	39.3	73.1	72.2	95.5	26.539	0.089

X	AD	1700	21.65	0.0174	18.48	21.5	29.3	74.8	100.0	26.191	0.094
	Integrated age ± 2σ			n=29	MSWD=229.93	480.9	48.8		K2O=12.24%	26.31	0.23
	Plateau ± 2σ steps X-AC			n=6	MSWD=2.07	332.3	74.9	±33.0	69.1	26.50	0.12
	Isochron±2σ steps B-AD			n=29	MSWD=179.85		$^{40}Ar/^{36}Ar$=	323.6±1.5		23.77	0.10
	MZQ-8, K-Feldspar, 14.5 mg, J=0.0009033±0.06%, D=1.002±0.001, NM-196L, Lab#=56285-01										
X	B	500	1958.0	0.2363	6437.7	0.390	2.2	2.8	0.1	88.5	14.2
X	C	500	273.5	0.3065	894.9	0.283	1.7	3.3	0.1	14.7	4.2
X	D	550	274.1	0.1640	881.2	0.562	3.1	5.0	0.3	22.2	3.2
X	E	550	153.0	0.1149	490.8	0.687	4.4	5.2	0.4	12.9	1.9
X	F	600	168.6	0.0490	522.6	2.23	10.4	8.4	0.9	23.0	1.4
X	G	600	67.36	0.0587	188.5	1.64	8.7	17.3	1.2	18.92	0.77
X	H	650	57.08	0.0368	151.5	2.83	13.9	21.6	1.8	19.96	0.57
X	I	650	44.46	0.0357	106.5	2.55	14.3	29.2	2.4	21.06	0.51
X	J	700	40.21	0.0306	89.46	3.59	16.7	34.3	3.1	22.31	0.40
X	K	700	29.16	0.0307	52.96	3.50	16.6	46.3	3.9	21.89	0.28
X	L	750	32.07	0.0239	60.91	5.19	21.4	43.9	5.0	22.79	0.28
X	M	750	21.53	0.0212	26.50	4.86	24.0	63.6	6.0	22.19	0.20
X	N	800	25.96	0.0190	40.22	7.39	26.8	54.2	7.6	22.80	0.20
X	O	800	18.64	0.0188	15.44	5.92	27.2	75.5	8.9	22.80	0.15
X	P	850	25.30	0.0162	36.84	7.20	31.5	57.0	10.4	23.34	0.20
X	Q	850	18.39	0.0196	14.63	5.99	26.1	76.5	11.7	22.78	0.16
X	R	900	29.36	0.0182	51.43	7.99	28.0	48.2	13.4	22.93	0.20
X	S	900	21.09	0.0196	23.63	6.49	26.0	66.9	14.8	22.84	0.17
X	T	950	35.22	0.0180	71.11	8.51	28.4	40.3	16.6	23.01	0.24
X	U	950	26.43	0.0179	42.01	6.59	28.6	53.0	18.0	22.70	0.21
	V	1000	37.51	0.0138	78.37	10.08	36.9	38.3	20.1	23.24	0.26
	X	1050	35.30	0.0123	70.70	18.7	41.6	40.8	24.1	23.33	0.20
	Y	1100	29.85	0.0097	52.30	44.7	52.4	48.2	33.7	23.31	0.14
	Z	1150	26.99	0.0088	42.47	50.8	58.0	53.5	44.5	23.38	0.12
	AA	1250	22.60	0.0045	26.84	122.5	112.9	64.9	70.6	23.747	0.081
	AB	1300	28.28	0.0092	46.12	21.6	55.5	51.8	75.2	23.73	0.13
X	AC	1400	26.69	0.0060	39.45	51.6	84.5	56.3	86.2	24.33	0.12
X	AD	1700	25.40	0.0078	34.95	64.7	65.7	59.3	100.0	24.40	0.10
	Integrated age ± 2σ			n=28	MSWD=17.84	469.1	47.5		K2O=13.76%	23.61	0.25
	Plateau ± 2σ steps V-AB			n=6	MSWD=3.09	268.4	80.0	±54.8	57.2	23.56	0.18
	Isochron±2σ steps B-AD			n=28	MSWD=17.44		$^{40}Ar/^{36}Ar$=	293.5±1.4		23.56	0.12
	MZQ-34, K-Feldspar, 18.03 mg, J=0.0007881±0.06%, D=1.004±0.001, NM-208L, Lab#=57190-01										
X	B	520	161.0	0.0304	480.1	0.315	16.8	11.9	0.1	26.9	2.9
X	C	570	153.2	0.0466	438.4	0.390	10.9	15.4	0.2	33.3	1.9
X	D	570	129.1	-7.3605	1530.8	0.032	-	-250.7	0.2	-528.3	######
X	E	620	85.91	0.0187	232.4	1.435	27.4	20.1	0.5	24.36	0.85
X	F	620	32.40	0.0174	59.02	1.887	29.4	46.2	0.9	21.15	0.45
X	G	670	36.79	0.0151	72.06	2.146	33.8	42.1	1.4	21.90	0.42
X	H	670	23.68	0.0089	29.82	2.31	57.6	62.8	1.9	21.02	0.28
X	I	720	28.47	0.0126	43.52	2.36	40.6	54.8	2.4	22.06	0.32
X	J	720	21.27	0.0088	19.94	3.00	57.9	72.3	3.1	21.74	0.23
X	K	770	31.84	0.0114	53.62	2.86	44.9	50.2	3.7	22.59	0.32
X	L	770	19.35	0.0082	12.52	3.99	62.1	80.9	4.6	22.12	0.18
X	M	820	24.27	0.0073	28.32	3.72	70.2	65.5	5.4	22.48	0.25
X	N	820	19.24	0.0107	10.73	4.23	47.6	83.5	6.3	22.70	0.15
X	O	870	26.34	0.0125	34.46	3.76	40.8	61.3	7.2	22.83	0.22
X	P	870	19.52	0.0077	12.88	4.16	66.1	80.5	8.1	22.20	0.16
X	Q	920	31.25	0.0087	50.98	3.31	58.9	51.8	8.8	22.87	0.29
X	R	920	22.78	0.0106	22.14	4.08	48.3	71.3	9.7	22.94	0.19
	S	970	38.60	0.0111	76.70	3.59	46.1	41.3	10.5	22.51	0.30
	T	970	26.31	0.0079	36.08	4.20	64.3	59.5	11.4	22.11	0.20

	U	1020	41.98	0.0081	88.17	5.07	63.0	37.9	12.5	22.50	0.30
	V	1020	30.20	0.0091	48.80	5.83	56.1	52.2	13.8	22.30	0.21
	W	1070	40.28	0.0069	82.87	7.28	73.9	39.2	15.4	22.31	0.27
	X	1070	32.08	0.0050	55.91	9.67	102.9	48.5	17.6	21.98	0.16
	Y	1120	36.43	0.0059	70.85	13.42	86.3	42.5	20.5	21.89	0.19
	Z	1120	31.07	0.0050	52.39	18.22	101.1	50.2	24.6	22.04	0.15
	AA	1170	30.56	0.0069	50.94	26.8	74.4	50.7	30.5	21.91	0.13
	AB	1170	26.66	0.0069	37.11	36.0	74.3	58.9	38.4	22.18	0.10
	AC	1170	22.63	0.0059	23.47	53.5	87.1	69.3	50.2	22.171	0.078
	AD	1170	21.23	0.0054	18.18	49.1	94.2	74.7	61.1	22.405	0.068
X	AE	1270	21.05	0.0036	17.27	39.7	141.4	75.8	69.8	22.532	0.072
X	AF	1320	21.43	0.0018	16.90	97.6	276.5	76.7	91.4	23.215	0.061
X	AG	1420	22.33	0.0030	19.82	16.83	168.9	73.8	95.1	23.28	0.10
X	AH	1770	23.35	0.0039	22.38	22.28	129.5	71.7	100.0	23.64	0.10
	Integrated age ± 2σ			n=33	MSWD=15.90	453.1	106.9	K2O=12.25%		22.54	0.17
	Plateau ± 2σ steps S-AD			n=12	MSWD=2.05	232.657	84.092±35.710		51.3	22.21	0.109
	Isochron±2σ steps B-AH			n=33	MSWD=15.29		$^{40}Ar/^{36}Ar$=	291.1±1.9		22.761	0.092

MZQ-9, K-Feldspar, 12.4 mg, J=0.0009034±0.05%, D=1.002±0.001, NM-196L, Lab#=56286-01

X	B	460	967.8	0.0236	2085.6	0.902	21.6	36.3	0.2	497.6	6.5
X	C	460	180.5	0.0826	510.0	0.208	6.2	16.5	0.2	47.9	3.8
X	D	510	152.6	0.0405	323.1	0.654	12.6	37.4	0.4	90.8	1.9
X	E	510	65.40	0.0347	157.6	0.670	14.7	28.8	0.5	30.4	1.2
X	F	560	119.2	0.0198	236.2	2.21	25.7	41.4	1.0	78.78	0.86
X	G	560	26.20	0.0337	44.53	1.85	15.2	49.8	1.3	21.13	0.41
X	H	610	50.33	0.0217	85.19	5.79	23.5	50.0	2.5	40.55	0.34
X	I	610	14.97	0.0178	13.18	4.11	28.6	74.0	3.4	17.96	0.17
X	J	660	15.14	0.0147	11.58	6.28	34.8	77.4	4.6	19.00	0.13
X	K	660	12.11	0.0114	5.004	6.06	44.6	87.8	5.9	17.24	0.11
X	L	710	11.81	0.0108	3.815	7.53	47.4	90.5	7.4	17.330	0.087
X	M	710	11.26	0.0077	2.662	7.81	66.3	93.0	9.0	16.985	0.087
X	N	760	11.63	0.0085	3.613	9.17	60.3	90.8	10.9	17.129	0.082
X	O	760	11.24	0.0072	2.957	8.48	70.8	92.2	12.6	16.819	0.087
X	P	810	12.58	0.0082	6.308	9.34	62.0	85.2	14.6	17.388	0.096
X	Q	810	11.34	0.0078	4.039	7.73	65.6	89.5	16.1	16.457	0.091
X	R	860	12.27	0.0096	6.437	6.99	53.0	84.5	17.6	16.82	0.11
X	S	860	11.87	0.0083	6.101	6.26	61.3	84.8	18.8	16.34	0.11
X	T	910	14.85	0.0117	14.77	6.79	43.5	70.6	20.2	17.01	0.13
X	U	910	14.15	0.0094	11.93	7.00	54.2	75.1	21.7	17.23	0.11
X	V	960	18.76	0.0106	24.16	9.51	48.0	62.0	23.6	18.85	0.13
X	W	960	17.74	0.0069	19.03	11.99	74.3	68.3	26.1	19.64	0.11
X	X	1010	20.50	0.0066	25.72	19.4	77.3	62.9	30.0	20.91	0.11
X	Y	1010	18.13	0.0058	18.57	24.0	87.2	69.7	35.0	20.495	0.091
X	Z	1060	19.28	0.0067	21.47	34.1	76.1	67.1	41.9	20.952	0.083
X	AA	1060	16.38	0.0064	14.34	27.5	79.3	74.1	47.6	19.679	0.070
X	AB	1110	17.34	0.0069	15.17	28.9	74.0	74.1	53.5	20.832	0.086
X	AC	1110	16.33	0.0079	13.04	23.2	64.2	76.4	58.3	20.228	0.072
X	AD	1110	15.57	0.0085	10.54	29.4	60.3	80.0	64.3	20.189	0.072
X	AE	1110	15.48	0.0092	9.475	31.3	55.7	81.9	70.7	20.546	0.063
X	AF	1210	16.11	0.0065	9.099	41.7	79.1	83.3	79.2	21.740	0.062
X	AG	1260	15.43	0.0054	7.074	55.6	94.1	86.5	90.6	21.611	0.055
X	AH	1360	16.40	0.0291	10.57	8.44	17.5	81.0	92.3	21.52	0.11
X	AI	1700	15.79	0.0309	9.393	37.5	16.5	82.4	100.0	21.085	0.064
	Integrated age ± 2σ			n=34	MSWD=856.31	488.4	49.9	K2O=16.75%		21.73	0.12
	Plateau ± 2σ no plateau			n=0	MSWD=0.00	0.000	0.000±0.000		0.0	0.00	0.000
	Isochron±2σ steps B-AI			n=34	MSWD=240.35		$^{40}Ar/^{36}Ar$=	445.8±2.5		17.267	0.061

MZQ-33, K-Feldspar, 16.69 mg, J=0.0007875±0.05%, D=1.004±0.001, NM-208L, Lab#=57189-01

X	B	520	546.8	0.0760	1382.5	0.339	6.7	25.3	0.1	186.5	4.0
X	C	520	172.5	0.0517	494.1	0.436	9.9	15.4	0.2	37.3	2.6
X	D	570	206.6	0.0345	438.3	1.221	14.8	37.3	0.5	106.3	1.4
X	E	570	54.11	0.0321	138.5	1.056	15.9	24.4	0.7	18.65	0.79
X	F	620	87.96	0.0158	165.9	3.12	32.3	44.3	1.5	54.49	0.53
X	G	620	24.93	0.0184	44.73	2.33	27.8	47.0	2.0	16.57	0.33
X	H	670	28.10	0.0123	41.49	4.04	41.3	56.4	3.0	22.36	0.26
X	I	670	17.88	0.0069	21.00	3.67	73.5	65.3	3.8	16.51	0.20
X	J	720	18.95	0.0070	19.66	4.65	73.3	69.4	4.9	18.58	0.17
X	K	720	15.34	0.0060	13.30	5.20	85.5	74.4	6.2	16.14	0.14
X	L	770	18.16	0.0066	16.62	6.87	77.6	73.0	7.8	18.73	0.14
X	M	770	14.24	0.0077	9.348	6.16	66.5	80.6	9.3	16.23	0.13
X	N	820	16.28	0.0049	12.11	6.35	105.1	78.0	10.8	17.96	0.14
X	O	820	14.58	0.0078	8.886	5.65	65.7	82.0	12.1	16.90	0.13
X	P	870	17.01	0.0039	13.80	5.89	131.2	76.0	13.5	18.28	0.13
X	Q	870	15.75	0.0096	13.46	4.39	53.4	74.8	14.5	16.65	0.18
X	R	920	18.39	0.0108	20.06	4.10	47.3	67.8	15.5	17.62	0.18
X	S	920	18.03	0.0100	19.67	3.71	50.9	67.8	16.4	17.28	0.20
X	T	970	25.22	0.0096	40.58	4.48	52.9	52.5	17.4	18.70	0.22
X	U	970	23.54	0.0071	34.49	5.17	71.4	56.7	18.7	18.87	0.19
X	V	1020	31.58	0.0068	53.15	7.73	75.0	50.3	20.5	22.41	0.18
X	W	1020	27.57	0.0066	41.01	9.77	77.2	56.0	22.8	21.81	0.16
X	X	1070	30.98	0.0055	47.03	16.32	92.5	55.1	26.7	24.10	0.15
X	Y	1070	24.89	0.0044	30.80	18.69	115.0	63.4	31.1	22.29	0.12
X	Z	1120	26.36	0.0052	33.06	28.4	98.8	62.9	37.8	23.43	0.11
X	AA	1120	21.39	0.0053	20.62	26.8	96.9	71.5	44.1	21.605	0.088
X	AB	1170	22.13	0.0064	21.16	36.2	79.8	71.7	52.7	22.417	0.080
X	AC	1170	19.95	0.0066	16.16	36.2	77.5	76.1	61.3	21.429	0.068
X	AD	1170	18.81	0.0056	13.66	38.6	91.9	78.5	70.4	20.867	0.059
X	AE	1170	19.26	0.0037	15.56	30.7	138.2	76.1	77.7	20.710	0.073
X	AF	1270	18.11	0.0046	8.992	19.98	111.9	85.3	82.4	21.827	0.071
X	AG	1320	18.73	0.0022	9.856	44.1	228.5	84.5	92.8	22.341	0.053
X	AH	1420	20.43	0.0048	14.52	12.29	107.0	79.0	95.7	22.78	0.11
X	AI	1770	20.40	0.0027	14.77	18.00	189.8	78.6	100.0	22.640	0.084
	Integrated age ± 2σ			n=34	MSWD=594.90	422.5	89.1	K2O=12.35%		21.96	0.13
	Plateau ± 2σ	no plateau		n=0	MSWD=0.00	0.000	0.000±0.000		0.0	0.00	0.000
	Isochron±2σ	steps B-AI		n=34	MSWD=268.25		$^{40}Ar/^{36}Ar$=	397.4±2.5		18.738	0.076

MZQ-10, K-Feldspar, 18.85 mg, J=0.0007906±0.05%, D=1.004±0.001, NM-208L, Lab#=57186-01

X	B	570	567.1	0.0050	1870.9	5.90	101.6	2.5	1.4	20.2	3.3
X	C	570	100.5	0.0064	303.1	5.05	79.2	10.9	2.7	15.52	0.65
X	D	620	63.16	0.0040	175.3	9.48	127.3	18.0	5.0	16.14	0.42
X	E	620	50.32	0.0029	130.1	6.41	175.5	23.6	6.5	16.84	0.35
X	F	670	43.71	0.0034	107.9	7.88	152.3	27.1	8.4	16.79	0.27
X	G	670	38.17	0.0056	90.42	5.76	90.4	30.0	9.8	16.26	0.32
X	H	720	34.10	0.0012	76.13	6.08	433.6	34.0	11.3	16.47	0.26
X	I	720	30.48	0.0058	65.65	4.87	87.7	36.4	12.5	15.74	0.22
	J	770	29.08	0.0027	58.89	6.64	186.0	40.1	14.1	16.57	0.22
	K	770	24.96	0.0035	46.12	5.38	146.0	45.4	15.4	16.09	0.22
	L	820	26.12	0.0034	49.14	6.00	150.1	44.4	16.8	16.47	0.21
	M	820	25.06	0.0027	46.68	5.07	186.0	45.0	18.1	16.00	0.23
	N	870	40.47	0.0020	97.12	5.64	254.0	29.1	19.4	16.71	0.30
	O	870	46.59	0.0046	118.9	5.24	111.2	24.6	20.7	16.26	0.37
	P	920	107.1	0.0050	324.2	7.02	101.4	10.5	22.4	16.00	0.74
	Q	920	106.6	0.0053	321.5	7.23	96.6	10.9	24.1	16.44	0.69
	R	970	161.3	0.0037	504.8	11.49	136.1	7.5	26.9	17.19	0.93
	S	970	128.9	0.0018	395.2	11.66	288.0	9.4	29.8	17.19	0.77
	T	1020	143.4	0.0041	443.1	18.42	124.4	8.7	34.2	17.70	0.82

	U	1020	99.82	0.0045	298.2	15.13	114.5	11.7	37.9	16.64	0.60
	V	1070	102.7	0.0042	306.0	20.70	121.1	11.9	42.9	17.37	0.58
	W	1070	69.43	0.0052	195.6	14.66	98.1	16.8	46.5	16.53	0.41
	X	1120	76.30	0.0052	219.0	18.74	98.1	15.2	51.0	16.43	0.42
	Y	1120	56.90	0.0040	153.1	14.16	129.1	20.5	54.4	16.54	0.33
	Z	1170	52.73	0.0073	140.2	9.31	69.8	21.4	56.7	16.05	0.32
	AA	1170	50.86	0.0040	132.1	9.63	127.8	23.2	59.0	16.79	0.33
	AB	1220	55.92	0.0034	150.6	12.42	149.6	20.4	62.0	16.23	0.34
	AC	1320	44.65	0.0021	110.9	101.2	237.5	26.6	86.5	16.84	0.21
	AD	1370	47.21	0.0021	119.3	29.3	248.6	25.3	93.7	16.97	0.26
X	AE	1470	55.19	0.0048	144.5	7.58	105.2	22.6	95.5	17.73	0.35
X	AF	1770	50.66	0.0037	127.9	18.60	137.7	25.4	100.0	18.26	0.27
	Integrated age ± 2σ			n=31	MSWD=3.20	412.7	145.3	K2O=10.64%		16.86	0.73
	Plateau ± 2σ steps J-AD			n=21	MSWD=1.24	335.1	175.8	±120.2	81.2	16.50	0.16
	Isochron±2σ steps B-AF			n=31	MSWD=2.86		$^{40}Ar/^{36}Ar$=	297.1±1.1		16.30	0.21

MZQ-19, K-Feldspar, 18.2 mg, J=0.0007029±0.04%, D=1.002±0.001, NM-203H, Lab#=56824-01

X	C	550	80.98	0.0699	190.4	0.474	7.3	30.5	0.1	31.1	1.1
X	D	600	68.62	0.0651	101.7	0.873	7.8	56.2	0.3	48.26	0.60
X	E	600	26.27	0.0468	37.89	0.615	10.9	57.4	0.5	19.03	0.60
X	F	650	30.56	0.0571	32.92	1.235	8.9	68.2	0.8	26.23	0.35
X	G	650	19.55	0.0496	17.60	1.217	10.3	73.4	1.1	18.12	0.31
X	H	700	22.80	0.0371	18.07	2.09	13.7	76.6	1.6	22.01	0.20
X	I	700	17.19	0.0409	8.931	2.02	12.5	84.7	2.1	18.36	0.19
X	J	750	19.48	0.0323	12.46	3.33	15.8	81.1	2.9	19.92	0.13
X	K	750	16.27	0.0311	5.776	3.12	16.4	89.5	3.6	18.38	0.12
X	L	800	16.99	0.0291	5.951	4.37	17.5	89.7	4.7	19.211	0.090
X	M	800	16.10	0.0276	4.327	3.89	18.5	92.1	5.7	18.70	0.11
X	N	850	16.48	0.0304	3.863	4.84	16.8	93.1	6.8	19.353	0.085
X	O	850	16.19	0.0289	4.043	4.31	17.7	92.6	7.9	18.915	0.091
X	P	900	16.83	0.0269	4.973	4.99	19.0	91.3	9.1	19.375	0.086
X	Q	900	16.82	0.0250	4.439	4.37	20.4	92.2	10.2	19.558	0.097
X	R	950	18.27	0.1211	8.531	4.92	4.2	86.3	11.4	19.870	0.088
X	S	950	17.82	0.0193	6.871	4.49	26.4	88.6	12.5	19.916	0.099
X	T	1000	20.13	0.0161	13.69	5.05	31.7	79.9	13.7	20.29	0.10
X	U	1000	19.50	0.0126	11.46	5.14	40.6	82.6	14.9	20.321	0.092
X	V	1050	23.21	0.0115	24.05	6.42	44.2	69.4	16.5	20.31	0.12
X	W	1050	21.24	0.0123	17.30	6.54	41.4	75.9	18.1	20.34	0.10
X	X	1100	25.78	0.0109	31.55	9.47	46.7	63.8	20.4	20.75	0.12
X	Y	1100	21.98	0.0105	18.91	8.73	48.6	74.6	22.5	20.673	0.095
X	Z	1150	24.02	0.0112	24.55	14.13	45.4	69.8	26.0	21.143	0.083
X	AA	1150	22.87	0.0117	20.49	13.56	43.8	73.5	29.3	21.200	0.075
X	AB	1150	21.65	0.0114	16.30	35.1	44.8	77.8	37.8	21.220	0.061
X	AC	1250	19.45	0.0060	7.866	98.2	85.2	88.1	61.7	21.583	0.039
X	AD	1350	18.93	0.0092	5.875	96.8	55.3	90.8	85.3	21.676	0.035
X	AE	1450	19.84	0.0278	8.415	13.09	18.3	87.5	88.4	21.881	0.061
X	AF	1750	22.06	0.0205	16.80	47.5	24.8	77.5	100.0	21.554	0.055
	Integrated age ± 2σ			n=30	MSWD=237.52	410.8	34.5	K2O=12.34%		21.265	0.081
	Plateau ± 2σ no plateau			n=0	MSWD=0.00	0.000	0.000±0.000		0.0	0.00	0.000
	Isochron±2σ steps C-AF			n=30	MSWD=169.73		$^{40}Ar/^{36}Ar$=	369.3±4.0		20.020	0.062

MZQ-21, K-Feldspar, 17.4 mg, J=0.0009049±0.05%, D=1.002±0.001, NM-196L, Lab#=56289-01

X	B	460	348.8	0.2572	1019.6	0.253	2.0	13.6	0.0	75.9	7.6
X	C	460	69.20	0.2210	234.7	0.306	2.3	-0.2	0.1	-0.2	4.3
X	D	510	61.74	0.1021	156.3	0.724	5.0	25.2	0.2	25.2	2.0
X	E	510	31.07	0.0643	80.38	1.032	7.9	23.6	0.4	11.9	1.3
X	F	560	30.64	0.0475	66.39	2.13	10.8	36.0	0.8	17.91	0.66
X	G	560	21.39	0.0391	43.64	2.73	13.0	39.7	1.2	13.82	0.51

X	H	610	21.04	0.0293	34.83	5.75	17.4	51.1	2.2	17.47	0.28
X	I	610	15.62	0.0273	20.12	5.18	18.7	61.9	3.1	15.72	0.28
X	J	660	15.52	0.0253	18.04	7.78	20.2	65.7	4.4	16.56	0.19
X	K	660	12.85	0.0242	9.070	7.23	21.0	79.2	5.6	16.53	0.19
X	L	710	12.99	0.0250	9.141	9.20	20.4	79.2	7.1	16.73	0.16
X	M	710	11.61	0.0208	5.171	9.17	24.6	86.8	8.7	16.38	0.14
X	N	760	12.03	0.0194	6.087	12.02	26.3	85.1	10.7	16.63	0.12
X	O	760	11.22	0.0153	3.087	12.36	33.2	91.9	12.8	16.75	0.11
X	P	810	11.69	0.0154	4.248	14.80	33.1	89.3	15.3	16.954	0.096
X	Q	810	11.28	0.0154	2.793	14.34	33.1	92.7	17.7	16.987	0.094
X	R	860	12.10	0.0155	5.108	15.5	32.8	87.5	20.3	17.205	0.093
X	S	860	11.62	0.0150	3.679	15.03	34.1	90.7	22.9	17.120	0.093
X	T	910	12.99	0.0162	7.817	13.15	31.6	82.2	25.1	17.35	0.11
X	U	910	12.69	0.0136	6.937	15.28	37.5	83.9	27.7	17.286	0.097
X	V	960	15.14	0.0146	14.54	11.68	35.0	71.6	29.7	17.62	0.14
X	W	960	14.81	0.0120	13.76	16.0	42.5	72.5	32.4	17.46	0.10
X	X	1010	17.05	0.0116	20.80	17.8	44.1	64.0	35.4	17.72	0.11
X	Y	1010	16.27	0.0097	18.05	20.2	52.7	67.2	38.8	17.77	0.10
X	Z	1060	17.48	0.0099	21.37	22.2	51.4	63.9	42.5	18.14	0.10
X	AA	1060	16.07	0.0095	16.51	23.4	53.5	69.6	46.5	18.180	0.088
X	AB	1110	17.49	0.0098	20.33	21.3	52.0	65.7	50.1	18.64	0.10
X	AC	1110	17.00	0.0125	18.49	24.1	40.7	67.9	54.1	18.728	0.095
X	AD	1110	17.13	0.0111	18.78	35.6	46.0	67.6	60.1	18.812	0.080
X	AE	1110	17.73	0.0099	20.58	42.9	51.3	65.7	67.4	18.919	0.080
X	AF	1210	18.20	0.0057	20.13	66.8	90.2	67.3	78.7	19.892	0.070
X	AG	1260	19.51	0.0044	24.09	61.7	116.1	63.5	89.1	20.111	0.077
X	AH	1360	25.95	0.0416	42.57	9.24	12.3	51.5	90.6	21.71	0.20
X	AI	1700	20.77	0.0113	27.13	55.5	45.3	61.4	100.0	20.698	0.087
	Integrated age ± 2σ			n=34	MSWD=132.55	592.3	40.1	K2O=14.45%		18.59	0.11
	Plateau ± 2σ	no plateau		n=0	MSWD=0.00	0.000	0.000±0.000		0.0	0.00	0.000
	Isochron±2σ	steps B-AI		n=34	MSWD=41.78		$^{40}Ar/^{36}Ar$=	371.2±3.2		16.376	0.091

MZQ-32, K-Feldspar, 17.83 mg, J=0.0007878±0.05%, D=1.004±0.001, NM-208L, Lab#=57188-01

X	B	520	158.0	0.0271	372.1	1.413	18.8	30.4	0.3	67.0	1.1
X	C	520	25.61	0.0112	48.85	1.196	45.7	43.6	0.5	15.82	0.51
X	D	570	20.14	0.0087	25.28	3.10	58.6	62.9	1.1	17.92	0.27
X	E	570	15.79	0.0080	14.82	2.99	64.0	72.3	1.7	16.15	0.21
X	F	620	18.56	0.0081	15.53	6.21	62.9	75.3	2.9	19.75	0.14
X	G	620	14.01	0.0021	5.296	5.09	240.1	88.8	3.8	17.60	0.13
X	H	670	13.69	0.0065	4.997	7.82	78.8	89.2	5.3	17.273	0.092
X	I	670	13.28	0.0064	4.127	8.04	79.6	90.8	6.9	17.068	0.089
X	J	720	12.93	0.0055	2.769	10.15	92.9	93.7	8.8	17.128	0.069
X	K	720	13.01	0.0055	3.494	10.22	92.6	92.1	10.8	16.943	0.066
X	L	770	12.81	0.0053	2.233	12.95	96.4	94.9	13.2	17.184	0.060
X	M	770	12.87	0.0035	2.430	13.80	144.4	94.4	15.9	17.190	0.057
X	N	820	12.77	0.0035	1.848	14.59	145.3	95.7	18.7	17.287	0.050
X	O	820	13.14	0.0054	3.047	13.51	94.8	93.2	21.2	17.313	0.055
X	P	870	13.07	0.0046	2.611	12.84	112.0	94.1	23.7	17.391	0.059
X	Q	870	13.48	0.0047	3.932	12.02	109.5	91.4	26.0	17.421	0.058
X	R	920	13.90	0.0054	4.955	11.16	95.3	89.5	28.1	17.584	0.068
X	S	920	14.35	0.0043	6.389	10.42	119.0	86.8	30.1	17.622	0.077
X	T	970	15.24	0.0053	9.394	9.72	96.5	81.8	32.0	17.637	0.085
X	U	970	15.69	0.0050	10.55	10.09	102.1	80.1	33.9	17.780	0.074
X	V	1020	16.96	0.0033	13.92	10.56	152.7	75.7	35.9	18.162	0.081
X	W	1020	16.91	0.0041	13.71	11.82	125.9	76.0	38.2	18.187	0.071
X	X	1070	17.84	0.0043	15.95	12.97	119.1	73.6	40.7	18.56	0.10
X	Y	1070	17.17	0.0040	13.49	14.25	128.5	76.8	43.4	18.645	0.080
X	Z	1120	17.96	0.0046	15.32	15.61	112.0	74.8	46.4	18.999	0.081

X	AA	1120	17.25	0.0060	12.82	16.32	85.4	78.0	49.5	19.035	0.067
X	AB	1170	18.03	0.0053	14.35	13.97	95.8	76.5	52.2	19.493	0.085
X	AC	1170	17.88	0.0056	14.70	17.69	91.6	75.7	55.6	19.143	0.081
X	AD	1170	18.28	0.0048	15.28	28.0	107.3	75.3	60.9	19.458	0.077
X	AE	1170	19.16	0.0029	18.04	32.4	176.4	72.2	67.1	19.554	0.076
X	AF	1270	18.74	0.0023	14.17	30.4	222.3	77.6	72.9	20.562	0.070
X	AG	1320	19.02	0.0013	14.45	81.6	387.8	77.6	88.5	20.852	0.058
X	AH	1420	19.87	0.0015	17.20	26.6	330.8	74.4	93.6	20.902	0.078
X	AI	1770	20.79	0.0015	18.28	33.4	334.4	74.0	100.0	21.745	0.075
	Integrated age ± 2σ			n=34	MSWD=381.08	522.8	135.2	K2O=14.30%		19.272	0.087
	Plateau ± 2σ	no plateau		n=0	MSWD=0.00	0.000	0.000±0.000		0.0	0.00	0.000
	Isochron±2σ	steps B-AI		n=34	MSWD=66.05		$^{40}Ar/^{36}Ar$=	432.8±3.5		16.656	0.057

Notes:

Isotopic ratios corrected for blank, radioactive decay, and mass discrimination, not corrected for interfering reactions.
Errors quoted for individual analyses include analytical error only, without interfering reaction or J uncertainties.
Integrated age calculated by summing isotopic measurements of all steps.
Integrated age error calculated by quadratically combining errors of isotopic measurements of all steps.
Plateau age is inverse-variance-weighted mean of selected steps.
Plateau age error is inverse-variance-weighted mean error (Taylor, 1982) times root MSWD where MSWD>1.
Plateau error is weighted error of Taylor (1982).
Decay constants and isotopic abundances after Steiger and Jäger (1977).
symbol preceding sample ID denotes analyses excluded from plateau age calculations.
Weight percent K_2O calculated from ^{39}Ar signal, sample weight, and instrument sensitivity.
Ages calculated relative to FC-2 Fish Canyon Tuff sanidine interlaboratory standard at 28.02 Ma
Decay Constant (LambdaK (total)) = 5.543e-10/a
Correction factors:
$(^{39}Ar/^{37}Ar)_{Ca}$ = 0.00068 ± 2e-05
$(^{36}Ar/^{37}Ar)_{Ca}$ = 0.00028 ± 1e-05
$(^{38}Ar/^{39}Ar)_{K}$ = 0.013
$(^{40}Ar/^{39}Ar)_{K}$ = 0 ± 0.0004

APPENDIX C

Appendix B contains Arrhenius and log (r/r_o) plots used for MDD thermal modeling of K-feldspars. Modeled age spectra and thermal histories, both monotonic and unconstrained, are located within the main body of the text. All MDD thermal histories were modeled using algorithms developed by Lovera et al., (1989, 1991). Arrhenius plots are constructed using the heating schedule and the fraction of $^{39}Ar_K$ released for each step. Log (r/r_o) plots are constructed by fitting an Arrhenius reference line (r_o) to the Arrhenius plot, calculating the deviation of the Arrhenius trend from r_o, and comparing that to the cumulative ^{39}Ar released. Black lines are the actual data and gray lines are the modeled data.

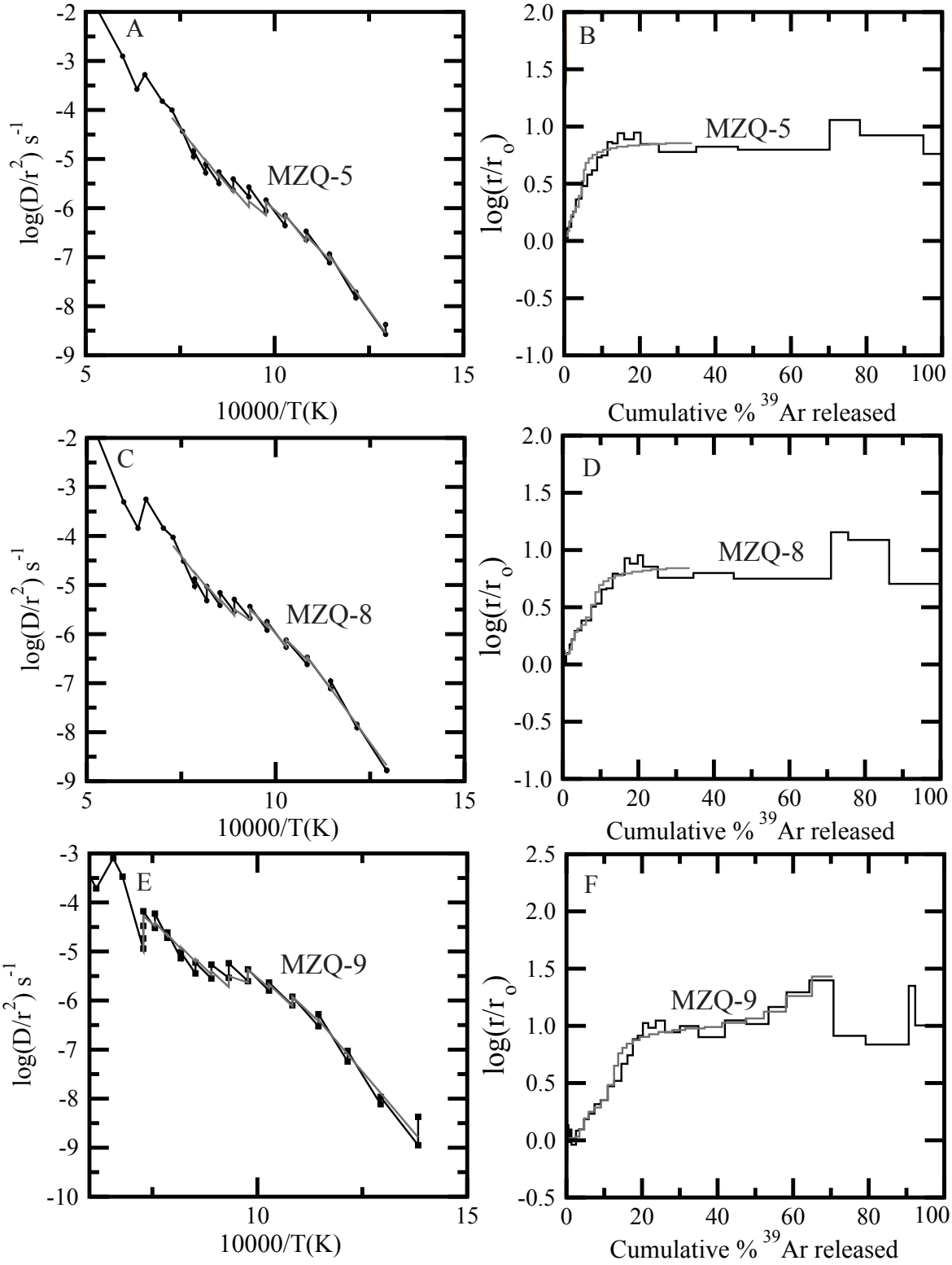
A
MZQ-5
log(D/r^2) s^{-1}
10000/T(K)
B
MZQ-5
log(r/r$_o$)
Cumulative % ^{39}Ar released
C
MZQ-8
log(D/r^2) s^{-1}
10000/T(K)
D
MZQ-8
log(r/r$_o$)
Cumulative % ^{39}Ar released
E
MZQ-9
log(D/r^2) s^{-1}
10000/T(K)
F
MZQ-9
log(r/r$_o$)
Cumulative % ^{39}Ar released

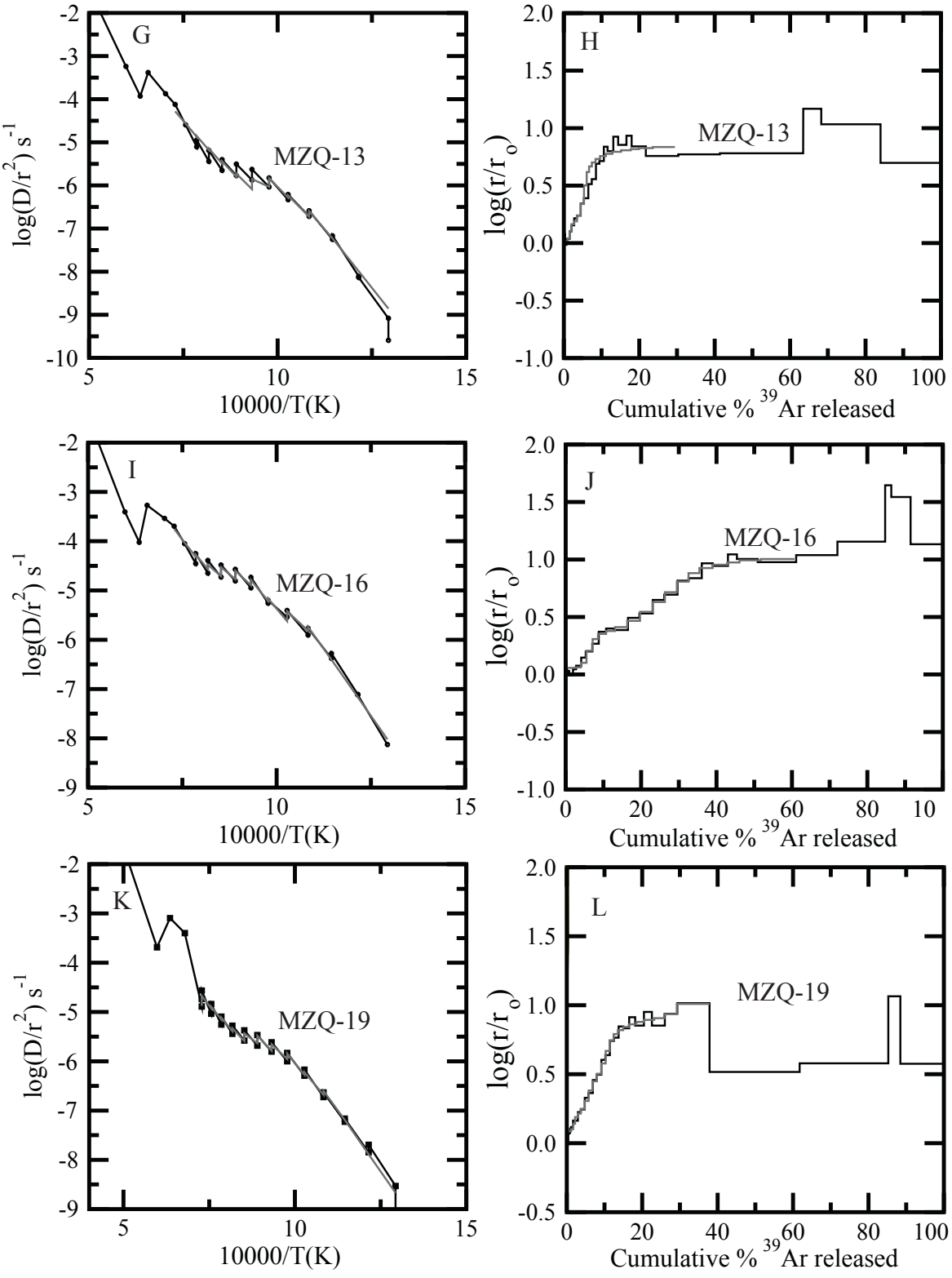
G
MZQ-13
log(D/r^2) s^{-1}
10000/T(K)
H
MZQ-13
log(r/r$_o$)
Cumulative % ^{39}Ar released
I
MZQ-16
log(D/r^2) s^{-1}
10000/T(K)
J
MZQ-16
log(r/r$_o$)
Cumulative % ^{39}Ar released
K
MZQ-19
log(D/r^2) s^{-1}
10000/T(K)
L
MZQ-19
log(r/r$_o$)
Cumulative % ^{39}Ar released

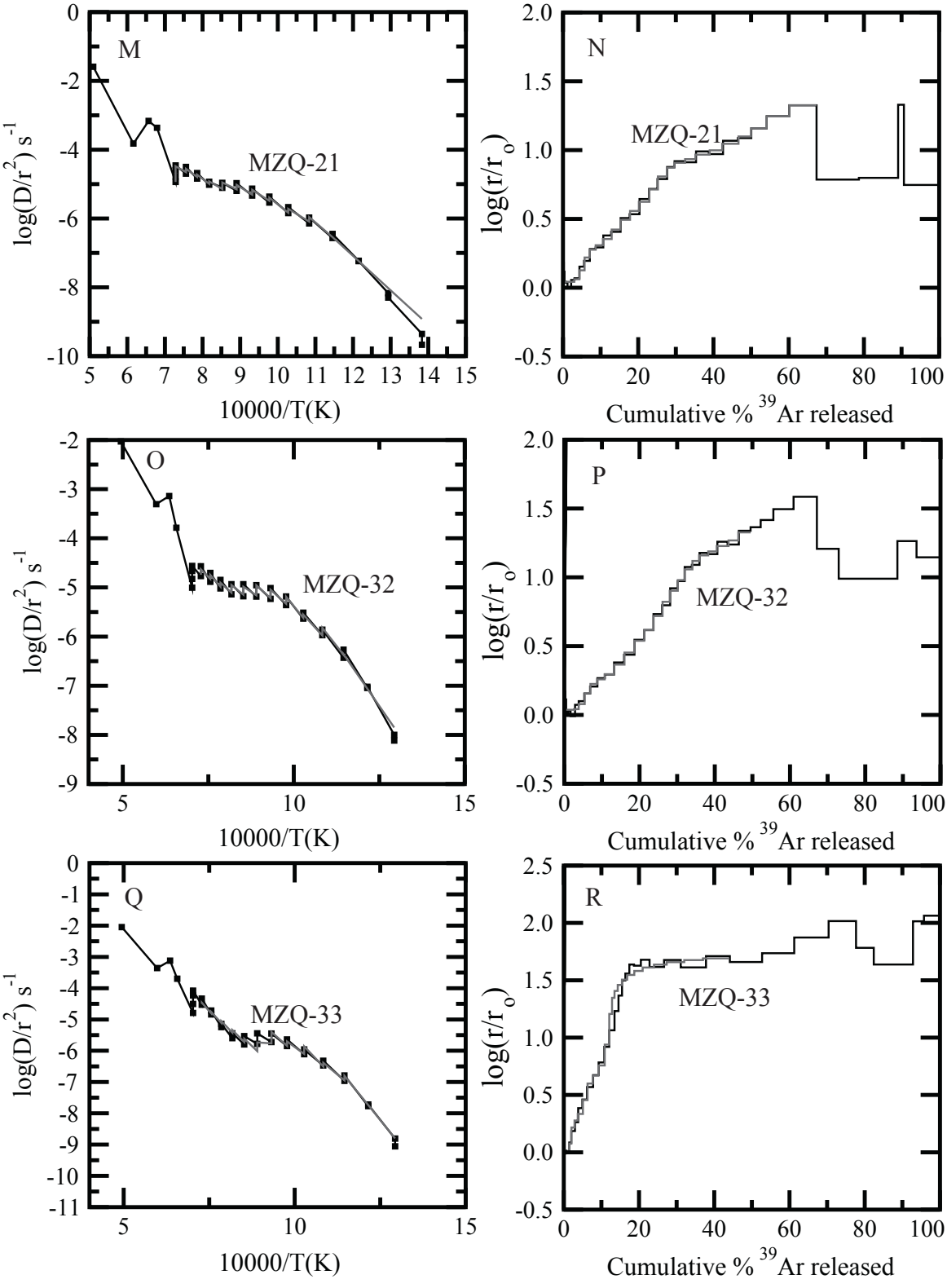
M
MZQ-21
log(D/r^2) s^{-1}
10000/T(K)
N
MZQ-21
log(r/r$_o$)
Cumulative % ^{39}Ar released
O
MZQ-32
log(D/r^2) s^{-1}
10000/T(K)
P
MZQ-32
log(r/r$_o$)
Cumulative % ^{39}Ar released
Q
MZQ-33
log(D/r^2) s^{-1}
10000/T(K)
R
MZQ-33
log(r/r$_o$)
Cumulative % ^{39}Ar released

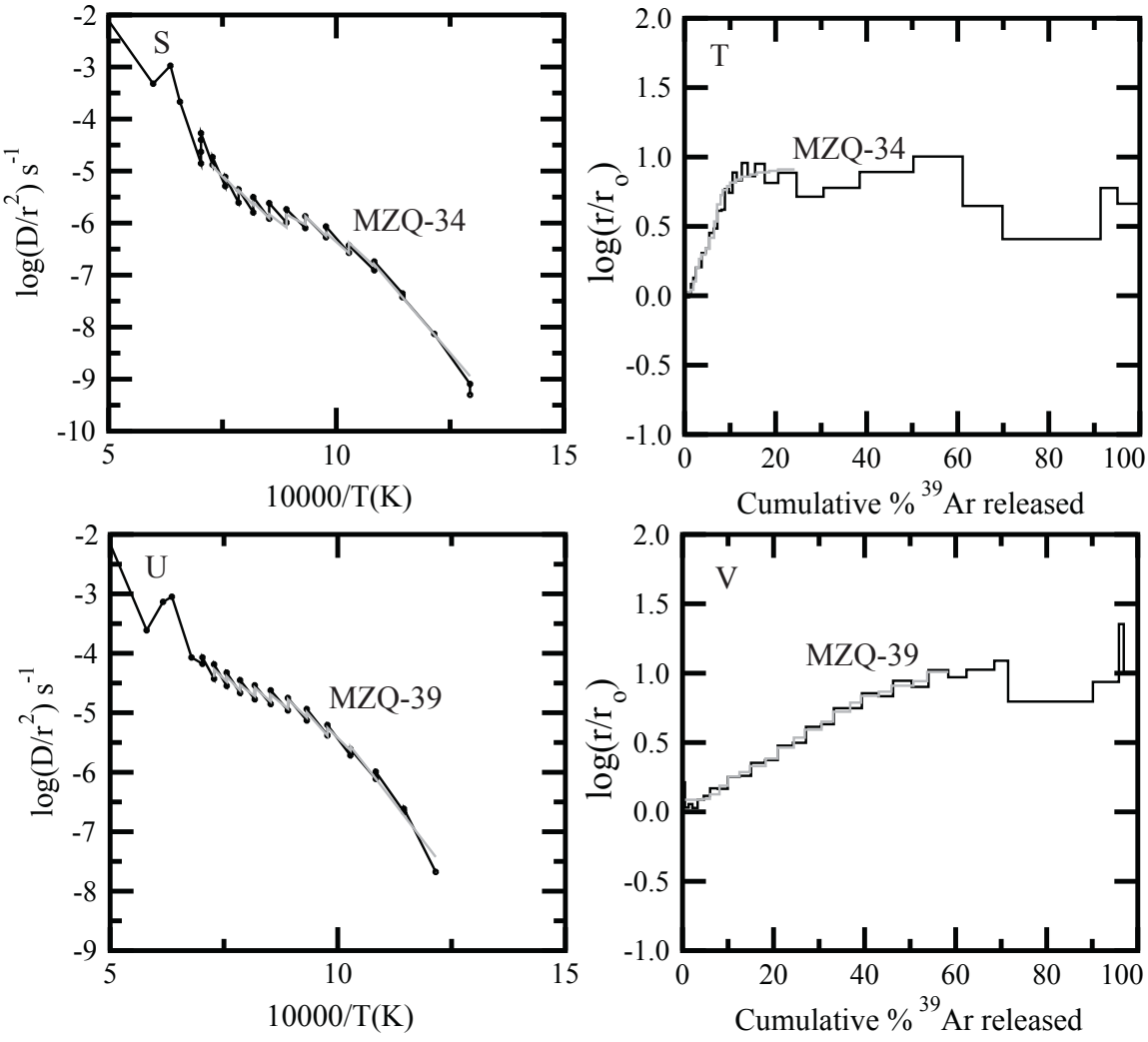
S
MZQ-34
log(D/r^2) s^{-1}
10000/T(K)
T
MZQ-34
log(r/r$_o$)
Cumulative % ^{39}Ar released
U
MZQ-39
log(D/r^2) s^{-1}
10000/T(K)
V
MZQ-39
log(r/r$_o$)
Cumulative % ^{39}Ar released